CHAPTER 4
RESULTS AND DISCUSSION

This chapter discussed the observations and findings of all the objectives undertaken in the current study. The results are discussed in the proposed order of the objectives, beginning with the development of a lab-scale continuous ohmic heating (COH) cell, the heating performance of different fruit juices like pineapple, orange, tomato, lemon, cucumber, and standardized pineapple juice based on different °Brix/Acid (18, 22, and 26 °Brix/Acid). Further, an isothermal holding section was developed to complete the heating and holding section of the COH system. Quality parameters like colour and vitamin C, enzyme, and microbial inactivation were studied under different COH treatment conditions, and the process parameters were optimized. Then, different kinetic models were fitted to enzyme and microbial inactivation and vitamin C degradation. Finally, the storage study of COH-treated (optimized level), conventional water bath-treated, and untreated pineapple juice was conducted at two different temperatures.

4.1 Design and development of continuous ohmic heating (COH) set-up and its performance evaluation

4.1.1 COH set-up and its operation

A lab-scale COH set-up was developed, as discussed in Chapter 3 in Section 3.2.2, which consisted of a cylindrical heating chamber placed horizontally with two platinized titanium electrodes fixed at both ends at a gap of 100 mm. An isothermal holding chamber was placed vertically over the outlet port of the heating chamber connected with a T-shaped hollow jointer. A peristaltic pump was used to pump the juice into the heating chamber, and a variac transformer (0-500 V, 1ϕ, 50 Hz) and a temperature controller were used to regulate the power supply. A K-type thermocouple (insulated with Teflon tape) placed at the outlet port of the heating chamber was used to measure the rise in temperature of the juice. A multimeter was used to measure the current flowing within the juice matrix. The COH setup was fabricated in the Central workshop at Tezpur University (Department of Mechanical Engineering). The schematic diagram of the COH set-up is shown in Fig. 3.8 and Fig. 3.9, respectively, and the actual set-up is shown in Fig. 4.1 and Fig. 4.2.

The juice was pumped to the COH heating chamber from the inlet storage tank through a peristaltic pump. The treatment chamber was filled with juice before providing the electric power supply to avoid any air pockets within the treatment chamber. The juice was heated until

the target temperature of 90 °C was achieved to study the heating performance of the COH system using different fruit juices, viz., cucumber, orange, pineapple, tomato, and lemon, as well as different °Brix/Acid pineapple juice, viz., 18, 22, and 26 °Brix/Acid.

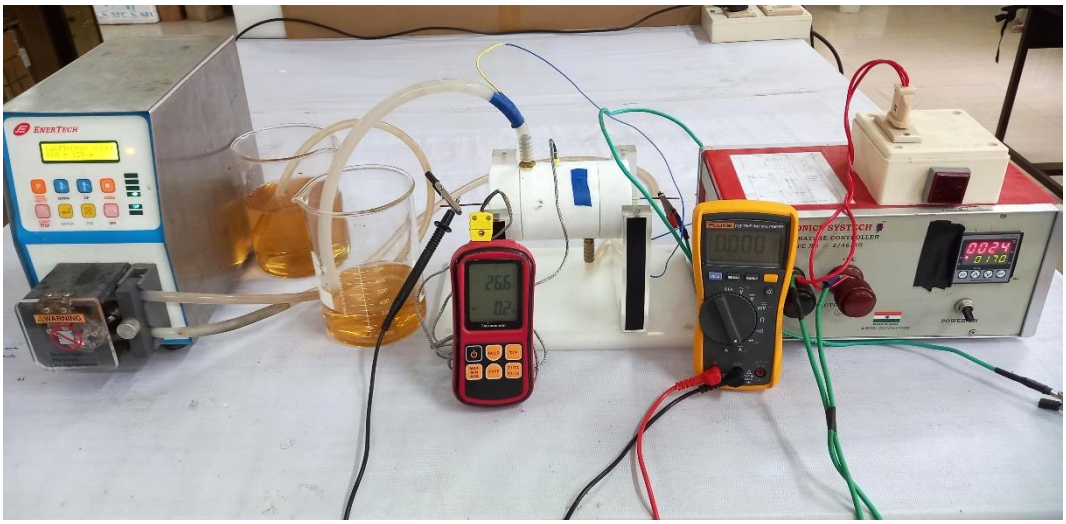

Fig. 4.1 Actual set-up of a lab-scale COH chamber

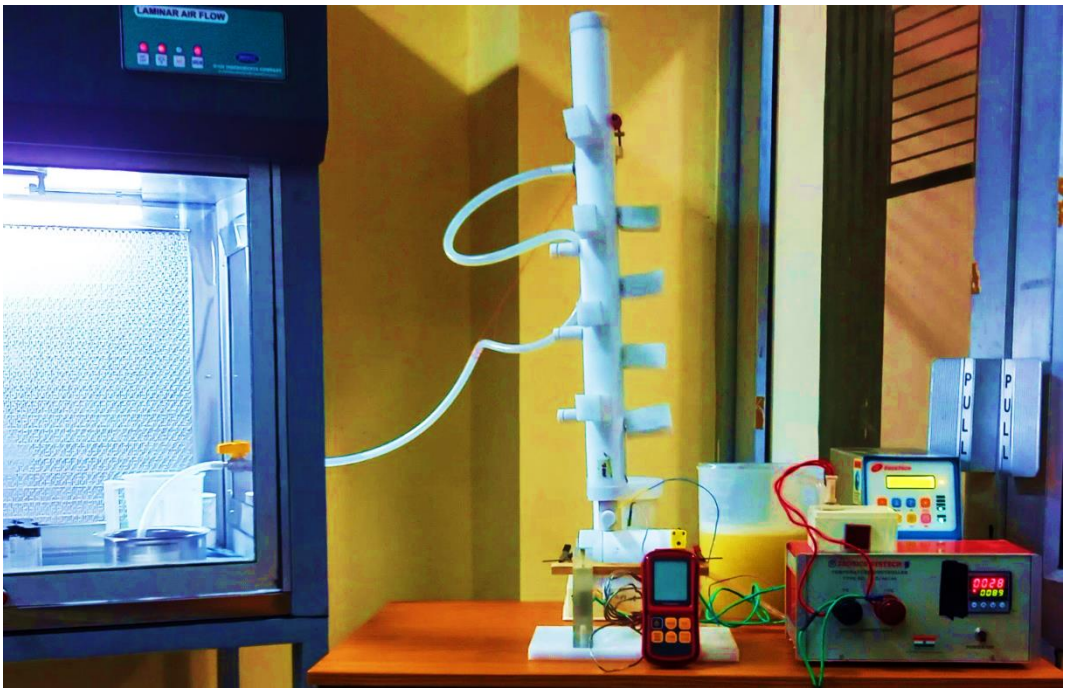

Fig. 4.2 Actual set-up of a lab-scale COH chamber equipped with an isothermal holding chamber

The ohmically heated standardized pineapple juice was passed to an isothermal holding chamber to study the temperature-time effect on parameters like enzyme and microbial inactivation and other quality parameters of juice. After holding for a certain period at the desired temperature, the juice sample was collected from the outlet port of the isothermal

holding chamber. The juice samples were immediately cooled in an ice bath and used for the experimental analysis.

4.1.2 Physico-chemical properties of fresh fruit juice

The physico-chemical properties of the fruit juice were measured as shown in Table 4.1. The pH of lemon juice (2.18) was the lowest, while cucumber juice (6.23) observed a maximum pH value. Consequently, the titratable acidity of the lemon juice was maximum (5.546%) and minimum for cucumber juice (0.085%). Also, the TSS value of the cucumber juice (3.6 °Brix) was the lowest, while the orange juice had a maximum TSS value of 12.0 °Brix. Even though the titratable acidity of tomato juice was lower than lemon, orange, and pineapple juice, it showed maximum electrical conductivity, which may be due to the higher TSS content in these juices, resulting in lower juice moisture content. The presence of sugar has a negative impact on the electrical conductivity (EC) of the fruit juice and, thus, a reduction in the heating rate during ohmic heating. The other reason is that lemon juice contains too much acid, allowing easy passage of electrical current through the juice sample, thus resulting in lower EC.

Table 4.1 Physico-chemical properties of the fresh fruit juice used in the present study

Parameters	Fruit Juice				
	Cucumber	**Tomato**	**Orange**	**Pineapple**	**Lemon**
pH	6.23 ± 0.00	4.34 ± 0.01	4.08 ± 0.02	3.38 ± 0.01	2.18 ± 0.01
TSS (°Brix)	3.6 ± 0.0	4.2 ± 0.0	12.0 ± 0.0	11.6 ± 0.1	6.0 ± 0.0
Titratable acidity (%)	0.085 ± 0.000	0.355 ± 0.025	0.597 ± 0.000	0.974 ± 0.062	5.546 ± 0.074
Specific heat (kJ/kg°C)	4.064 ± 0.003	4.053 ± 0.002	3.875 ± 0.003	3.870 ± 0.009	4.017 ± 0.004
Electrical Conductivity (S/m)	0.284 ± 0.001	0.297 ± 0.003	0.261 ± 0.000	0.246 ± 0.000	0.291 ± 0.003
Moisture content (%wb)	95.55 ± 0.13	95.12 ± 0.06	87.98 ± 0.13	87.80 ± 0.37	93.69 ± 0.18
Density (Kg/m^3)	1017.1 ± 9.6	1030.9 ± 7.5	1071.7 ± 7.5	1090.1 ± 0.3	1053.2 ± 3.8

The density of the cucumber juice was closer to the density of the water because of the high moisture content (95.55%) and low TSS and acid content. On the other hand, the pineapple and orange juice showed maximum density of 1090.1 and 1071.7 kg/m^3, respectively, due to higher TSS and acid content than cucumber juice, resulting in lower moisture content of the juice samples. The specific heat capacity of the juice samples was 3.870 to 4.064 kJ/kg°C. The specific heat capacity had a direct relation with the amount of moisture content, and it increased with an increase in moisture content.

4.1.3 Ohmic heating behaviour of fresh fruit juice

4.1.3.1 Effect of electric field strength on ohmic heating behaviour

Heating rate (HR) is an important parameter determining how efficiently thermal processing occurs. Higher HR will gradually reduce the processing time, ensuring uniform heating and a lower temperature gradient within the samples. The heating profile of cucumber, tomato, orange, pineapple, and lemon juice are shown in Fig. 4.3, 4.4, 4.5, 4.6, and 4.7, respectively, between temperatures 28 °C and 90 °C. The come-up time (CUT) required to achieve a target temperature of 90 °C from an initial temperature of 28 °C at different EFS and flow rates for all five fruit juices are shown in Table 4.2. With an increase in EFS value, the CUT period of all five fruit juices was reduced significantly ($p < 0.05$), irrespective of the flow rate. The reason was that the flow of higher electric current at higher EFS brought more electrical energy within the juice samples, thus heating fruit juice at a faster rate and reducing overall heating time (Al-Hilphy et al., 2020; Jo & Park, 2019). The CUT period of tomato juice was lowest followed by lemon, orange, cucumber, and pineapple at respective EFS of 25, 30, and 35 V/cm. It was observed that the CUT period of lemon juice was lesser than orange juice at a lower EFS value of 25 V/cm at all flow rates. On the other hand, the CUT period of both lemon and orange juice became similar at EFS 30 and 35 V/m, while at higher EFS of 40 and 45 V/cm, the CUT period of orange juice became lesser than lemon juice at all three flow rates. It was also observed that the CUT period of cucumber juice became less than that of lemon juice at a higher EFS of 45 V/cm. The orange juice took the least time (16.0 s) to reach the desired temperature of 90 °C at 45 V/cm and 80 mL/min. On the other hand, the pineapple juice took maximum time to achieve the target temperature of 90 °C at all EFS and flow rates with a maximum CUT period of 214.5 s at 25 V/cm and 120 mL/min. The CUT period of cucumber, tomato, orange, pineapple, and lemon juice was in the range of 19.5 to 93.0 s, 17.0 to 70.0 s, 16.0 to 77.0 s, 30.0 to 214.5 s, and 20.0 to 71.5 s, respectively as shown in Table 4.2. The variations in the CUT period and, therefore, variations in heating rate among different fruit changes were observed because of the fruit juice's intrinsic properties like acid content, EC at room temperature, sugar content, consistency/viscosity, and ionic concentrations. Apart from juice's intrinsic properties, the ohmic heating behaviour is also influenced by factors like EFS and the frequency of the electric current (Ramaswamy et al., 2014). EC depends on the ionic concentration of the juice and helps in the flow of the current. The resistance to the flow of these currents results in the temperature rise. Therefore, the EC of the juice greatly influences the HR, and therefore, the CUT period of the fruit juice during ohmic heating (Makroo et al., 2022).

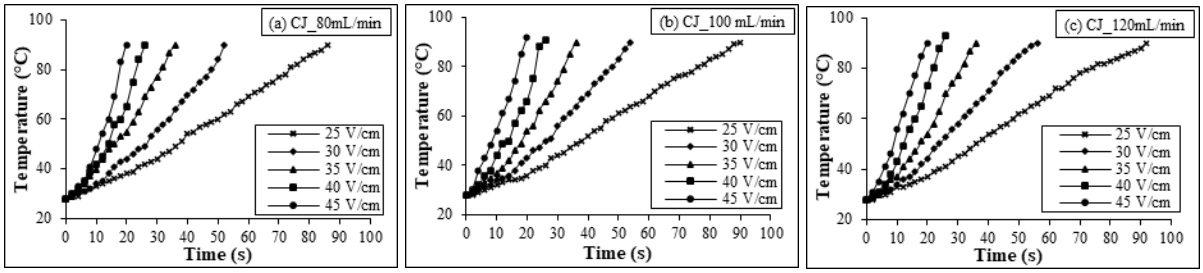

Fig. 4.3 Effect of EFS on the heating profile of cucumber juice during COH at (a) 80 mL/min, (b) 100 mL/min, and (c) 120 mL/min

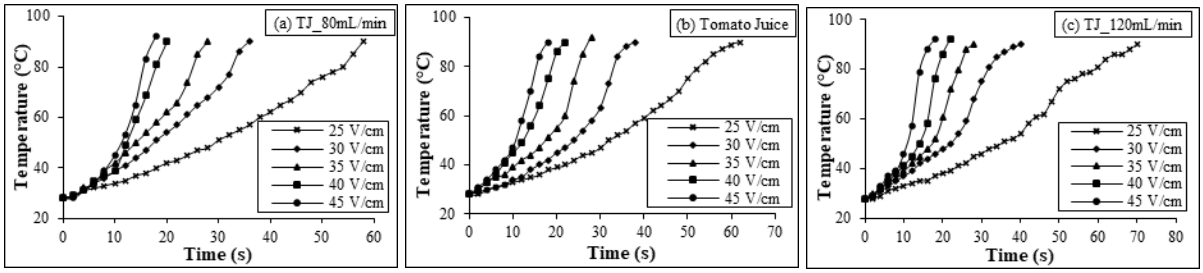

Fig. 4.4 Effect of EFS on the heating profile of tomato juice during COH at (a) 80 mL/min, (b) 100 mL/min, and (c) 120 mL/min

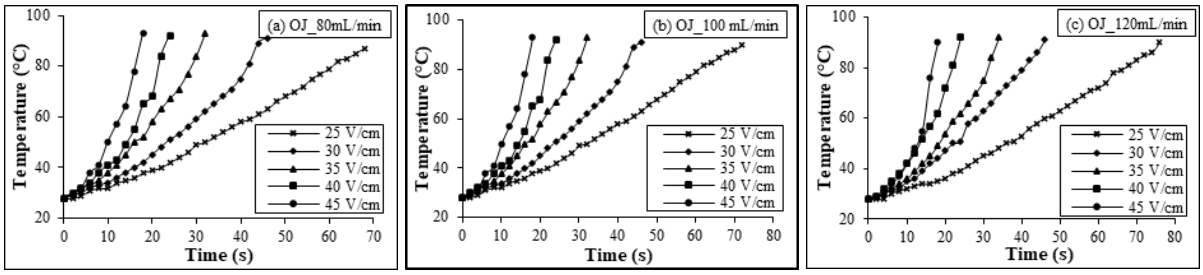

Fig. 4.5 Effect of EFS on the heating profile of orange juice during COH at (a) 80 mL/min, (b) 100 mL/min, and (c) 120 mL/min

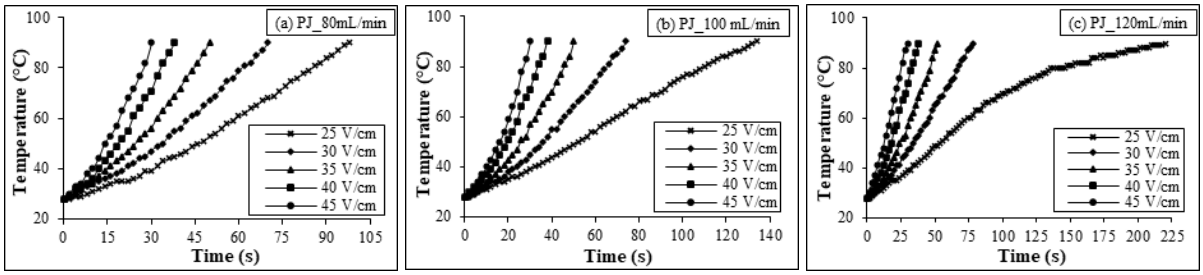

Fig. 4.6 Effect of EFS on the heating profile of pineapple juice during COH at (a) 80 mL/min, (b) 100 mL/min, and (c) 120 mL/min

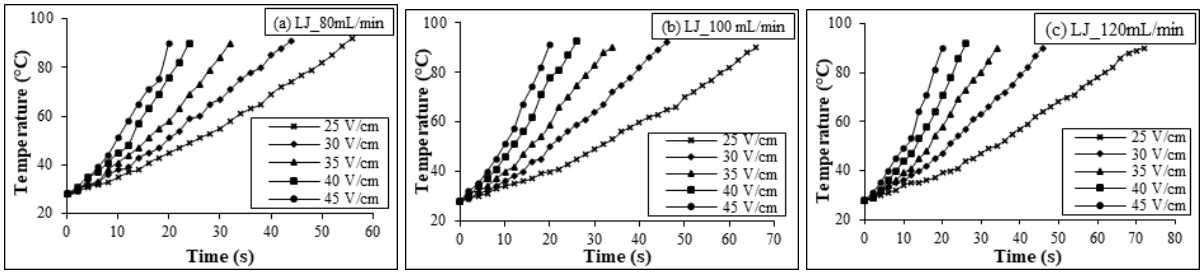

Fig. 4.7 Effect of EFS on the heating profile of lemon juice during COH at a flow rate of (a) 80 mL/min, (b) 100 mL/min, and (c) 120 mL/min

Table 4.2 Come-up time of different fruit juices at varied EFS and flow rates during COH to achieve a target temperature of 90 °C

Fruit Juice	Flow Rate (mL/min)	EFS (V/cm)				
		25	30	35	40	45
Cucumber	80	86.5 ± 0.7^{eA}	52.5 ± 0.7^{dA}	34.5 ± 0.7^{cA}	24.5 ± 0.7^{bA}	19.5 ± 0.7^{aA}
	100	89.5 ± 0.7^{eAB}	54.5 ± 0.7^{dAB}	36.0 ± 0.0^{cA}	25.0 ± 0.0^{bA}	19.5 ± 0.7^{aA}
	120	93.0 ± 1.4^{eB}	55.5 ± 0.7^{dB}	36.5 ± 0.7^{cA}	25.0 ± 0.0^{bA}	20.0 ± 0.0^{aA}
Tomato	80	57.0 ± 1.4^{dA}	34.5 ± 0.7^{cA}	26.5 ± 0.7^{bA}	20.0 ± 0.0^{a}	17.0 ± 0.0^{aA}
	100	61.5 ± 0.7^{eA}	37.5 ± 0.7^{dB}	28.0 ± 0.0^{cA}	21.0 ± 0.0^{b}	17.0 ± 0.0^{aA}
	120	70.0 ± 1.4^{eB}	39.5 ± 0.7^{dB}	28.5 ± 0.7^{cA}	22.0 ± 0.0^{b}	17.5 ± 0.7^{aA}
Orange	80	67.0 ± 1.4^{eA}	42.5 ± 0.7^{dA}	30.5 ± 0.7^{cA}	22.0 ± 0.0^{bA}	16.0 ± 0.0^{aA}
	100	72.5 ± 0.7^{eB}	45.5 ± 0.7^{dB}	32.5 ± 0.7^{cAB}	22.5 ± 0.7^{bAB}	18.0 ± 0.0^{aB}
	120	77.0 ± 1.4^{eB}	46.5 ± 0.7^{dB}	34.5 ± 0.7^{cB}	24.5 ± 0.7^{bB}	18.5 ± 0.7^{aB}
Pineapple	80	96.0 ± 1.4^{eA}	70.5 ± 0.7^{dA}	50.5 ± 0.7^{cA}	38.0 ± 0.0^{b}	30.0 ± 0.0^{a}
	100	132.0 ± 2.8^{eB}	75.0 ± 1.4^{dAB}	50.5 ± 0.7^{cA}	38.0 ± 0.0^{b}	30.0 ± 0.0^{a}
	120	214.5 ± 6.4^{dC}	78.0 ± 1.4^{cB}	51.5 ± 0.7^{bA}	38.0 ± 0.0^{a}	30.0 ± 0.0^{a}
Lemon	80	55.5 ± 0.7^{eA}	42.5 ± 0.7^{dA}	32.0 ± 0.0^{cA}	23.5 ± 0.7^{bA}	20.0 ± 0.0^{aA}
	100	67.0 ± 1.4^{eB}	44.5 ± 0.7^{dAB}	32.5 ± 0.7^{cAB}	24.5 ± 0.7^{bAB}	20.0 ± 0.0^{aA}
	120	71.5 ± 0.7^{eC}	46.5 ± 0.7^{dB}	34.5 ± 0.7^{cB}	26.0 ± 0.0^{bB}	20.5 ± 0.7^{aA}

Values in the same row with different small superscripts significantly ($p < 0.05$) different with a change in EFS at a constant flow rate of specific fruit juice. Also, values in the same column with different capital superscripts are significantly ($p < 0.05$) different with a change in flow rate at a constant EFS of specific fruit juice.

The rate of temperature rise of the fruit juice was higher at higher applied EFS. The HR increased multiple folds when EFS increased from 25 to 45 V/cm at all three flow rates, as shown in Fig. 4.8. The HR increased by more than 4.4, 3.4, 4.1, 3.2, and 2.7 folds, respectively, for cucumber, tomato, orange, pineapple, and lemon juice when the EFS applied across the juice samples increased from 25 to 45 V/cm. The higher EFS generated a higher heat generation rate due to the increased ionic movement rate and ionic flow resistance within the juice matrix (Ramaswamy et al., 2014).

The minimum HR of cucumber, tomato, orange, pineapple, and lemon juice was 40.0 ± 0.6, 53.2 ± 1.1, 48.3 ± 0.9, 17.4 ± 0.5, and 52.0 ± 0.5 °C/min, respectively when the EFS supplied across juice samples was 25 V/cm with a mass flow rate of 120 mL/min. While the maximum HR of cucumber, tomato, orange, pineapple, and lemon juice was significantly ($p < 0.05$) increased to 192.4 ± 4.8, 222.4 ± 5.0, 232.5 ± 0.0, 124.0 ± 0.0, and 189.0 ± 4.2 °C/min, respectively when the juice was heated at 45 V/cm with a flow rate of 80 mL/min. Statistical analysis showed that HR increased significantly ($p < 0.05$) with an increase in EFS for all the samples and under all three flow rates. These results were also in agreement with the volumetric energy generation equation $Q = \sigma \times \nabla V^2$ (Darvishi et al., 2021), which interpreted that the

amount of generated heat was directly proportional to the current produced by the voltage gradient and the EC of the foodstuff (Ramaswamy et al., 2014). So, the inherent properties of the food material and EC influenced the HR (Norouzi et al., 2021).

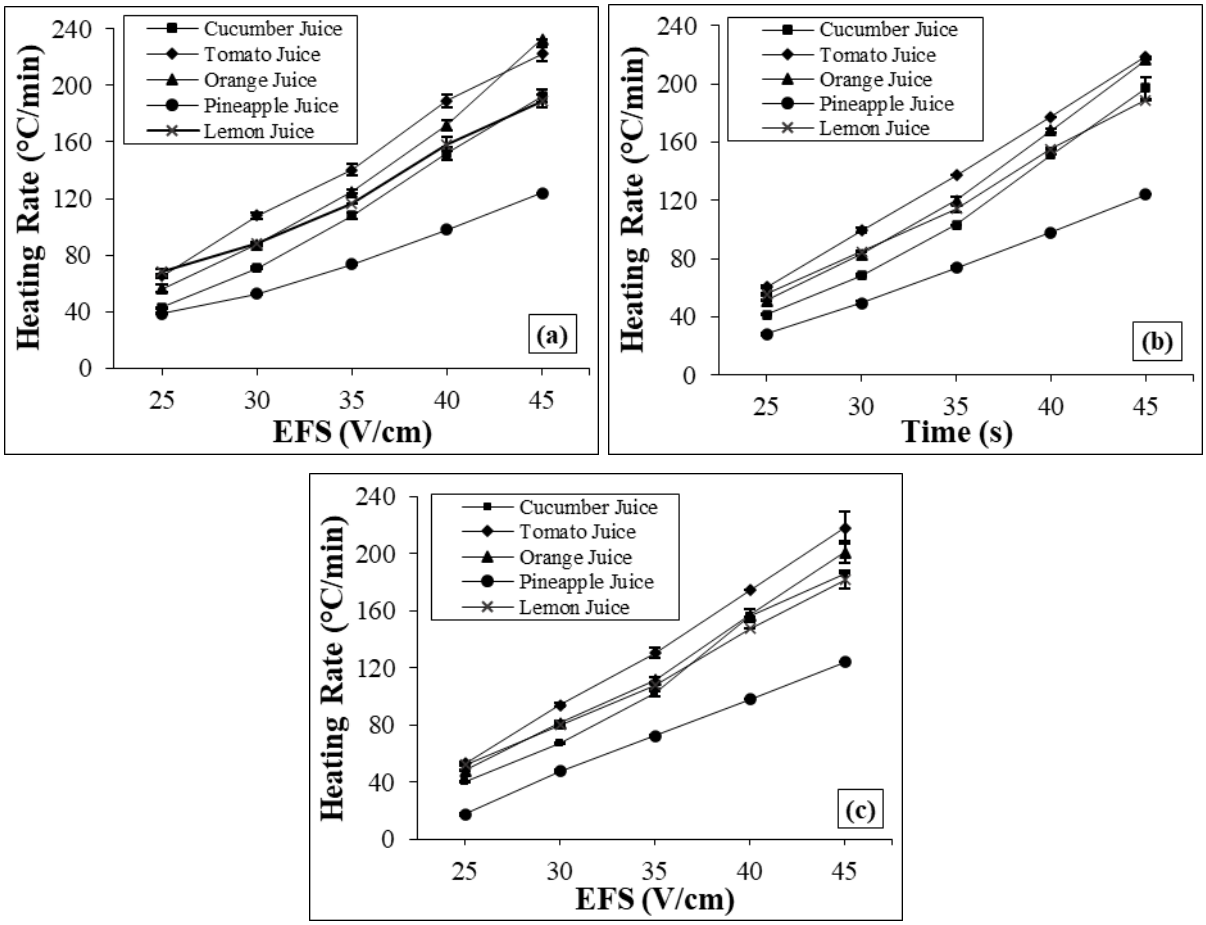

Fig. 4.8 The heating rate curve during COH of different fruit juices at varied EFS at a flow rate of (a) 80 mL/min, (b) 100 mL/min, and (c) 120 mL/min

4.1.3.2 Effect of flow rate on ohmic heating behaviour

The heating profile of cucumber, tomato, orange, pineapple, and lemon juice at different flow rates of 80, 100, and 120 mL/min between temperatures 28 °C to 90 °C are shown in Fig. 4.3, 4.4, 4.5, 4.6, and 4.7, respectively. It was observed that the flow rate had a significant effect on the CUT period at lower EFS of 25 and 30 V/cm, while a non-significant change was observed at higher EFS of 40 and 45 V/cm during COH of different fruit juice as shown in Table 4.2. When the flow rate of the juice was increased from 80 mL/min to 120 mL/min at a constant EFS of 25 V/cm, the CUT period of cucumber, tomato, orange, pineapple, and lemon juice was increased by 1.08, 1.23, 1.15, 2.23, and 1.29 times, respectively. On the other hand, at an elevated EFS of 45 V/cm, there was a minor change (< 1 s) in the CUT period for all the fruit juice samples except for orange juice (~ 2.5 s) when the flow rate was increased from 80 to

120 mL/min. Chen et al. (2010) also studied the effect of flow rate on temperature rise during COH of soup products.

The effect of flow rate on HR was significantly ($p < 0.05$) affected at lower EFS of 25 V/cm. In comparison, the change was non-significant ($p > 0.05$) at higher EFS of 40 and 45 V/cm, as shown in Fig. 4.8. This may be due to larger voltage gradients that allowed greater current to pass through the sample, causing faster heat generation (Ramaswamy et al., 2014). At lower EFS of 25 V/cm, pineapple juice showed a maximum increase in the HR (2.23 folds) when the flow rate was decreased from 120 to 80 mL/min, followed by lemon juice (1.31 folds), tomato juice (1.23 folds), orange juice (1.17 folds), and lastly cucumber juice (1.08 folds). Three-factor ANOVA also showed a significant ($p < 0.05$) change in come-up time and HR with EFS, flow rates, and °Brix/Acid individually and with its combined effect.

4.1.3.3 Performance evaluation of continuous ohmic heating

The performance evaluation of the COH system was done by calculating system performance coefficient (SPC) parameters to check the system's energy efficiency. Since OH is a pure volumetric and direct resistance heating, almost all the energy supplied to the system is used in heating the food samples; thus, 90% and above efficiency can be achieved (Ramaswamy et al., 2014). SPC was evaluated for the COH system for all the combinations of EFS and flow rate of cucumber, tomato, orange, pineapple, and lemon juice as shown in Fig. 4.9. The maximum SPC obtained was 0.971, 0.990, 0.982, 0.985, and 0.980, respectively for cucumber, tomato, orange, pineapple, and lemon juice. Thus, it showed that more than 95% energy efficiency can be achieved with ohmic heating. The study showed that the SPC was in the range of 0.781 to 0.971 for cucumber juice, 0.947 to 0.990 for tomato juice, 0.933 to 0.982 for orange juice, 0.939 to 0.980 for lemon juice, and 0.478 to 0.985 for pineapple juice when EFS and flow rate was in the range of 25 to 45 V/cm and 80 to 120 mL/min, respectively. The only exception was that when pineapple juice was heated at a lower EFS of 25 V/cm and a higher flow rate of 100 mL/min and 120 mL/min, the SPC was observed to be lowest. The reason was the lowest electrical conductivity of pineapple juice at room temperature than other juice with the presence of high level of sugar content that has influenced a lower rate of electric current flow in the juice sample. The lower rate of current flow resulted in a slower heating of the pineapple juice, and therefore, the electrical energy consumption duration was high leading to a greater amount of energy consumption. Therefore, the energy efficiency of the COH system became low with pineapple juice at 25 V/cm resulting in a lower SPC value. Srivsatav (2016) reported that at a lower electric field, higher heating duration was required and resulted in

higher electrical energy; thus, the SPC of the system was reduced. Icier and Ilicali (2005) also reported that the SPC of the ohmic heating system greatly depended on the EFS across the food sample. This showed that more than 93% energy efficiency can be achieved for tomato, orange, and lemon juice and more than 78% for cucumber juice under applied EFS of 25 to 45 V/cm with a flow rate of 80 to 120 mL/min. Also, more than 81% energy efficiency was observed for pineapple juice under similar treatment conditions except the heating at 25V/cm and 120 mL/min, where energy efficiency achieved was only 47.8%.

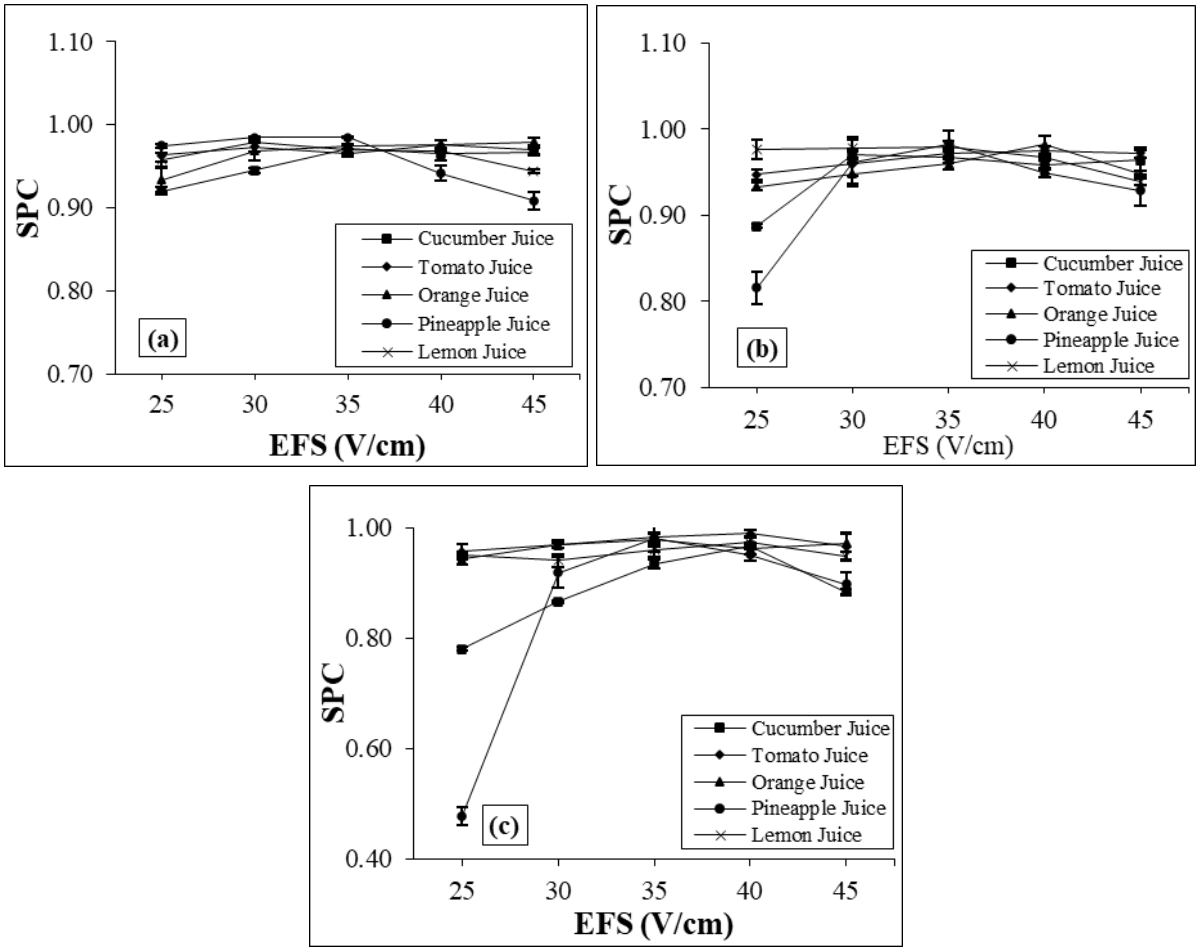

Fig. 4.9 System performance coefficient (SPC) of different fruit juices at varied EFS during COH at a flow rate of (a) 80 mL/min, (b) 100 mL/min, and (c) 120 mL/min

It was also observed that with an increase in EFS value, the SPC was found to increase and reach a maximum value, and then a further increase in the EFS resulted in the reduction of the SPC. Therefore, the EFS where maximum SPC or energy efficiency is achieved was termed a critical EFS. This phenomenon may be due to all supplied electrical energy having converted into thermal energy, i.e., a critical limit of heat generation has been reached. Excess electrical energy was lost beyond this threshold, resulting in a decrease in SPC value. Darvishi et al. (2021) have reported that voltage gradient considerably impacts the thermal performance of

the ohmic heating process. They also mentioned that high energy losses at larger voltage gradients may be caused by physical, chemical, and electrochemical changes during heating. The critical EFS for tomato and pineapple juice was 40 and 35 V/cm, respectively. On the other hand, the critical EFS for cucumber and lemon juice was 30 to 40 V/cm, depending on the flow rates of the juice during ohmic heating. The critical EFS for orange juice ranged from 35 to 45 V/cm, depending on the flow rate. This phenomenon may be due to all supplied electrical energy having converted into thermal energy, i.e., a critical limit of heat generation has been reached. Excess electrical energy was lost beyond this threshold, resulting in a decrease in SPC value. Darvishi et al. (2021) have reported that voltage gradient considerably impacts the thermal performance of the ohmic heating process. They also mentioned that high energy losses at larger voltage gradients may be caused by physical, chemical, and electrochemical changes during heating. Jo and Park (2019) studied the effect of EFS on SPC and observed that when EFS was 10, 15, and 17.5 V/cm, the SPC was found to be 0.46 ± 0.02, 0.63 ± 0.05, and 0.58 ± 0.02 respectively. They concluded that the 15 V/cm gave the highest SPC value of 0.63 ± 0.05 among the three tested EFS.

4.1.3.4 Electrical conductivity behaviour during continuous ohmic heating of fruit juices

The effect of temperature rise during COH on the EC of fruit juice at different EFS ranging from 25 to 45 V/cm and flow rate ranging from 80 to 120 mL/min are shown in Fig. 4.10 for cucumber juice, Fig. 4.11 for tomato juice, Fig. 4.12 for orange juice, Fig. 4.13 for pineapple juice, and Fig. 4.14 for lemon juice. The EC of all the fruit juices was increased with an increase in EFS and temperature during COH at different flow rates between 80 to 100 mL/min. The EC at the initial stage of COH of the cucumber, tomato, orange, pineapple, and lemon juice at a temperature of 30 °C with a constant flow rate of 100 mL/min between EFS of 25 to 45 V/cm was in the range of 0.394 to 0.588, 0.565 to 0.654, 0.435 to 0.619, 0.284 to 0.334, and 0.479 to 0.516 S/m, respectively. At the same time, the EC at the final stage of ohmic heating at a temperature of 90 °C under similar conditions was increased in the range of 0.626 to 0.850, 0.834 to 0.849, 0.759 to 0.921, 0.491 to 0.635, 0.802 to 0.935 S/m, respectively for each fruit juice. The EC of the tomato juice was maximum at the initial stage of COH (30 °C), followed by lemon, orange, cucumber, and pineapple juice. At the final stage of COH (90 °C), maximum EC was observed for lemon juice, followed by tomato, orange, cucumber, and pineapple juice. The changes in the EC with change in fruit juice were due to differences in the acid content and TSS of the juice samples, which resulted in variations of ionic movement and current flow across the juice samples (Sabanci and Icier, 2017). This also significantly ($p < 0.05$) affected the heating time.

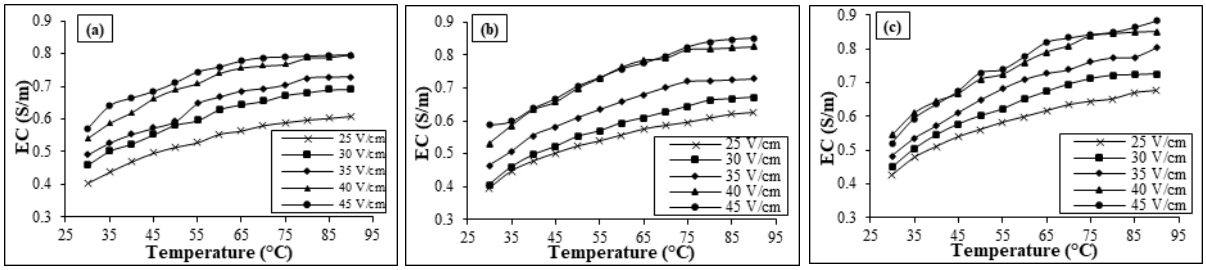

Fig. 4.10 Electrical conductivity – temperature curve of cucumber juice at different EFS during COH at a flow rate of (a) 80 mL/min, (b) 100 mL/min, and (c) 120 mL/min

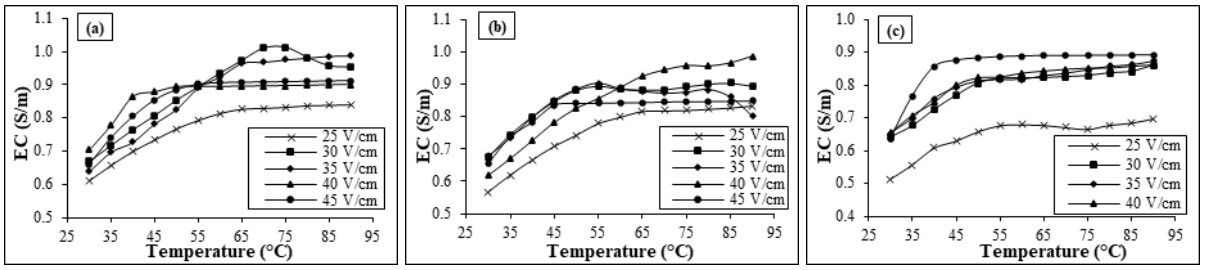

Fig. 4.11 Electrical conductivity – temperature curve of tomato juice at different EFS during COH at a flow rate of (a) 80 mL/min, (b) 100 mL/min, and (c) 120 mL/min

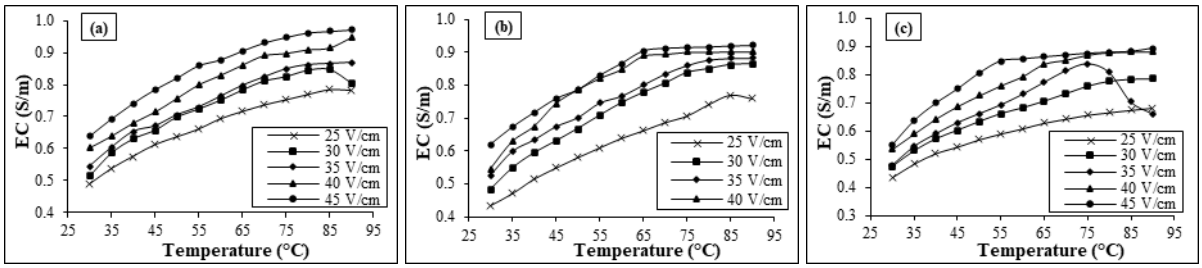

Fig. 4.12 Electrical conductivity – temperature curve of orange juice at different EFS during COH at a flow rate of (a) 80 mL/min, (b) 100 mL/min, and (c) 120 mL/min

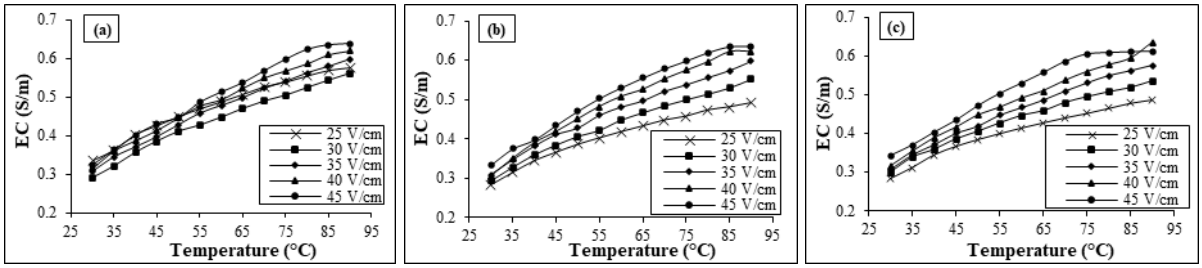

Fig. 4.13 Electrical conductivity – temperature curve of pineapple juice at different EFS during COH at a flow rate of (a) 80 mL/min, (b) 100 mL/min, and (c) 120 mL/min

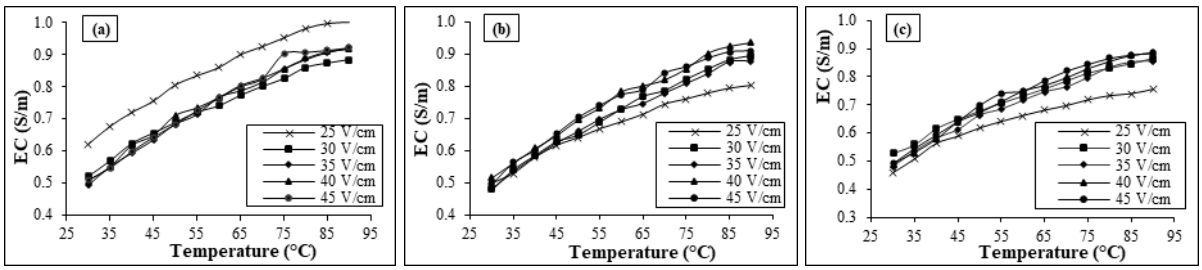

Fig. 4.14 Electrical conductivity – temperature curve of lemon juice at different EFS during COH at a flow rate of (a) 80 mL/min, (b) 100 mL/min, and (c) 120 mL/min

The study also showed that with increased concentrations of the soluble solids in orange juice concentrates (Icier and Ilicali, 2005) and sour cherry juice (Sabanci and Icier, 2017), the EC decreased at any constant temperature and voltage gradients. The EC of the fruit juices during COH changes with a temperature change. The results showed that the EC of all the fruit juices increased significantly with the temperature. When the temperature was raised from 30 °C to 90 °C at a constant flow rate of 100 mL/min and EFS 30 V/cm, the EC was increased by 65.5, 32.8, 79.3, 88.4, and 86.4%, respectively, for cucumber, tomato, orange, pineapple, and lemon juice. Similar observations were made at different EFS and flow rates. The present study was in line with other studies that also observed an increase in the EC with an increase in the temperature of different fruit juices like grape juice (Icier et al., 2008) and sour cherry juice (Sabanci and Icier, 2017) during ohmic heating. The study also observed a rise in the EC when the supplied EFS increased from 25 to 45 V/cm across the fruit juice during COH. As the EFS increases, more charge carriers are mobilized, resulting in higher EC and more efficient current flow through fruit juice (Ramaswamy et al., 2014). The EC was increased by 33.7, 17.7, 38.8, and 15.3% for cucumber, tomato, orange, and pineapple juice at a constant temperature of 40 °C and a 100 mL/min flow rate. Similar observations were made at different temperature and flow rates. On the other hand, because of the very high acid content, lemon juice showed an unclear trend in the EC with a change in EFS.

The present study also showed a linear relationship of EC with temperature during COH of cucumber, orange, pineapple, and lemon juice under different EFS and flow rates of the juice. On the other hand, the EC and temperature relationship of tomato juice during COH was better explained with a second-order polynomial relationship with $R^2 \geq 0.910$. The R^2 of the linear relationship of EC and temperature was ≥ 0.950 under all treatment conditions of COH of pineapple and lemon juice. On the other hand, the R^2 of the linear relationship of cucumber and orange juice was ≥ 0.945 between the EFS 25 to 35 V/cm under all flow rates. In comparison, at higher EFS of 40 and 45 V/cm, the R^2 was reduced further, and the linear relationship was explained poorly. At the higher EFS of 40 and 45 V/cm of COH of cucumber and orange juice, the electrical conductivity – temperature relationship was better explained by a second-order polynomial relationship with $R^2 \geq 0.980$. Studies on batch-type ohmic heating of various food samples (like orange juice, sour cherry juice, banana pulp, and others) also observed a similar relationship between EC and temperature (Icier and Ilicali, 2005; Norouzi et al., 2021; Poojitha and Athmaselvi, 2018; Sabanci and Icier, 2017). The increase in the EC with an increase in temperature might be because of the reduction in the viscosity of the fruit juice, which reduced the drag force on the movement of the ions in the samples. Thus, the flow

of electric current across the samples increased, and subsequently, the EC increased with an increase in the temperature (Ramaswamy et al., 2014).

4.2 Standardization of pineapple juice and ohmic heating behaviour

4.2.1 Standardization of pineapple juice and its characterization

The pineapple juice was standardized at varied °Brix/Acid of 18, 22, and 26 following the methods explained in Section 3.2.5. The TSS was maintained constant at 12 °Brix, and different °Brix/Acid of pineapple juice was obtained by maintaining the desired acid content. The moisture content of the unstandardized pineapple juice (PJ) was measured to be 87.80 ± 0.37%, which was in line with Hounhouigan et al. (2014), who also reported 85% of the moisture content in the edible portion of the pineapple. The pH, TSS, titratable acidity, specific heat, and density of the unstandardized pineapple juice were measured to be 3.38 ± 0.01, 11.6 ± 0.1 °Brix, 0.974 ± 0.062%, 3.870 ± 0.009 kJ/kg°C, and 1.046 ± 0.001 g/cm^3, respectively. Vollmer et al. (2020) also reported 3.7 ± 0.0, 1.047 ± 0.001 g/cm^3, 11.8 ± 0.1 °Brix, and 0.5 ± 0.0 5%, respectively, for pH, density, TSS, and titratable acidity which was in line with the present study except for the acid content which was higher in the current pineapple juice.

Table 4.3 Physico-chemical properties of different °Brix/Acid of the pineapple juice

Parameters	Samples (°Brix/Acid)			
	PJ	18	22	26
pH	3.38 ± 0.01^a	3.41 ± 0.01^b	3.43 ± 0.01^c	3.44 ± 0.01^c
TSS (°Brix)	11.6 ± 0.1^a	12.0 ± 0.0^b	12.0 ± 0.0^b	12.0 ± 0.0^b
TA (%)	0.974 ± 0.062^d	0.661 ± 0.000^c	0.548 ± 0.012^b	0.462 ± 0.012^a
C_p (kJ/kg°C)	3.870 ± 0.009^a	3.866 ± 0.005^a	3.869 ± 0.006^a	3.864 ± 0.004^a
MC (%wb)	87.80 ± 0.37^a	87.63 ± 0.19^a	87.77 ± 0.23^a	87.54 ± 0.15^a
Density (g/cm^3)	1.046 ± 0.001^a	1.057 ± 0.001^b	1.058 ± 0.001^b	1.058 ± 0.001^b
EC (S/m)	0.246 ± 0.000^d	0.196 ± 0.001^c	0.164 ± 0.001^b	0.140 ± 0.001^a

Values in the same row with different superscripts are significantly different ($p < 0.05$), while those with the same superscripts are significantly different ($p > 0.05$) among themselves. TSS, TA, C_p, and MC are total soluble solids, titratable acidity, specific heat, and moisture content on weight basis

Krueger et al. (1992) studied the composition of pineapple juice from various locations. They observed that the TSS value ranged from 11.2 to 16.2 °Brix (average 13.8 °Brix), and the total acidity values ranged from 0.46 to 1.21% (average 0.83%) depending on the cultivar type. Thus, the composition of the pineapple juice varies significantly depending on the culture, cultivar, geography, maturity, and harvest season. Table 4.3 showed that the acid content of the juice was significantly ($p < 0.05$) reduced with an increase in °Brix/Acid at a constant TSS of

12 °Brix while a non-significant ($p > 0.05$) change was observed in the moisture content and specific heat. A significant ($p < 0.05$) increase in pH value was observed with an increase in the °Brix/Acid of the juice. This increase in pH of the juice sample was due to the reduction in the acid content with an increase in °Brix/Acid. The physical composition of the juice greatly affects the heating rate during ohmic heating. Dissolved ionic salts, acids, and water content over 30% render the juice sample electrically conductive and are functional parameters for ohmic heating (Ramaswamy et al., 2014).

4.2.2 Ohmic heating behaviour of standardized pineapple juice

4.2.2.1 Effect of °Brix/Acid

The heating profile of varied °Brix/Acid of pineapple juice from temperature 28 °C to 90 °C at different EFS are shown in Fig. 4.15, 4.16, and 4.17, respectively, for 80, 100, and 120 mL/min flow rates of juice. At low °Brix/Acid, there was a quick temperature rise, and the increment followed a non-linear path. The degree of non-linearity increased with an increase in the °Brix/Acid ratio of juice. The results also showed that with the increase in °Brix/Acid, the come-up time (time required to reach 90 °C) was significantly ($p < 0.05$) increased (Table 4.4).

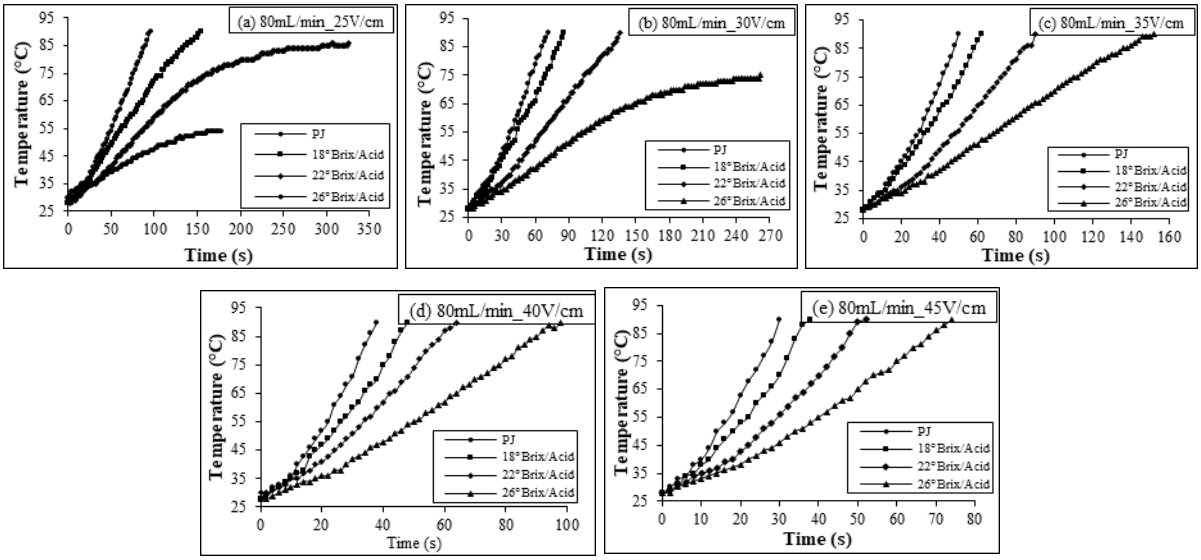

Fig. 4.15 Effect of °Brix/Acid of pineapple juice on heating profile at a constant flow rate of 80 mL/min during COH at EFS (a) 25 V/cm, (b) 30 V/cm, (c) 35 V/cm, (d) 40 V/cm, and (e) 45 V/cm

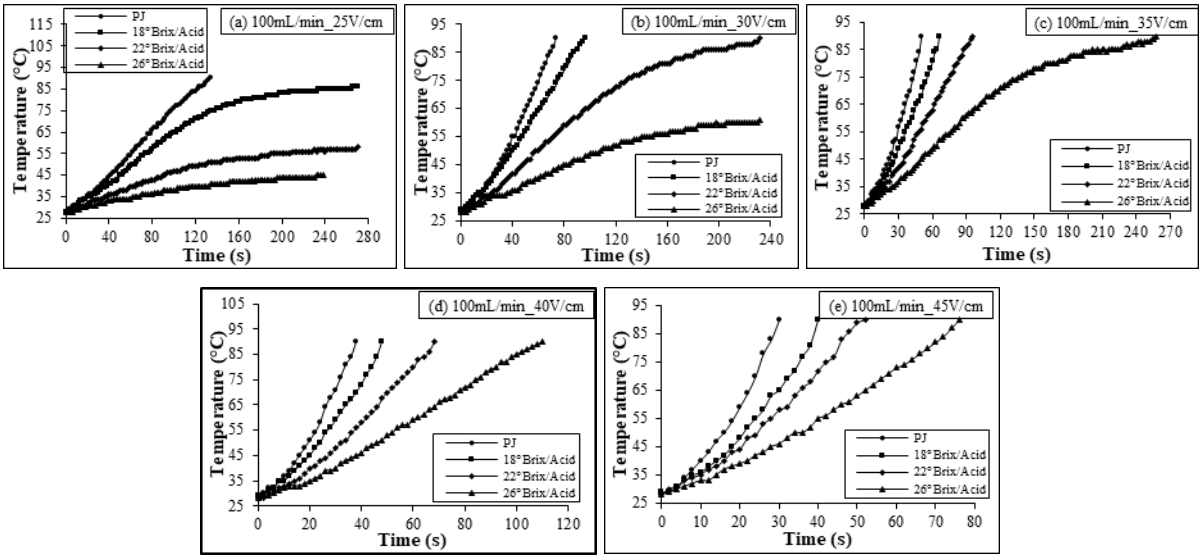

Fig. 4.16 Effect of °Brix/Acid of pineapple juice on heating profile at a constant flow rate of 100 mL/min during COH at EFS (a) 25 V/cm, (b) 30 V/cm, (c) 35 V/cm, (d) 40 V/cm, and (e) 45 V/cm

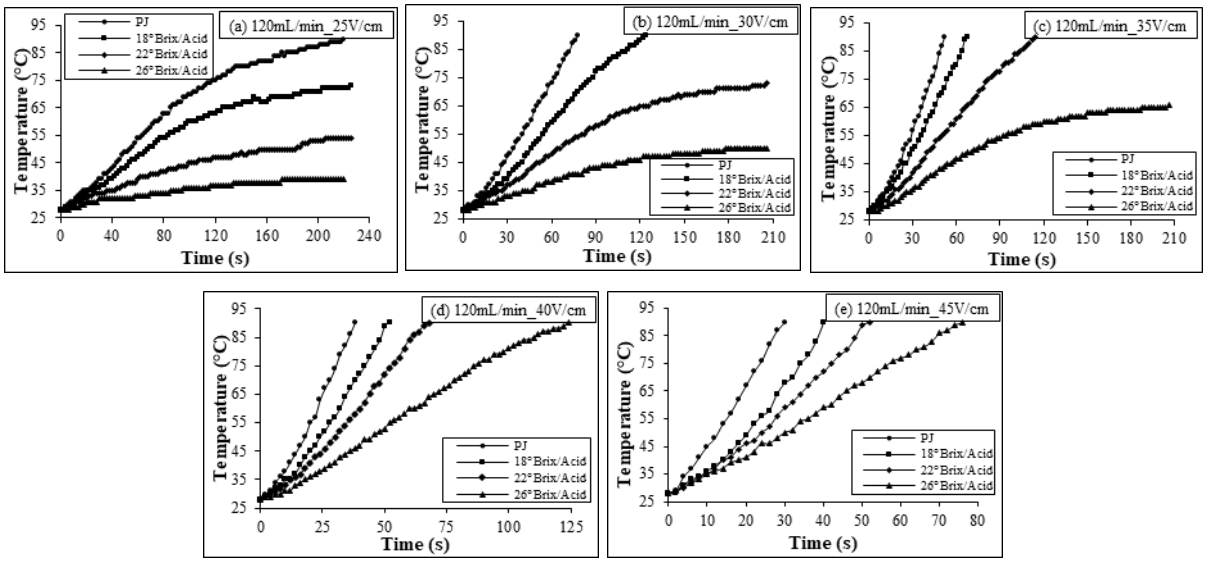

Fig. 4.17 Effect of °Brix/Acid of pineapple juice on heating profile at a constant flow rate of 120 mL/min during COH at EFS (a) 25 V/cm, (b) 30 V/cm, (c) 35 V/cm, (d) 40 V/cm, and (e) 45 V/cm

Come-up times for the unstandardized pineapple juice, 18, 22, and 26 °Brix/Acid juices were 50, 67, 97, and 262 s, respectively, at 35 V/cm and 100 mL/min flow rate. Statistical studies showed that the HR reduced significantly ($p < 0.05$) with an increase in °Brix/Acid (Fig. 4.18). The maximum HR of unstandardized PJ, 18, 22, and 26 °Brix/Acid was observed in decreasing trend at higher EFS and lower flow rates, and the HR was found to be 124.0 ± 0.0, 99.2 ± 1.9, 72.2 ± 1.0, and 49.9 ± 0.5 °C/min, respectively. This might be due to the reduction in the juice's

acid content and EC with an increase in °Brix/Acid, which subsequently reduced the current carrying capacity during ohmic heating (Ramaswamy et al., 2014). Poojitha and Athmaselvi (2018) studied the impact of different levels of sucrose content on the ohmic heating of banana pulp. They observed that the come-up time to achieve 100 °C increased with increased sucrose content. Icier and Ilicali (2005) also observed similar results with different soluble solids concentrations in orange juice. They concluded that heating time increased with increased concentration because of a lower HR. It was also seen that with an increase in °Brix/Acid and at lower EFS, the desired temperature of 90 °C was not achieved, and the heating reached its saturation level.

Table 4.4 Come-up time of different °Brix/Acid pineapple juices at different EFS and flow rate during COH to achieve a target temperature of 90 °C

Flow rate (mL/min)	EFS (V/cm)	Come-up time (s)			
		PJ	18 °Brix/Acid	22 °Brix/Acid	26 °Brix/Acid
80	25	96.0 ± 1.4^{e}	157.0 ± 4.2^{e}	NA	NA
	30	70.5 ± 0.7^{dA}	87.5 ± 2.1^{dB}	140.0 ± 5.7^{cC}	NA
	35	50.5 ± 0.7^{cA}	62.5 ± 2.1^{cA}	92.5 ± 3.5^{bB}	155.0 ± 4.2^{cC}
	40	38.0 ± 0.0^{bA}	48.0 ± 1.4^{bB}	64.5 ± 0.7^{aC}	100.0 ± 2.8^{bD}
	45	30.0 ± 0.0^{aA}	37.5 ± 0.7^{aB}	51.5 ± 0.7^{aC}	74.5 ± 0.7^{aD}
100	25	132.0 ± 2.8^{e}	NA	NA	NA
	30	75.0 ± 1.4^{dA}	97.5 ± 3.5^{dB}	236.0 ± 5.7^{dC}	NA
	35	50.5 ± 0.7^{cA}	67.0 ± 1.4^{cB}	97.5 ± 2.1^{cC}	262.0 ± 5.7^{cD}
	40	38.0 ± 0.0^{bA}	49.0 ± 1.4^{bB}	67.5 ± 0.7^{bC}	111.0 ± 2.8^{bD}
	45	30.0 ± 0.0^{aA}	40.5 ± 0.7^{aB}	51.5 ± 0.7^{aC}	76.5 ± 0.7^{aD}
120	25	214 ± 6.4^{d}	NA	NA	NA
	30	78.0 ± 1.4^{c}	127.0 ± 4.2^{c}	NA	NA
	35	51.5 ± 0.7^{bA}	68.5 ± 2.1^{bB}	116.5 ± 3.5^{cC}	NA
	40	38.0 ± 0.0^{aA}	51.5 ± 0.7^{aB}	68.0 ± 1.4^{bC}	126.0 ± 2.8^{D}
	45	30.0 ± 0.0^{aA}	41.5 ± 2.1^{aB}	52.0 ± 1.4^{aC}	77.0 ± 1.4^{D}

Values in the same row with different capital superscripts significantly ($p < 0.05$) different with change in °Brix/Acid at constant EFS and flow rate. Also, values in the same column with different small superscripts are significantly ($p < 0.05$) different with a change in EFS at a constant °Brix/Acid and flow rate.

4.2.2.2 Effect of electric field strength

The time required to raise the sample temperature from 28 °C to 90 °C at different applied EFS of 25 to 45 V/cm are shown in Fig. 4.15, 4.16, and 4.17. It was observed that with an increase in EFS, the time required to achieve the desired temperature of 90 °C was significantly ($p <$

0.05) reduced for all the samples (Table 4.4). The increment rate of temperature was very high at higher applied EFS. In the juice with high °Brix/Acid, higher HR can be achieved at a higher level of EFS applied. Statistical analysis showed that HR increased significantly ($p < 0.05$) with an increase in EFS for all the samples and under all three flow rates (Fig. 4.18). These results were also in agreement with the volumetric energy generation equation $Q = \sigma \times \nabla V^2$ (Darvishi et al., 2021), which interpreted that the amount of generated heat was directly proportional to the current produced by the voltage gradient and the EC of the foodstuff (Ramaswamy et al., 2014). So, the inherent properties of the food material and electrical conductivity influenced the heating rate (Norouzi et al., 2021).

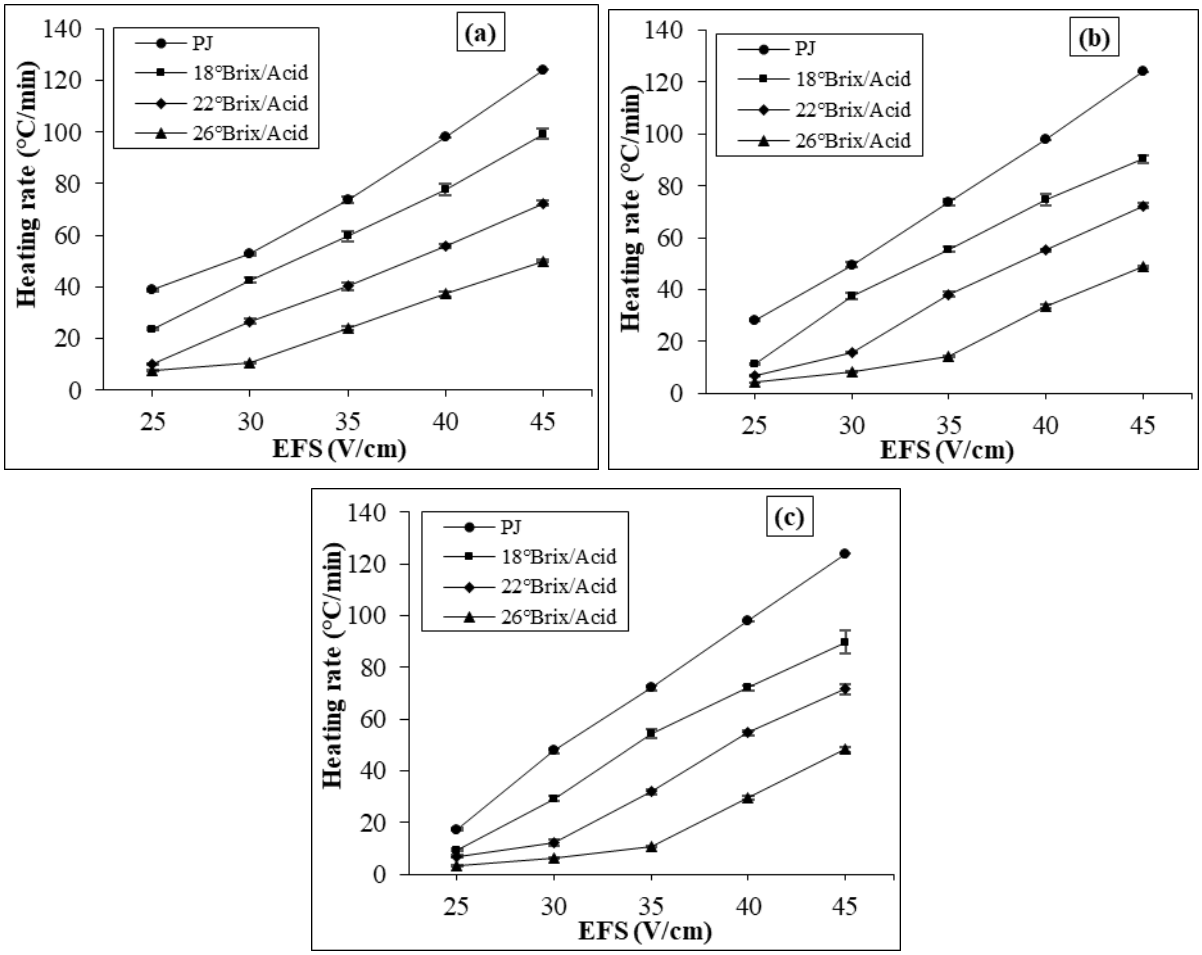

Fig. 4.18 The heating rate curve of different °Brix/Acid pineapple juices at different EFS during COH at a flow rate of (a) 80 mL/min, (b) 100 mL/min, and (c) 120 mL/min

The time required to reach 90 °C by 22 °Brix/Acid juice at 100 mL/min flow rate was 51, 67, 97, 236 s when applied EFS were 45, 40, 35, and 30 V/cm, respectively. The reason was that the flow of higher electric current at higher EFS brought greater electrical energy within the juice samples (Al-Hilphy et al., 2020; Jo and Park, 2019). However, at the same condition, when the applied voltage was 25V/cm, the sample temperature, instead of reaching 90 °C,

achieved a new equilibrium temperature of 58 °C after 262 s. This result showed that a low EFS is unsuitable (insufficient energy) to reach high temperatures when the sample's high flow rate and °Brix/Acid value are high. It was seen that when EFS was reduced from 40 to 30 V/cm, come-up time was increased by 2 to 4 folds. This showed that a lower electric field could be used for slow heating whenever required. Lee et al. (2012) also observed that at a lower EFS of 25 V/cm, the temperature rise of orange juice did not exceed 60 °C even after 300 s during COH. Thus, heating came to saturation level. The authors of earlier studies also observed approximately three times higher come-up time to reach the desired temperature of 80 °C when the EFS was reduced from 40 V/cm to 20 V/cm (Bozkurt and Icier, 2010). Also, the come-up time to heat the grape juice from 30 °C to 80 °C at EFS 20 V/cm was 3.7 and 2.2 times higher than at 40 and 30 V/cm, respectively (Icier et al., 2008). Al-Hilphy et al. (2020) also observed a significant increase in HR from 5.83 to 17.50 °C/min with an increase in EFS from 4.28 to 15.71 V/cm. Similarly, in the OH of well water, the HR was increased from 1.14 to 3.28 °C/s when the voltage gradient increased from 15 to 30 V/cm (Darvishi et al., 2021). Several studies on OH (Norouzi et al., 2021; Poojitha and Athmaselvi, 2018) also concluded similar results that showed HR increased with an increase in EFS. So, the voltage gradient across the food sample during OH is an essential parameter that influences the heating rate of the food product.

4.2.2.3 Effect of flow rate

The heating profile of the pineapple juice at varied flow rates of 80, 100, and 120 mL/min are shown in Fig. 4.15, 4.16, and 4.17, respectively. It was observed that the effect of flow rate on come-up time was high at lower EFS. When the flow rate was increased from 80 mL/min to 120 mL/min at 18 °Brix/Acid, come-up time was increased by 1.45 and 1.1 times at 30 V/cm and 45 V/cm, respectively. At lower EFS and higher °Brix/Acid ratio, the sample temperature attained a new equilibrium temperature at all flow rate conditions instead of attaining the target temperature. For example, in juice having 26 °Brix/Acid, the temperature achieved was 54 °C (181.0 ± 4.2 s), 45 °C (245.0 ± 9.9 s), and 39 °C (216.0 ± 5.7 s) when heated at 25 V/cm with a flow rate of 80 mL/min, 100 mL/min and 120 mL/min, respectively. Similarly, the temperature attained with 30 V/cm was 75 °C (270.0 ± 2.8 s), 61 °C (241.0 ± 9.9 s), and 50 °C (214.0 ± 0.0 s), respectively, for the flow rate of 80, 100 and 120 mL/min. Chen et al. (2010) studied the effect of the flow rate on temperature during soup products' continuous ohmic heating. The effect of flow rate on HR was not significant ($p > 0.05$) at higher EFS (45 V/cm). This may be due to larger voltage gradients that allowed greater current to pass through the sample, causing faster heat generation. At a lower EFS, the effect of the flow rate on HR was

significant. Similar results were observed with the unstandardized PJ, 18, 22, and 26 °Brix/Acid. Kim et al. (2018) also observed that the HR of the buffered peptone water was inversely proportional to the flow rate as the sample was subjected to a longer heating duration at lower flow rates, ultimately resulting in higher HR. Three-factor ANOVA also showed a significant ($p < 0.05$) change in come-up time with EFS, flow rates, and °Brix/Acid individually and with its combined effect.

4.2.2.4 Performance evaluation

System performance coefficient (SPC) was used to study the COH system's performance based on energy efficiency (Ramaswamy et al., 2014). SPC was evaluated for COH for all EFS, °Brix/Acid, and flow rate combinations. Fig. 4.19 illustrates the influence of the EFS, °Brix/Acid, and flow rate on the SPC of the pineapple juice during COH treatment. With an increase in the EFS from 25 V/cm to 35 V/cm, the SPC of the unstandardized pineapple juice increased significantly and attained a maximum value at 35 V/cm under all three flow rate levels. Further, with an increase in the EFS from 35 to 45 V/cm, the SPC of the juice was reduced. Similar observations were made for the standardized pineapple juice at 18 °Brix/Acid. Therefore, the maximum SPC of the unstandardized pineapple juice and 18 °Brix/Acid juice was observed at 35 V/cm (critical EFS). When the °Brix/Acid of the juice increased, the critical EFS for maximum SPC was observed at higher EFS values. This phenomenon may be due to all supplied electrical energy having converted into thermal energy, i.e., a critical limit of heat generation has been reached. Excess electrical energy was lost beyond this threshold, decreasing the SPC value (Darvishi et al., 2021). Jo and Park (2019) studied the effect of EFS on SPC and observed that when EFS was 10, 15, and 17.5 V/cm, the SPC was found to be 0.46 ± 0.02, 0.63 ± 0.05, and 0.58 ± 0.02, respectively. They concluded that the 15 V/cm gave the highest SPC value of 0.63 ± 0.05 among the three tested EFS. Similarly, the current study observed the maximum SPC for unstandardised pineapple juice and 18 °Brix/Acid at EFS 35 V/cm among five different EFS tested under all three flow rates. At the same time, the maximum SPC for 22 and 26 °Brix/Acid juice was observed at EFS 45 V/cm.

SPC of the COH was decreased significantly with an increase in °Brix/Acid. SPC value of unstandardized pineapple juice, 18, 22, and 26 °Brix/Acid juice was 0.986 ± 0.02, 0.932 ± 0.03, 0.870 ± 0.03, and 0.450 ± 0.01, respectively, at 35 V/cm EFS and 100 mL/min flow rate. This value indicated that a higher EFS value was required for high °Brix/Acid juice to reach maximum SPC. This might be due to the reduction in the acid content with increased

°Brix/Acid of the juice, which reduced the current flow across the samples and ultimately reduced the heating rates (Ramaswamy et al., 2014).

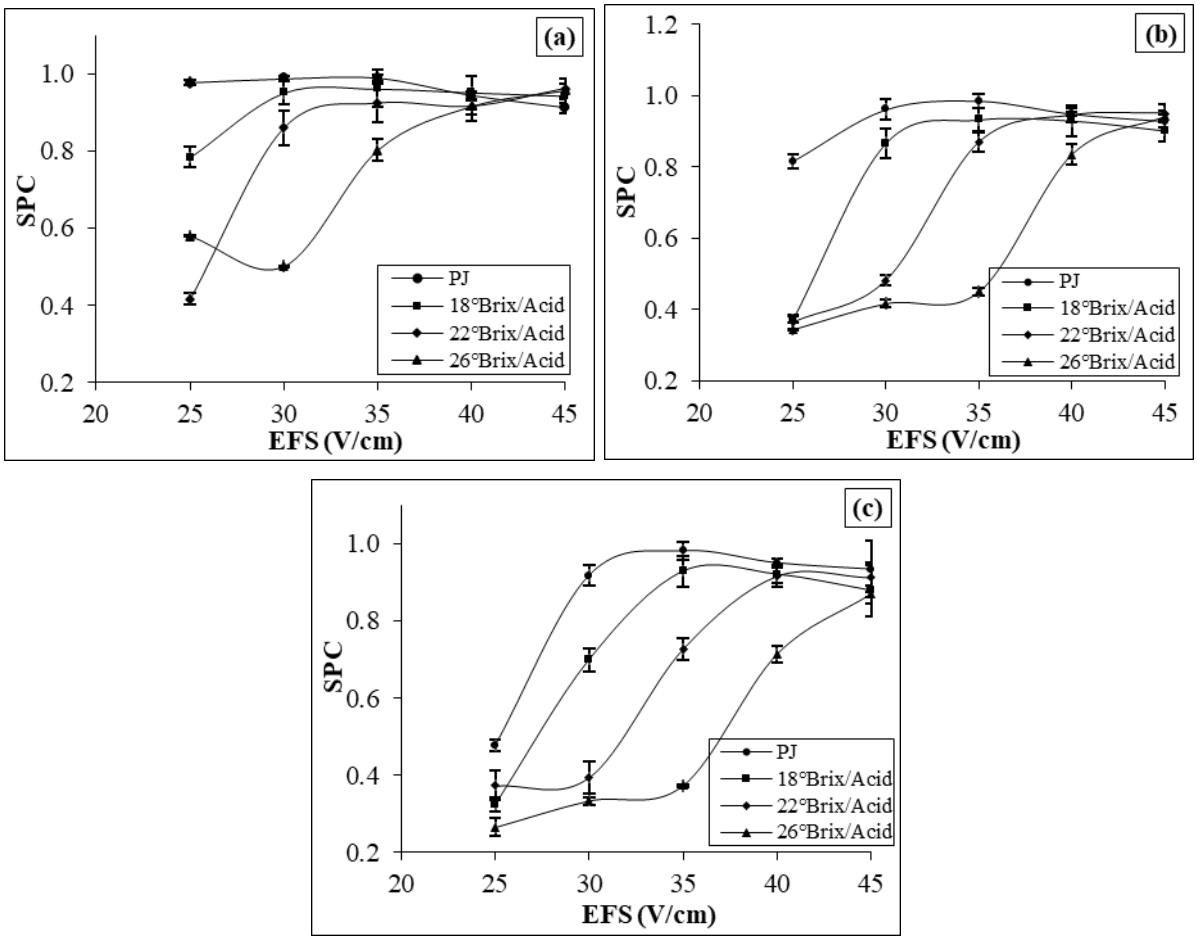

Fig. 4.19 The SPC curve of different °Brix/Acid pineapple juices at different EFS during COH at flow rates of (a) 80 mL/min, (b) 100 mL/min, and (c) 120 mL/min

Thus, a longer duration of electrical energy supply was required to achieve the target temperature; therefore, the SPC of the system was reduced (Cokgezme et al., 2017). Also, the maximum SPC value was observed at a flow rate of 80 mL/min, and the observed SPC value for unstandardized pineapple juice, 18, 22, and 26 °Brix/Acid pineapple juice was found to be 0.990 ± 0.01, 0.961 ± 0.05, 0.962 ± 0.03 and 0.957 ± 0.02, respectively. The higher SPC at lower flow rates obtained might be due to the rapid heating of the fruit juice, which needed a shorter electrical energy duration and reduced the required energy supply (Ramaswamy et al., 2014). Icier and Ilicali (2005) also reported that the SPC of the ohmic heating system greatly depended on the EFS across the food sample.

4.2.2.5 Electrical conductivity behaviour of standardized pineapple juice during continuous ohmic heating

The effect of °Brix/Acid and temperature on the EC of the pineapple juice during COH at a different EFS ranging from 25 to 45 V/cm and flow rate of 80 mL/min (Fig. 20), 100 mL/min (Fig. 4.21), and 120 mL/min (Fig. 4.22) are shown. The EC of the juice decreased significantly ($p < 0.05$) with an increase in the °Brix/Acid.

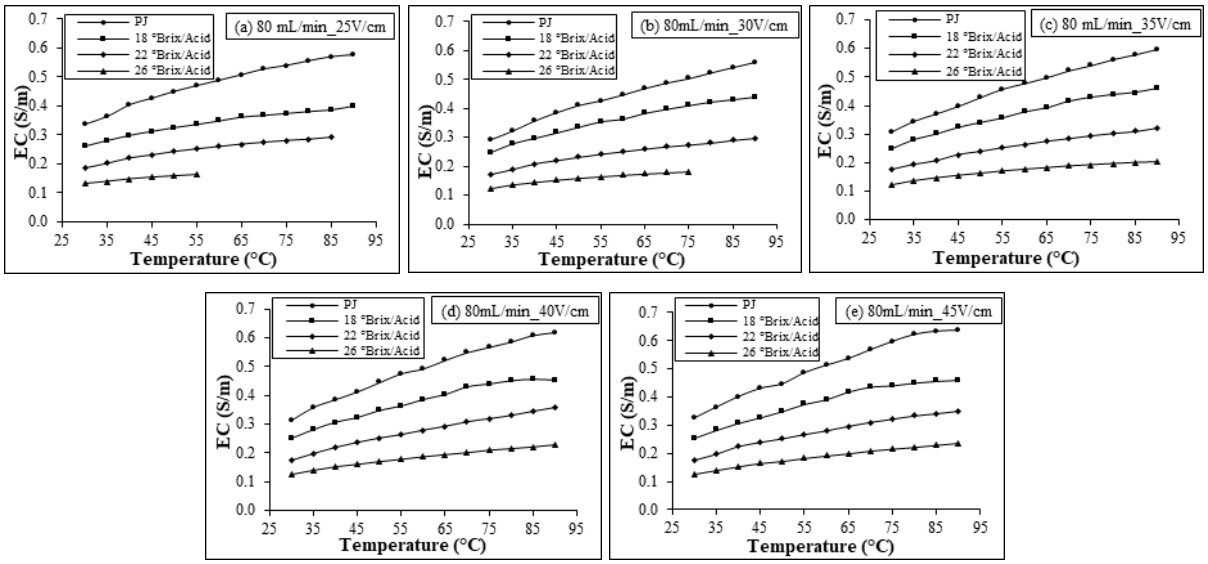

Fig. 4.20 Electrical conductivity – temperature curve of different °Brix/Acid pineapple juice during COH at flow rate of 80 mL/min at different EFS (a) 25 V/cm, (b) 30 V/cm, (c) 35 V/cm, (d) 40 V/cm, and (e) 45 V/cm

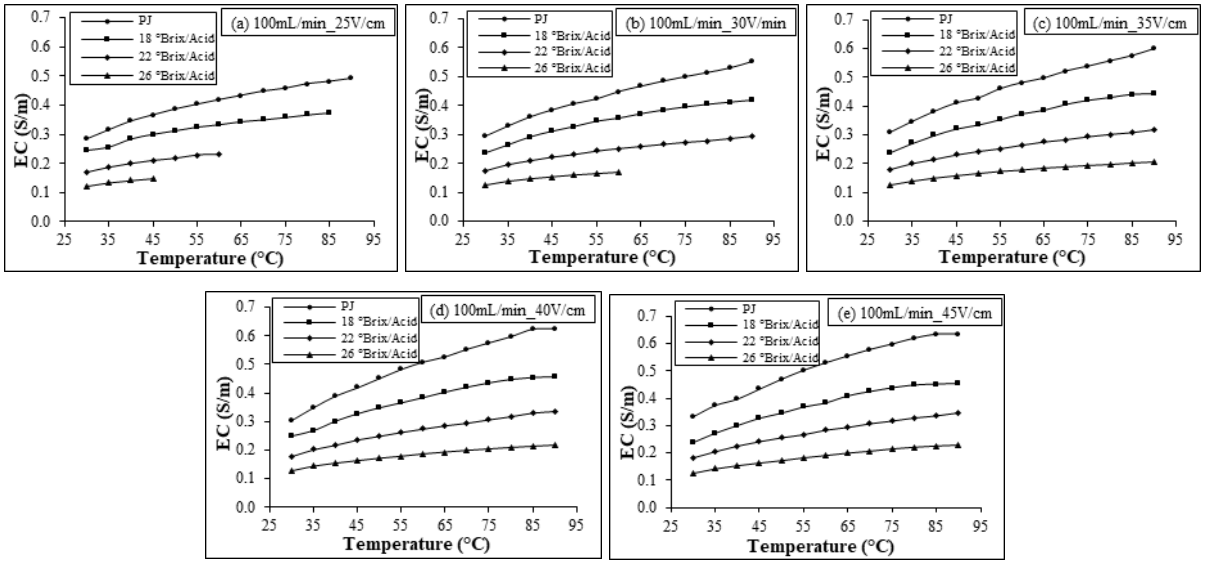

Fig. 4.21 Electrical conductivity – temperature curve of different °Brix/Acid pineapple juice during COH at a flow rate of 100 mL/min at different EFS (a) 25 V/cm, (b) 30 V/cm, (c) 35 V/cm, (d) 40 V/cm, and (e) 45 V/cm

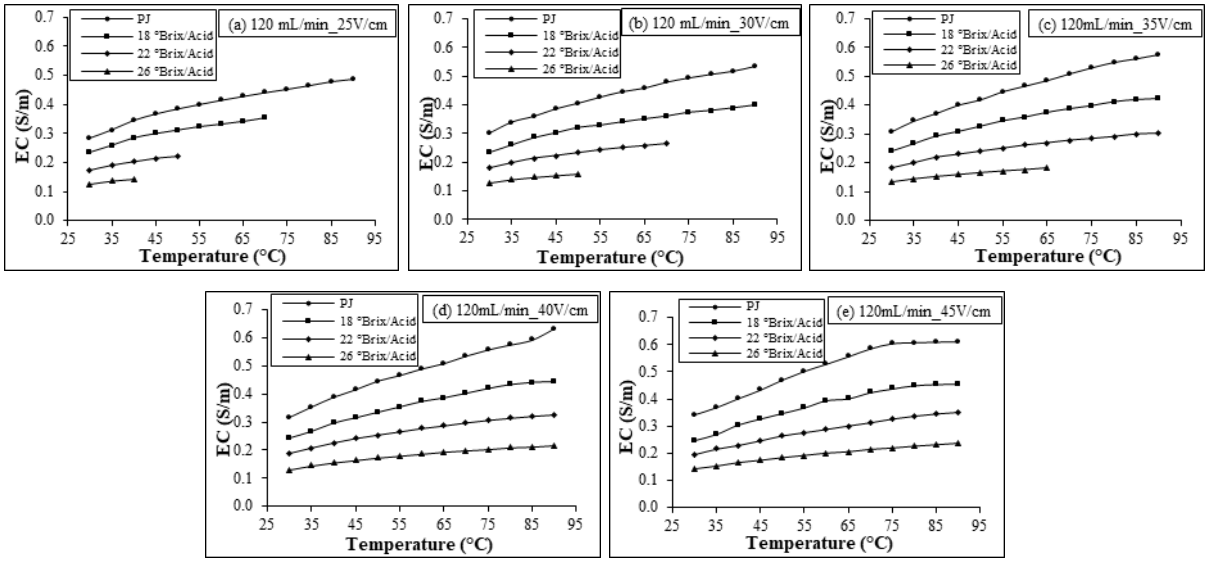

Fig. 4.22 Electrical conductivity – temperature curve of different °Brix/Acid pineapple juice during COH at a flow rate of 120 mL/min at different EFS (a) 25 V/cm, (b) 30 V/cm, (c) 35 V/cm, (d) 40 V/cm, and (e) 45 V/cm

At the initial temperature of 30 °C, the EC of unstandardized pineapple juice was 0.309 S/m, which was reduced to 0.239, 0.181, and 0.125 S/m for the 18, 22, and 26 °Brix/Acid pineapple juice, respectively, when the juice was heated at 35 V/cm and 100 mL/min. Similarly, at 90 °C under similar treatment conditions, the EC of unstandardized pineapple juice, 18, 22, and 26 °Brix/Acid was 0.598, 0.442, 0.318, and 0.205 S/m, respectively. Similarly, the EC was reduced with an increase in °Brix/Acid of the juice in other COH treatment conditions. Decrement in EC was higher when °Brix/Acid of the juice was increased from 22 to 26 compared to 18 to 22 at all temperatures. This reduction in EC with an increase in °Brix/Acid was due to a lowering of acid content and a decline of ionic movement that resulted in low current flow across the juice samples (Sabanci and Icier, 2017). This also significantly ($p < 0.05$) increased the heating time. The study also showed that with increased concentrations of the soluble solids in orange juice concentrates (Icier and Ilicali 2005) and sour cherry juice (Sabanci and Icier, 2017), the EC decreased at any temperature and voltage gradients.

Since EC changed during the heating period, it was also necessary to investigate the effect of temperature on EC. The results showed that the EC increased significantly ($p < 0.05$) with an increased temperature for all °Brix/Acid pineapple juice. When the temperature was raised from 30 °C to 90 °C during ohmic heating at 35 V/cm and 100 mL/min, the EC of unstandardized pineapple juice, 18, 22, and 26 °Brix/Acid juices were increased by 93.5, 84.9, 75.7, and 64.0%, respectively. So, when the °Brix/Acid of pineapple juice was low, the effect of temperature on EC increment was more significant because of higher acid content that

allowed rapid heating and higher EC. Similar, results were observed when the pineapple juice of different °Brix/Acid was heated at different EFS (25 to 45 V/cm) and flow rates (80 to 120 mL/min) as shown in Fig. 4.20, 4.21, and 4.22. The present study was in line with other studies that also observed an increase in EC with an increase in the temperature of different fruit juices like grape juice (Icier et al. 2008) and sour cherry juice (Sabanci and Icier 2017) during ohmic heating. The present study also showed a linear relationship of EC with temperature. The $R^2 \geq$ 0.950, 0.957, 0.959, and 0.960, respectively for unstandardized pineapple juice, 18, 22, and 26 °Brix/Acid pineapple juice during COH under different EFS (25 to 45 V/cm) and flow rate (80 to 120 mL/min). Studies on batch-type ohmic heating of various food samples (like orange juice, sour cherry juice, banana pulp, and others) also observed a similar relationship between EC and temperature (Icier and Ilicali 2005; Norouzi et al., 2021; Poojitha and Athmaselvi 2018; Sabanci and Icier, 2017). The increase in the EC with an increase in temperature might be because of the reduction in the viscosity of the fruit juice, which reduced the drag force on the movement of the ions in the samples. Thus, the flow of electric current across the samples increased, and subsequently, the EC increased with an increase in the temperature (Ramaswamy et al., 2014).

4.3 Design and development of isothermal holding section for COH system

The conceptual design consideration of the holding chamber was discussed in Section 3.2.2. The inner and outer diameters of the holding chamber were 23 and 51 mm, respectively. The length of the outlet ports from the base/inlet port was determined based on the designed flow rates of the standardized pineapple juice (22 °Brix/Acid) for respective EFS – temperature combinations. There was a total of nine combinations of EFS – temperature where EFS was 30, 35, and 40 V/cm, and temperature was 70, 80, 90 °C and for each combination, there are four outlet ports O1, O2, O3, and O4, respectively for holding period of 15, 30, 45, and 60 s as shown in Fig. 3.11. Prior to designing the location of the outlet ports for the isothermal holding section, the volume flow rate of the standardized pineapple juice (22 °Brix/Acid) was determined (Table 4.5) under which the juice attained a steady temperature of 70, 80, and 90 °C, respectively at each EFS of 30, 35, and 40 V/cm (Fig. 4.23). After reaching the desired steady temperature and no further rise in temperature occurred during COH, the juice samples were passed to the holding chamber for isothermal treatment.

The volume flow rate of the standardized pineapple juice was determined following a trial-and-error iterative approach to achieving a steady temperature of 70, 80, and 90 °C, respectively, for 30, 35, and 40 V/cm, as shown in Table 4.5. The flow rate was significantly ($p < 0.05$)

increased with an increase in EFS at any constant temperature, while the flow rate was significantly ($p < 0.05$) decreased with a rise in desired temperature at any constant EFS. As the EFS increases, more electrical power is dissipated into the juice, leading to higher temperatures. To prevent localized overheating and ensure uniform heating throughout the juice volume to a pre-determined temperature, the juice flow rate needs to be increased.

Table 4.5 Design of volume flow rate of juice

Temperature (°C)	Flow rates (mL/min)		
	30 V/cm	35 V/cm	40 V/cm
70	100.0 ± 0.8^{aC}	147.0 ± 1.2^{aB}	213.0 ± 1.2^{aA}
80	92.8 ± 0.5^{bC}	136.3 ± 1.3^{bB}	189.5 ± 0.6^{bA}
90	84.5 ± 0.6^{cC}	119.5 ± 1.0^{cB}	173.5 ± 1.3^{cA}

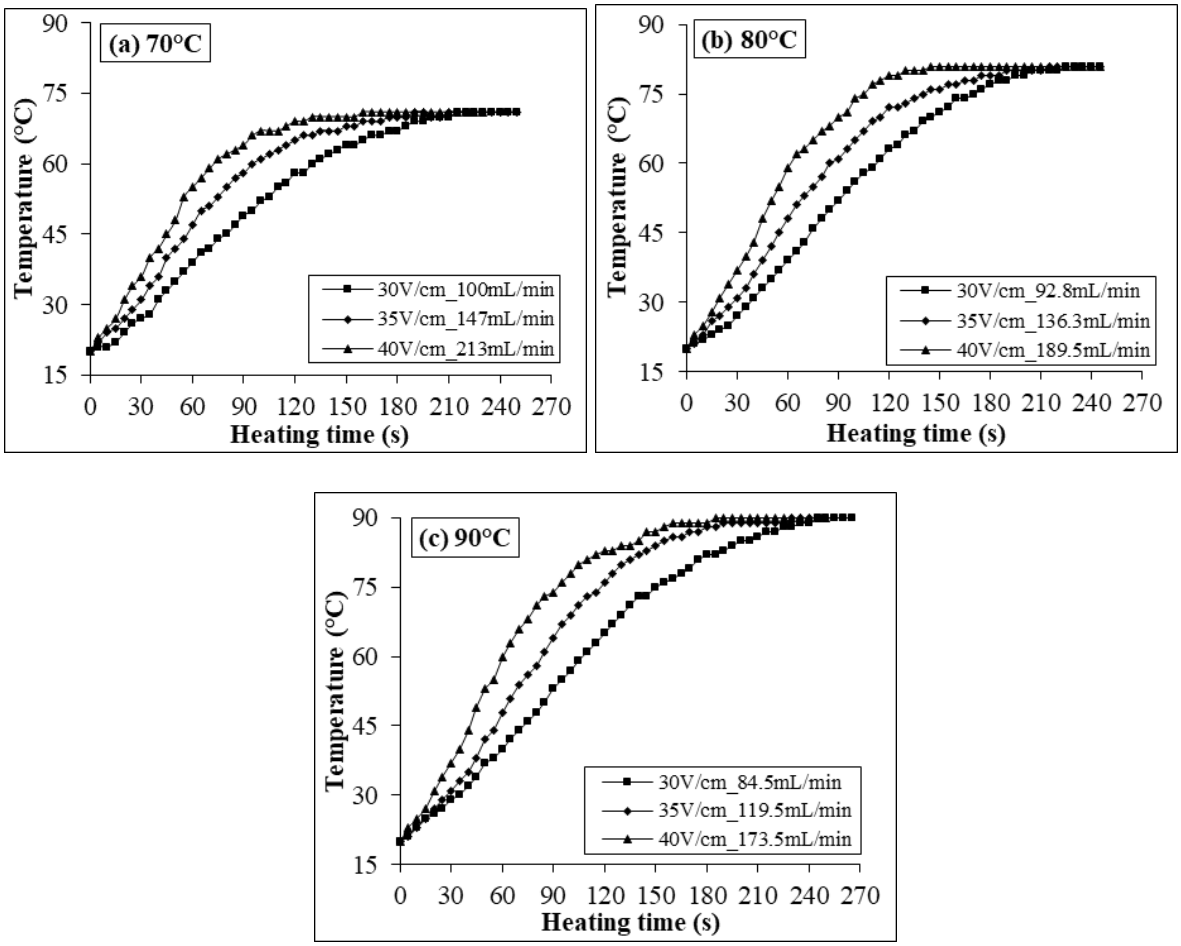

Fig. 4.23 Effect of electric field strength on heating profile during continuous ohmic heating of standardized pineapple juice (22 °Brix/Acid) at different temperatures (a) 70 °C, (b) 80 °C, and (c) 90 °C

This helps continuously bring fresh, cooler juice into the heating zone, thereby managing the overall rise in temperature. It also ensures that the electrical energy input is effectively utilized

to heat the juice, minimizing energy losses and maximizing throughput (Ramaswamy et al. 2014). The minimum flow rate of 84.5 ± 0.6 mL/min was observed to achieve at steady temperature of 90 °C at 30 V/cm which was increased significantly ($p < 0.05$) to 173.5 ± 1.3 mL/min at 40 V/cm. On the other hand, the maximum flow rate of 213.0 ± 1.2 mL/min was observed to achieve a steady temperature of 70 °C at 40 V/cm which was decreased significantly ($p < 0.05$) to 100.0 ± 0.8 mL/min at 30 V/cm. The heating profile and current profile of the standardised pineapple juice during continuous ohmic heating at different EFS (30 to 40 V/cm) and temperature (70 to 90 °C) to attain a steady temperature are shown in Fig. 4.23 and Fig. 4.24, respectively. Initially, the juice was heated at a faster rate, and thus, the rapid rise in temperature was observed in the initial period as shown in Fig. 4.23. Also, because of the rapid rise in temperature, the flow of electric current was also increased at a faster rate during these periods as shown in Fig. 4.24.

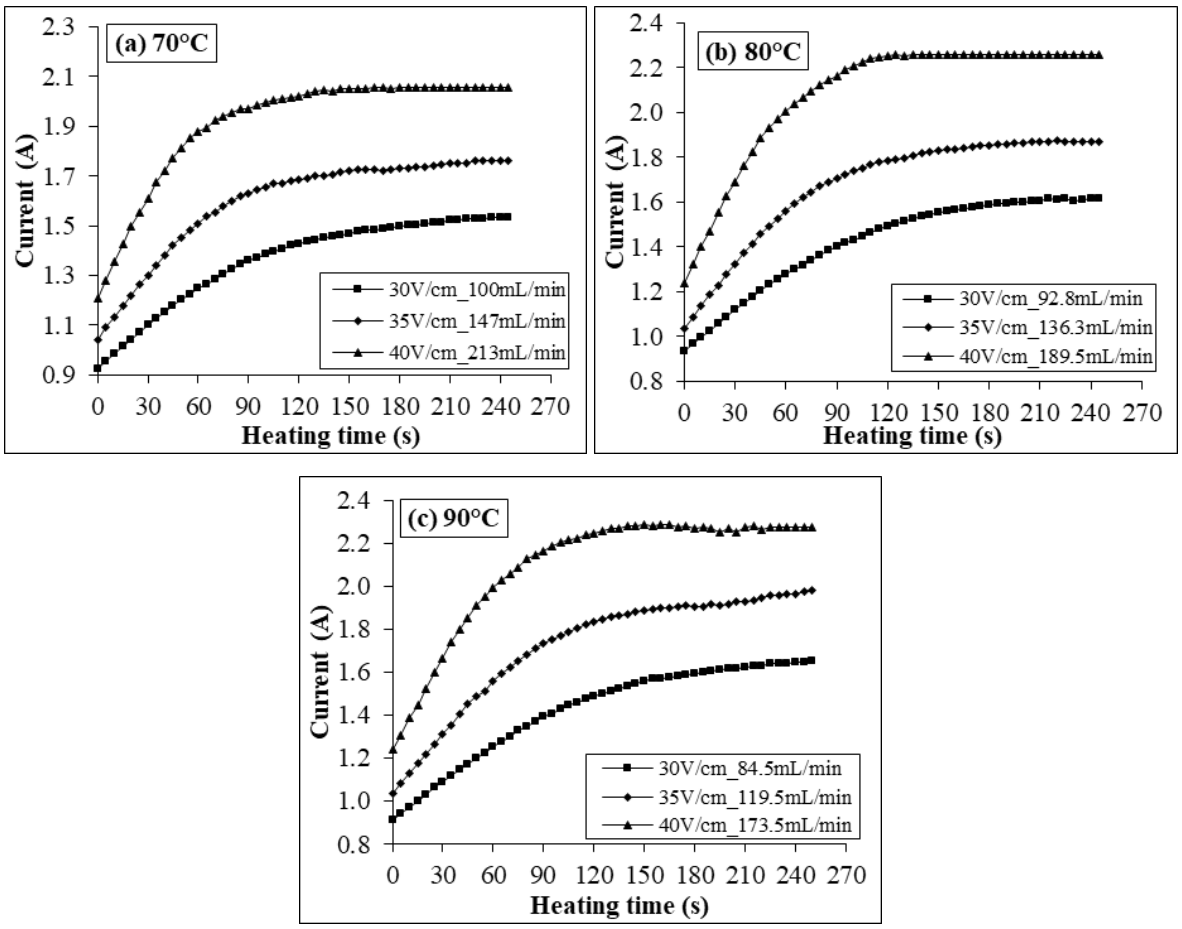

Fig. 4.24 Effect of electric field strength on current profile during continuous ohmic heating of standardized pineapple juice (22 °Brix/Acid) at different temperatures (a) 70 °C, (b) 80 °C, and (c) 90 °C

After the rapid heating period, the rate of heating of the juice was slowed down and it reached to a negligible amount at the end part of the heating. When the rate of change of temperature

becomes approximately zero, the juice attained a steady temperature of the desired value and no further rise in temperature was observed. During this period, the heating curve became almost parallel to the horizontal time axis as shown in Fig. 4.23. Similarly, the flow of electric current also started increasing slowly during the slower heating period and reached to almost a constant value during the last stage of heating when the juice attained a steady temperature. The come-up time (CUT) to achieve the steady temperature of all the nine EFS – temperature combinations is shown in the Table 4.6. The CUT period was significantly ($p < 0.05$) reduced with an increase in EFS, while on the other hand, the CUT period increased significantly ($p < 0.05$) with an increase in the desired temperature. The minimum CUT period was obtained to be 128.0 ± 2.8 s when the standardised pineapple juice was heated at 40 V/cm to achieve a steady temperature of 70 °C. While the maximum CUT period of 246.5 ± 4.9 s was obtained to achieve a desired steady temperature of 90 °C at 30 V/cm.

Table 4.6 Come-up time for steady temperature state

Temperature (°C)	CUT period (s)		
	30 V/cm	35 V/cm	40 V/cm
70	202.5 ± 3.5^{cA}	176.5 ± 4.9^{bA}	128.0 ± 2.8^{aA}
80	206.5 ± 4.9^{cA}	188.0 ± 2.8^{bA}	132.5 ± 3.5^{aA}
90	246.5 ± 4.9^{bB}	232.5 ± 3.5^{bB}	187.5 ± 3.5^{aB}

Values in the same row with different small superscripts significantly ($p < 0.05$) different with a change in EFS at a constant temperature. Also, values in the same column with different capital superscripts are significantly ($p < 0.05$) different with a change in temperature at a constant EFS.

The location of the outlet ports on the isothermal holding chamber was designed using the volume flow rates of the juice for the respective EFS – temperature combination (Table 4.5) and the inner base area of the holding chamber which was calculated using the inner radius of the chamber. The exact volume of the juice was calculated using the volume flow rate, respectively for a holding period of 15, 30, 45, and 60 s and then it was divided by the inner base area of the holding chamber to determine the length of the outlet port from the base. The location of the outlet port from the base of the holding chamber for different holding periods of 15, 30, 45, and 60 s for each EFS – temperature combination is shown in Table 4.7. The closest location of the outlet port from the base was observed at 50.8 mm for holding the juice for 15 s when heated at 30 V/cm for 90 °C while the farthest location was 512.7 mm for holding juice for 60 s when heated at 40 V/cm for 70 °C desired temperature. The closest or farthest location of the outlet port or any other location depended on the juice's flow rate and holding

period. After the location of the outlet port was designed, a hole of diameter 12.5 mm (as a thread diameter) was made at each location L1, L2, L3, and L4 and fixed with an I-shaped jointer with a cap serving as outlet ports for each location. The isothermal holding chamber was then placed over the COH heating cell, and the inlet port of the holding chamber was connected with the outlet port of the COH cell with a T-shaped jointer, as shown in Fig. 4.25.

Table 4.7 Location of the outlet port of the isothermal holding section for different treatment conditions

EFS (V/cm)	T (°C)	Location of outlet port from base for different holding periods (mm)			
		L1	L2	L3	L4
40	70	128.2	256.3	384.5	512.7
	80	114.0	228.0	342.0	456.1
	90	104.4	208.8	313.2	417.5
35	70	88.5	176.9	265.4	353.8
	80	82.0	164.0	245.9	327.9
	90	71.9	143.8	215.7	287.6
30	70	60.2	120.3	180.4	240.7
	80	55.8	111.6	167.4	223.3
	90	50.8	101.7	152.5	203.3

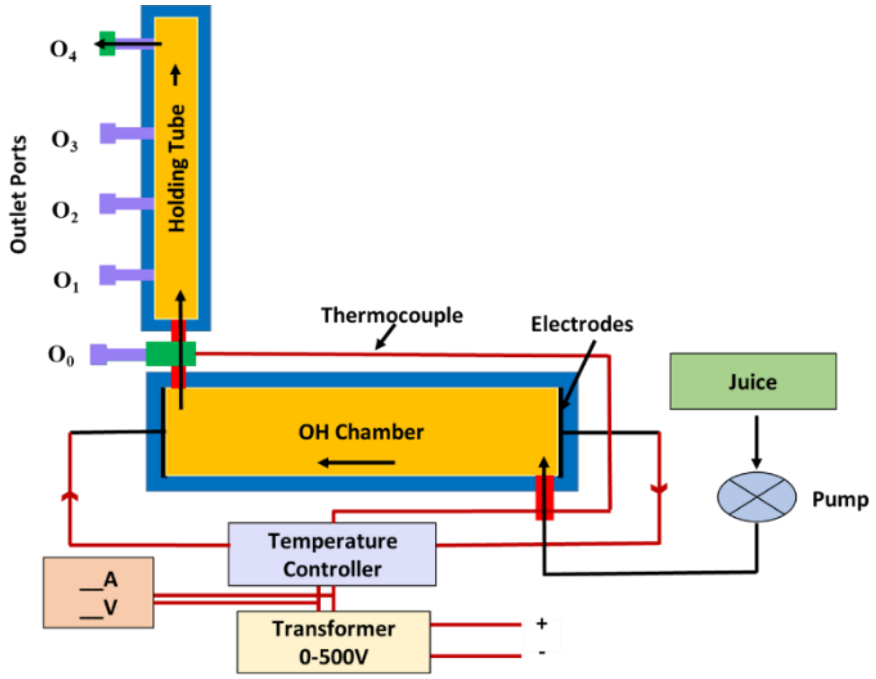

Fig. 4.25 Schematic diagram of a lab scale continuous type ohmic heating system with isothermal holding section

4.4 Effect of continuous ohmic heating on pH, TSS, and colour

The pH and TSS of the untreated pineapple juice were 3.43 ± 0.01 and 12.0 ± 0.0 °Brix, respectively. A non-significant ($p > 0.05$) effect of COH treatment parameters was observed on the pH and TSS of the treated pineapple juice. The L^*, a^*, and b^* value of the untreated pineapple juice was observed to be 28.16 ± 0.22, -0.41 ± 0.01 and 1.09 ± 0.02, respectively. The colour parameters, including the total colour change (ΔE) of the treated pineapple juice, are shown in Table 4.8. The L^* of the COH-treated juice had a significant ($p < 0.05$) effect on temperature, time, and EFS and was in the range of 28.07 ± 0.78 to 31.82 ± 0.24. This slight increase in the L^* values indicated that the COH-treated pineapple juice was comparatively lighter than the untreated juice. More minor differences in the L^* values were also reported during the OH of apples compared to fresh samples (Moreno et al., 2013). Also, a^* and b^* values of the treated juice were comparatively lower than untreated juice and were in the range of -0.88 ± 0.37 to -0.39 ± 0.06 and -0.43 ± 0.19 to 1.07 ± 0.14, respectively. A significant ($p < 0.05$) effect of temperature was observed on the a* and b* values of the treated juice, while treatment time and EFS had a non-significant effect. Rattanathanalerk et al. (2005) observed a decrease in L^* and b^* values and an increase in a^* values during thermal processing (non-OH) of pineapple juice because of non-enzymatic browning, carotenoid isomerization and degradation at high temperatures and longer treatment time. Similarly, Rodriguez et al. (2021) also observed significantly ($p < 0.05$) lower L^* and higher a^* values and non-significant ($p > 0.05$) changes in b^* values as compared to control samples during the ohmic pasteurization of carrot juice.

The ΔE of the COH-treated pineapple juice was observed to be less at 70 °C than at 80 °C and 90 °C. The ΔE at 70 °C was found to be in the range of 0.43 ± 0.15 to 1.84 ± 0.59, which was less as compared to 80 °C and 90 °C whose values were in the range of 0.87 ± 0.43 to 3.82 ± 0.02 and 0.98 ± 0.11 to 3.54 ± 0.24, respectively (Table 4.8). Statistical analysis showed a significant ($p < 0.05$) effect of EFS, treatment time, and temperature on the ΔE of the COH-treated juice. Rattanathanalerk et al. (2005) also reported a significant increase in the ΔE values at higher temperatures and longer processing times because of non-enzymatic browning and pigment destruction. Abedelmaksoud et al. (2019) observed a total colour change of 1.77 ± 0.2 at 80 °C and 40 V/cm during ohmic heating of Elstar apple juice, which was in accordance with the present study.

Table 4.8 Colour parameters and overall colour change of COH treated pineapple juice

EFS (V/cm)	T (°C)	t (s)	L^*	a^*	b^*	ΔE
		0	29.24 ± 0.28^{ab}	-0.50 ± 0.04^{a}	0.53 ± 0.04^{b}	1.23 ± 0.03^{a}
		15	29.50 ± 0.21^{a}	-0.58 ± 0.05^{a}	0.72 ± 0.02^{ab}	1.40 ± 0.03^{a}
	70	30	29.41 ± 0.06^{a}	-0.58 ± 0.11^{a}	0.90 ± 0.21^{ab}	1.29 ± 0.21^{a}
		45	29.05 ± 0.02^{ab}	-0.59 ± 0.05^{a}	1.07 ± 0.14^{a}	0.92 ± 0.24^{ab}
		60	28.60 ± 0.15^{b}	-0.63 ± 0.06^{a}	0.94 ± 0.15^{ab}	0.52 ± 0.14^{b}
		0	29.76 ± 0.36^{a}	-0.76 ± 0.02^{a}	0.30 ± 0.11^{a}	1.82 ± 0.06^{b}
		15	30.44 ± 0.27^{a}	-0.73 ± 0.08^{a}	0.31 ± 0.01^{a}	2.43 ± 0.02^{a}
30	80	30	30.43 ± 0.10^{a}	-0.71 ± 0.10^{a}	0.28 ± 0.05^{a}	2.43 ± 0.11^{a}
		45	29.76 ± 0.02^{a}	-0.74 ± 0.11^{a}	0.45 ± 0.07^{a}	1.76 ± 0.23^{b}
		60	29.58 ± 0.40^{a}	-0.79 ± 0.07^{a}	0.38 ± 0.12^{a}	1.64 ± 0.18^{b}
		0	29.20 ± 0.30^{b}	-0.64 ± 0.00^{ab}	0.09 ± 0.25^{a}	1.47 ± 0.21^{c}
		15	30.06 ± 0.46^{ab}	-0.59 ± 0.01^{a}	-0.11 ± 0.12^{a}	2.26 ± 0.12^{bc}
	90	30	30.80 ± 0.48^{a}	-0.58 ± 0.05^{a}	-0.18 ± 0.15^{a}	2.93 ± 0.29^{ab}
		45	31.16 ± 0.41^{a}	-0.68 ± 0.10^{ab}	-0.16 ± 0.31^{a}	3.26 ± 0.27^{a}
		60	31.02 ± 0.28^{a}	-0.78 ± 0.00^{b}	-0.23 ± 0.10^{a}	3.18 ± 0.08^{a}
		0	28.07 ± 0.78^{a}	-0.45 ± 0.06^{a}	0.93 ± 0.05^{a}	0.43 ± 0.15^{a}
		15	29.11 ± 1.17^{a}	-0.58 ± 0.25^{a}	0.59 ± 0.19^{a}	1.20 ± 0.69^{a}
	70	30	28.36 ± 1.69^{a}	-0.40 ± 0.05^{a}	0.81 ± 0.01^{a}	1.08 ± 0.26^{a}
		45	28.99 ± 0.95^{a}	-0.39 ± 0.06^{a}	0.77 ± 0.01^{a}	0.93 ± 0.64^{a}
		60	29.08 ± 0.94^{a}	-0.41 ± 0.06^{a}	0.68 ± 0.15^{a}	1.07 ± 0.56^{a}
		0	29.05 ± 0.88^{c}	-0.70 ± 0.35^{a}	0.18 ± 0.00^{a}	1.37 ± 0.49^{c}
		15	30.07 ± 0.17^{bc}	-0.50 ± 0.11^{a}	0.13 ± 0.02^{ab}	2.14 ± 0.06^{bc}
35	80	30	30.94 ± 0.32^{ab}	-0.68 ± 0.19^{a}	0.14 ± 0.04^{ab}	2.95 ± 0.09^{ab}
		45	31.45 ± 0.33^{ab}	-0.58 ± 0.06^{a}	0.05 ± 0.05^{b}	3.46 ± 0.09^{a}
		60	31.82 ± 0.24^{a}	-0.66 ± 0.17^{a}	0.03 ± 0.02^{b}	3.82 ± 0.02^{a}
		0	28.92 ± 0.00^{a}	-0.54 ± 0.12^{a}	0.40 ± 0.10^{a}	1.05 ± 0.13^{bc}
		15	28.51 ± 0.73^{a}	-0.46 ± 0.01^{a}	0.25 ± 0.06^{ab}	0.98 ± 0.11^{c}
	90	30	28.90 ± 0.66^{a}	-0.58 ± 0.15^{a}	-0.02 ± 0.09^{bc}	1.39 ± 0.12^{abc}
		45	29.37 ± 0.66^{a}	-0.48 ± 0.01^{a}	-0.10 ± 0.10^{c}	1.72 ± 0.22^{a}
		60	29.14 ± 0.15^{a}	-0.49 ± 0.04^{a}	-0.15 ± 0.03^{c}	1.58 ± 0.05^{ab}
		0	28.78 ± 0.06^{a}	-0.58 ± 0.03^{a}	0.67 ± 0.00^{a}	0.77 ± 0.23^{a}
		15	28.86 ± 0.47^{a}	-0.54 ± 0.09^{a}	0.77 ± 0.03^{a}	0.83 ± 0.57^{a}
	70	30	29.49 ± 0.28^{a}	-0.54 ± 0.19^{a}	0.50 ± 0.10^{a}	1.47 ± 0.48^{a}
		45	29.68 ± 0.25^{a}	-0.67 ± 0.10^{a}	0.71 ± 0.09^{a}	1.60 ± 0.41^{a}
		60	29.90 ± 0.45^{a}	-0.56 ± 0.10^{a}	0.58 ± 0.15^{a}	1.84 ± 0.59^{a}
		0	28.96 ± 0.24^{c}	-0.54 ± 0.03^{a}	0.81 ± 0.02^{a}	0.87 ± 0.43^{b}
		15	29.13 ± 0.19^{c}	-0.66 ± 0.11^{a}	0.62 ± 0.05^{a}	1.13 ± 0.32^{ab}
40	80	30	29.74 ± 0.21^{bc}	-0.55 ± 0.01^{a}	0.59 ± 0.01^{a}	1.66 ± 0.42^{ab}
		45	29.98 ± 0.13^{ab}	-0.65 ± 0.02^{a}	0.62 ± 0.10^{a}	1.90 ± 0.32^{ab}
		60	30.55 ± 0.18^{a}	-0.70 ± 0.13^{a}	0.65 ± 0.13^{a}	2.45 ± 0.36^{a}
		0	29.80 ± 0.22^{b}	-0.59 ± 0.15^{a}	-0.28 ± 0.11^{a}	2.15 ± 0.07^{b}
		15	30.65 ± 0.68^{ab}	-0.88 ± 0.37^{a}	-0.43 ± 0.19^{a}	3.01 ± 0.61^{ab}
	90	30	30.86 ± 0.19^{ab}	-0.58 ± 0.14^{a}	-0.24 ± 0.05^{a}	3.02 ± 0.05^{ab}
		45	31.33 ± 0.14^{a}	-0.67 ± 0.19^{a}	-0.18 ± 0.03^{a}	3.43 ± 0.08^{a}
		60	31.46 ± 0.05^{a}	-0.66 ± 0.08^{a}	-0.16 ± 0.05^{a}	3.54 ± 0.24^{a}

Different lowercase superscripts show a significant ($p < 0.05$) effect of time at constant EFS and. Values are shown in mean ± standard deviation

4.5 Effect of COH on enzyme inactivation and their kinetic modelling

4.5.1 Polyphenol oxidase (PPO)

4.5.1.1 Effect of COH on PPO inactivation

PPO was inactivated significantly ($p < 0.05$) during the CUT period, as shown in Fig. 4.26. Approximately 20% of the PPO inactivation occurred during this period when juice was heated to 90 °C at 40 V/cm from room temperature. This was due to the inactivation of highly thermal-sensitive fractions of the PPO enzymes during the rise in temperature of ohmic heating. A partial inactivation of PPO and POD in sugarcane juice (Brochier et al., 2016) and tyrosinase enzyme in *Agaricus bisporus* (Barron-Garcia et al., 2019) was also reported during the CUT period of ohmic heating. Juice samples with partially inactivated enzymes (during the CUT period) were passed to an isothermal holding section for thermal treatment.

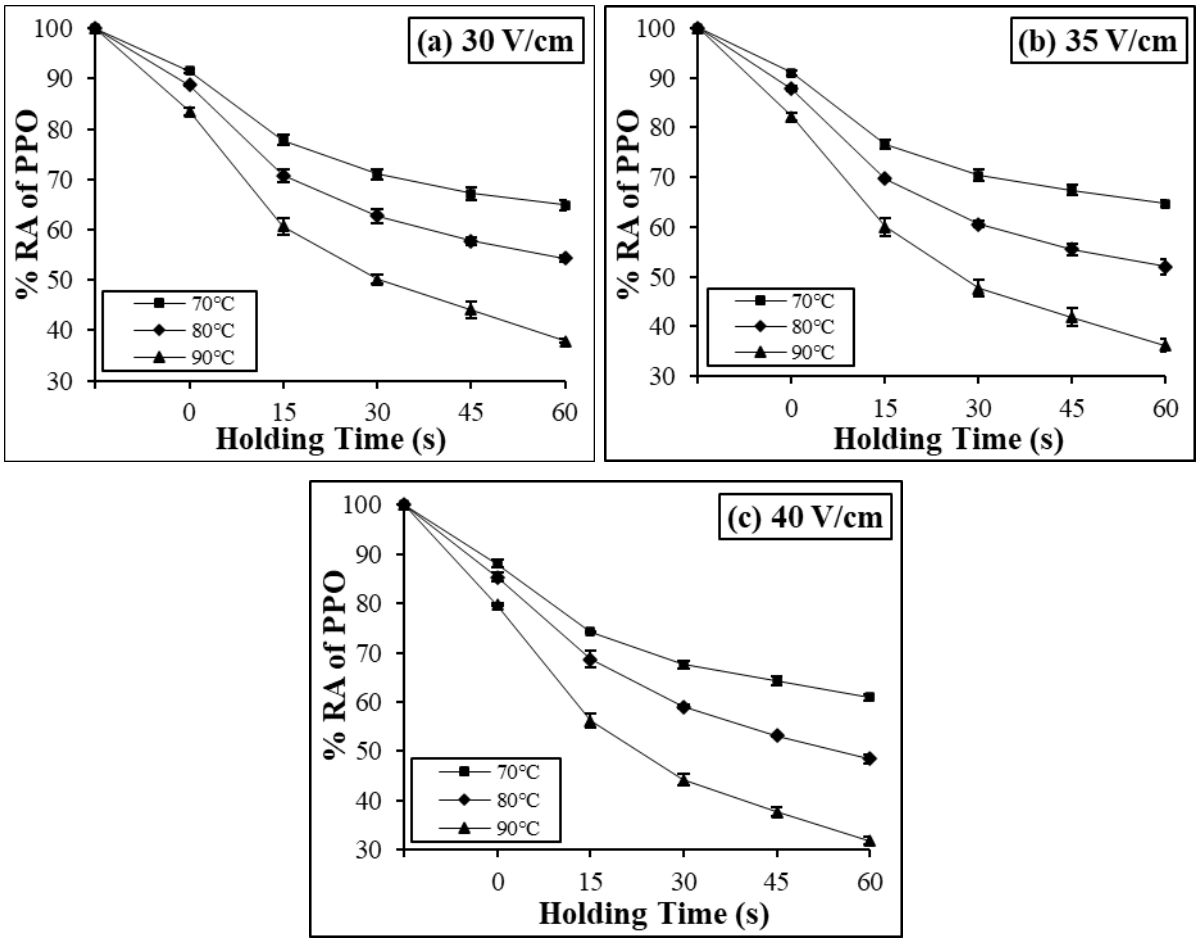

Fig. 4.26 Effect of continuous ohmic heating on PPO inactivation at EFS (a) 30 V/cm, (b) 35 V/cm, and (c) 40 V/cm

Time and temperature had a significant ($p < 0.05$) effect on PPO inactivation during isothermal holding (Fig. 4.26). PPO inactivation increased significantly ($p < 0.05$) from 20.2% to 68.2% with an increase in the treatment time from 0 s to 60 s at 90 °C and 40 V/cm. Also, with a rise

in temperature from 70 °C to 90 °C, the inactivation of PPO increased significantly from 39.1% to 68.2% at a constant treatment time of 60 s and EFS 40 V/cm. Similar results were observed in different treatment conditions. Also, PPO residual activity decreased numerically with an increase in EFS at constant temperature and time, but the reduction was statistically non-significant ($p > 0.05$) in most conditions. PPO inactivation significantly ($p < 0.05$) increased with an increase in EFS from 30 V/cm to 40 V/cm at a treatment temperature of 90 °C. The mechanism of enzyme inactivation may be due to the conformational change of the secondary structures in the enzymes from an α-helix to β-sheet, aggregation between the molecules, and distortion of the tertiary structures during thermal or non-thermal treatment (Kanjanapongkul and Baibua, 2021). Also, the biochemical reactions might have influenced the presence of an electric field by altering molecular spacing and increasing inter-chain reactions that resulted in the additional inactivation of the enzymes during ohmic treatment (Makroo et al., 2022). The other reason may be removing the metallic prosthetic groups of the PPO in the presence of an electric field, causing higher enzyme inactivation (Icier et al., 2008; Abedelmaksoud et al., 2019). The effect of temperature and time on PPO inactivation has been studied on several food samples, such as pineapple, garlic, grape juice, and coconut water. PPO inactivation is significantly affected by temperature, time, and their interaction during the ohmic heating of grape juice (Icier et al., 2008). The reduction rate of PPO activity increased from 0.04/min to 0.06/min with an increase in temperature from 70 °C to 80 °C during ohmic pasteurization of coconut water (Kanjanapongkul and Baibua, 2021).

4.5.1.2 Inactivation kinetic modelling of PPO enzyme

The model parameters and goodness of fit parameters of first order, distinct isozymes, Weibull distribution, sigmoidal logistic, and fractional conversion kinetic models are shown in Table 4.9 and Table 4.10, respectively. The reaction rate constant (k) of the first order model was significantly ($p < 0.05$) increased with an increase in temperature at any particular EFS applied. The rate constant increased more than 2.2-fold when the temperature rose from 70 °C to 90 °C at any constant EFS. Also, a maximum increment in the rate constant of 1.17-fold at 90 °C was observed when the EFS increased from 30 V/cm to 40 V/cm. As the temperature raised, the molecules in the system gained more kinetic energy, leading to more frequent collisions and increased reaction rates (k).

Table 4.9 Model parameters of different inactivation kinetic modelling of PPO enzymes in COH-treated pineapple juice

	EFS (V/cm)	Parameters	PPO		
			70 °C	80 °C	90 °C
First Order	30	k (min^{-1})	0.408 ± 0.017^{aA}	0.579 ± 0.021^{bA}	0.900 ± 0.014^{cA}
	35	k (min^{-1})	0.404 ± 0.012^{aA}	0.617 ± 0.020^{bA}	0.942 ± 0.047^{cAB}
	40	k (min^{-1})	0.428 ± 0.004^{aA}	0.639 ± 0.017^{bA}	1.052 ± 0.037^{cB}
Weibull Distribution	30	δ (min)	7.232 ± 0.214^{cAB}	3.528 ± 0.197^{bA}	1.460 ± 0.055^{aB}
		n	0.527 ± 0.010^{aA}	0.554 ± 0.041^{aA}	0.644 ± 0.049^{aA}
	35	δ (min)	9.282 ± 0.539^{bB}	2.985 ± 0.504^{aA}	1.324 ± 0.060^{aAB}
		n	0.480 ± 0.022^{aA}	0.580 ± 0.047^{abA}	0.673 ± 0.024^{bA}
	40	δ (min)	6.378 ± 0.721^{bA}	2.317 ± 0.373^{aA}	1.125 ± 0.031^{aA}
		n	0.537 ± 0.023^{aA}	0.680 ± 0.114^{aA}	0.683 ± 0.026^{aA}
Distinct Isozymes	30	K_L (min^{-1})	3.082 ± 0.018^{aA}	4.294 ± 0.033^{abA}	6.266 ± 0.924^{bB}
		K_S (min^{-1})	0.065 ± 0.010^{aA}	0.213 ± 0.035^{aA}	0.525 ± 0.079^{bA}
		A_L	0.256 ± 0.017^{aA}	0.247 ± 0.033^{aA}	0.229 ± 0.055^{aA}
		A_S	0.744 ± 0.017^{aA}	0.753 ± 0.033^{aA}	0.771 ± 0.055^{aA}
	35	K_L (min^{-1})	2.299 ± 2.632^{aA}	3.352 ± 0.320^{aA}	3.675 ± 0.003^{aA}
		K_S (min^{-1})	0.218 ± 0.174^{aA}	0.166 ± 0.020^{aA}	0.406 ± 0.030^{aA}
		A_L	0.112 ± 0.155^{aA}	0.314 ± 0.009^{aA}	0.349 ± 0.040^{aA}
		A_S	0.869 ± 0.129^{aA}	0.686 ± 0.009^{aA}	0.652 ± 0.040^{aA}
	40	K_L (min^{-1})	4.704 ± 1.334^{aA}	3.443 ± 1.919^{aA}	4.581 ± 0.496^{aAB}
		K_S (min^{-1})	0.165 ± 0.033^{aA}	0.260 ± 0.070^{aA}	0.563 ± 0.015^{bA}
		A_L	0.186 ± 0.034^{aA}	0.292 ± 0.093^{aA}	0.302 ± 0.002^{aA}
		A_S	0.814 ± 0.033^{aA}	0.708 ± 0.093^{aA}	0.698 ± 0.002^{aA}
Sigmoid Logistic	30	A_{min}	0.614 ± 0.001^{cA}	0.370 ± 0.088^{bA}	0.000 ± 0.000^{aA}
		t_{50}	0.375 ± 0.026^{aA}	0.602 ± 0.238^{aA}	0.823 ± 0.005^{aB}
		P	1.138 ± 0.025^{bA}	0.900 ± 0.075^{aA}	0.827 ± 0.058^{aA}
	35	A_{min}	0.558 ± 0.092^{bA}	0.425 ± 0.047^{bA}	0.161 ± 0.031^{aB}
		t_{50}	0.526 ± 0.284^{aA}	0.434 ± 0.061^{aA}	0.518 ± 0.080^{aA}
		P	0.921 ± 0.205^{aA}	1.065 ± 0.001^{aA}	1.024 ± 0.026^{aB}
	40	A_{min}	0.400 ± 0.190^{aA}	0.217 ± 0.085^{aA}	0.001 ± 0.001^{aA}
		t_{50}	1.085 ± 0.821^{aA}	0.825 ± 0.182^{aA}	0.645 ± 0.033^{aAB}
		P	0.826 ± 0.224^{aA}	0.953 ± 0.220^{aA}	0.909 ± 0.026^{aAB}
Fractional Conversion	30	K (min^{-1})	2.537 ± 0.088^{aA}	2.522 ± 0.296^{aA}	2.296 ± 0.301^{aA}
		A_O	1.000 ± 0.000^{bA}	0.998 ± 0.000^{abA}	0.996 ± 0.001^{aA}
		A_R	0.686 ± 0.007^{cAB}	0.583 ± 0.005^{bA}	0.405 ± 0.025^{aB}
	35	K (min^{-1})	2.842 ± 0.195^{aA}	2.432 ± 0.257^{aA}	2.247 ± 0.175^{aA}
		A_O	0.999 ± 0.000^{aA}	0.999 ± 0.000^{aA}	0.999 ± 0.000^{aB}
		A_R	0.700 ± 0.001^{cB}	0.556 ± 0.028^{bA}	0.382 ± 0.001^{aAB}
	40	K (min^{-1})	2.458 ± 0.117^{aA}	1.920 ± 0.544^{aA}	2.282 ± 0.164^{aA}
		A_O	0.999 ± 0.001^{aA}	0.999 ± 0.002^{aA}	0.998 ± 0.000^{aAB}
		A_R	0.670 ± 0.009^{cA}	0.489 ± 0.058^{bA}	0.341 ± 0.004^{aA}

Values in the same row with different small superscripts significantly ($p < 0.05$) different with change in temperature at constant EFS. Also, values in the same column with different capital superscripts are significantly ($p < 0.05$) different with a change in EFS at a constant temperature.

Table 4.10 Goodness of fit parameters for different inactivation kinetic modelling of PPO enzymes in continuous ohmic-treated pineapple juice

	EFS (V/cm)	Parameters	PPO		
			70 °C	80 °C	90 °C
First Order	30	R^2	0.885	0.906	0.949
		RMSE ($\times10^{-2}$)	3.980	4.732	4.806
		SSE ($\times10^{-3}$)	6.344	9.031	9.337
	35	R^2	0.856	0.918	0.958
		RMSE ($\times10^{-2}$)	4.351	4.656	4.554
		SSE ($\times10^{-3}$)	7.593	8.713	8.332
	40	R^2	0.894	0.953	0.963
		RMSE ($\times10^{-2}$)	3.967	3.570	4.570
		SSE ($\times10^{-3}$)	6.300	5.453	8.396
Weibull	30	R^2	0.997	0.999	0.999
		RMSE ($\times10^{-2}$)	0.729	0.534	0.638
		SSE ($\times10^{-4}$)	1.600	0.891	1.690
	35	R^2	0.998	0.998	0.998
		RMSE ($\times10^{-2}$)	0.541	0.804	1.008
		SSE ($\times10^{-4}$)	0.915	1.942	3.055
	40	R^2	0.999	0.999	0.999
		RMSE ($\times10^{-2}$)	0.471	0.550	0.658
		SSE ($\times10^{-4}$)	0.715	1.033	1.302
Distinct Isozymes	30	R^2	1.000	1.000	0.999
		RMSE ($\times10^{-2}$)	0.085	0.168	0.872
		SSE ($\times10^{-4}$)	0.011	0.049	1.304
	35	R^2	0.955	1.000	0.999
		RMSE ($\times10^{-2}$)	3.487	0.094	1.036
		SSE ($\times10^{-4}$)	23.208	0.014	1.130
	40	R^2	1.000	1.000	1.000
		RMSE ($\times10^{-2}$)	0.354	0.291	0.693
		SSE ($\times10^{-4}$)	0.126	0.157	0.488
Sigmoid Logistic	30	R^2	1.000	1.000	0.999
		RMSE ($\times10^{-2}$)	0.056	0.098	0.636
		SSE ($\times10^{-4}$)	0.012	0.020	2.086
	35	R^2	1.000	1.000	0.999
		RMSE ($\times10^{-2}$)	0.271	0.086	0.797
		SSE ($\times10^{-4}$)	0.168	0.022	1.330
	40	R^2	1.000	1.000	1.000
		RMSE ($\times10^{-2}$)	0.337	0.231	0.603
		SSE ($\times10^{-4}$)	0.229	0.138	0.739
Fractional Conversion	30	R^2	1.000	0.999	0.996
		RMSE ($\times10^{-2}$)	0.227	0.757	1.802
		SSE ($\times10^{-4}$)	0.103	1.149	6.748
	35	R^2	0.998	1.000	0.999
		RMSE ($\times10^{-2}$)	0.663	0.460	1.103
		SSE ($\times10^{-4}$)	0.948	0.423	2.468
	40	R^2	0.998	0.999	0.999
		RMSE ($\times10^{-2}$)	0.788	0.712	1.293
		SSE ($\times10^{-4}$)	1.341	1.186	3.397

R^2, RMSE, SSE, and R_d are the coefficient of determination, residual sum of square errors, sum of square errors, and relative deviation, respectively.

Thus, enzymes like PPO may undergo denaturation or structural changes at an enhanced rate at an elevated temperature, leading to a higher rate constant. On the other hand, higher EFS resulted in more efficient and intense heating, affecting the inactivation rate. The electric field can induce electrothermal effects, increasing energy dissipation within the system. This additional heat contributed to the overall thermal inactivation process, influencing the rate constant. The coefficient of determination (R^2) ranged from 0.856 to 0.963. The RMSE and SSE were lower than 0.05 and 0.01, respectively. Also, the R_d were lower than 6.5%. This model showed comparatively lower R^2 values and higher RMSE, SSE, and R_d than other models, which was also in line with the observation of Gomes et al. (2018), who suggested that the first-order kinetic model that is based on the assumption of single bond or structure rupture sufficient for enzyme inactivation is too simplistic to explain the mechanism of PPO and POD inactivation.

On the other hand, the different thermal resistance of the enzymes can be explained by the distinct isozymes model in which the enzymes are divided into thermal labile and thermal resistance fractions (Brochier et al., 2016). The R^2 (> 0.950) was high, and RMSE (< 0.035) and SSE (< 0.0024) values were comparatively lower than the first-order model. But the reaction rate constant for both the thermal labile and thermal stable fraction either decreased or was unpatterned except at 30 V/cm. Since, the reaction rate constant directly relates to temperature and should increase with the increase in temperature. Therefore, the model was unsuitable because of these unpatterned rate constant parameters even though the goodness of fit statistical parameters were in acceptable accuracy. The unsuitability of the distinct isozymes model was also explained by Gomes et al. (2018), Brochier et al. (2016), and Icier et al. (2008), who also rejected the model in the absence of acceptable physical parameters and the presence of uncertainties and unpatterned in the model parameters.

The scale factor, δ (min), of the Weibull distribution model decreased significantly ($p < 0.05$) with an increase in temperature. Temperature affected the scale factor by influencing the overall rate of inactivation. Higher temperatures typically result in a greater inactivation rate of enzymes due to increased denaturation or structural changes leading to lowering δ-values (Gomes et al., 2018). The δ-value decreased more than 4.9-fold when the temperature rose from 70 °C to 90 °C at any constant EFS between 30 to 40 V/cm. EFS also influences the overall rate of inactivation.

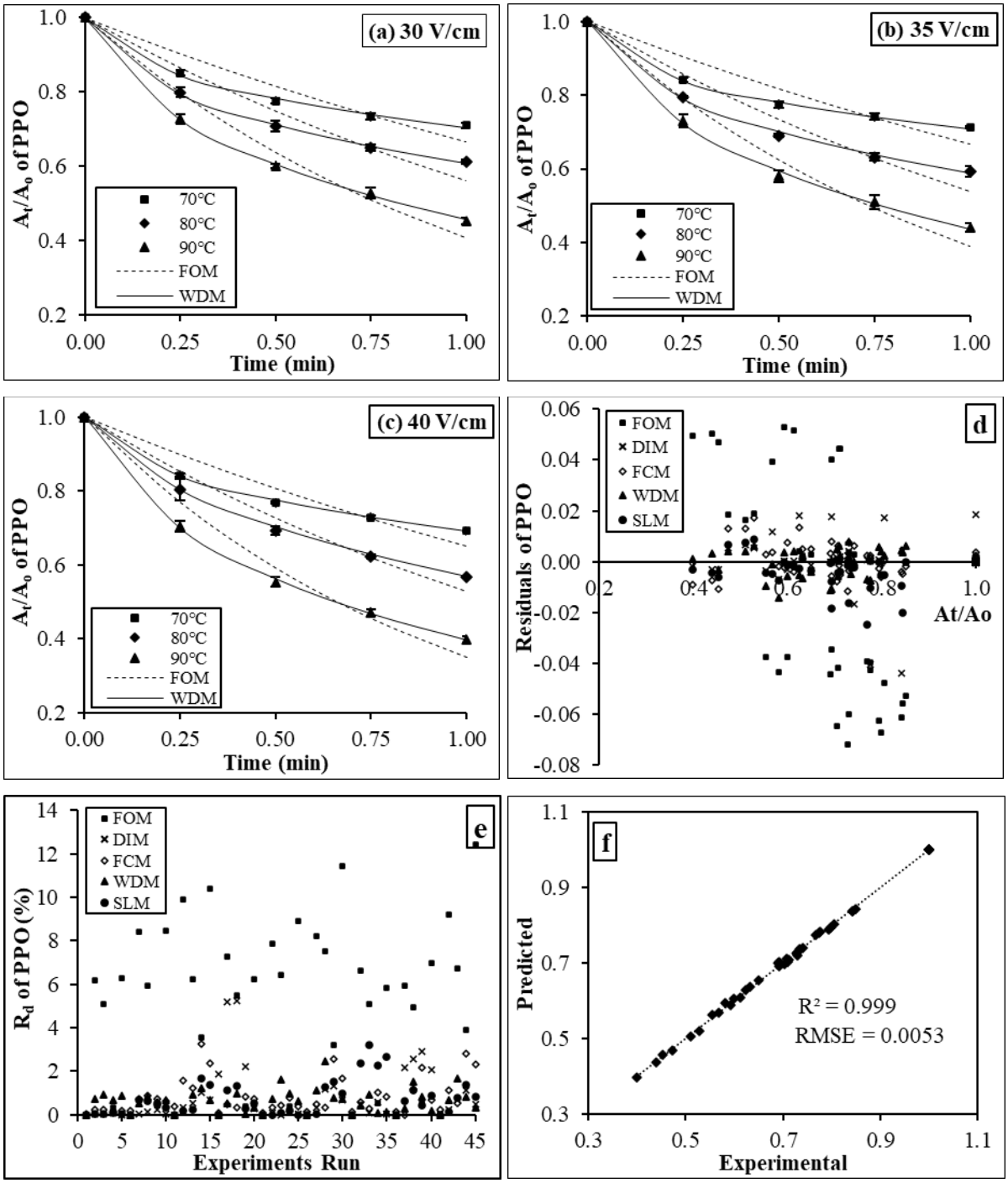

Fig. 4.27 Model curve fitting of experimental and predicted values of PPO enzymes at EFS (a) 30 V/cm, (b) 35 V/cm, and (c) 40 V/cm, (d) residual plot of PPO inactivation, (e) relative deviation plot of PPO inactivation, (f) predicted vs experimental residual activity of PPO using Weibull distribution model. Where FOM, DIM, FCM, WDM, and SLM are first-order models, distinct isozymes model, fractional conversion model, Weibull distribution model, and sigmoidal logistic model, respectively

A maximum increment of 1.5-fold in the δ-value was also observed at 80 °C when the applied EFS increased from 30 V/cm to 40 V/cm. A stronger EFS may result in more rapid inactivation of PPO because of electrothermal effects, affecting the δ-value. The reasons for thermal and

electric field effects on enzyme inactivation are explained in Section 4.5.1.1. The shape factor, $n < 1$, suggested the concave nature of the model curve (Fig. 4.27) and explained the 'tailing phenomena' that indicated the presence of highly heat-resistant enzymatic fractions (Gomes et al., 2018). Higher temperatures often increase the n-value, indicating a more pronounced enzyme inactivation and reflected in an increased sensitivity to heat at an elevated temperature (Pereira et al., 2020). The tailing phenomena became more prominent at lower n-values, which was observed at lower treatment temperatures. The R^2 of the Weibull model was greater than 0.990. Also, the RMSE, SSE, and R_d were lower than 0.0101, 0.00031, and 1.1%, respectively, which were comparatively lower than first-order and distinct isozymes models. Thus, the goodness of fit parameters like high R^2 and low RMSE, SSE, and R_d values suggested the acceptability and accuracy of the Weibull model. This was also explained by Pipliya et al. (2022) in pineapple juice (PPO and POD inactivation by cold plasma), who selected the Weibull distribution model as the best kinetic model for enzyme inactivation.

Similarly, the logistic model parameters like A_{min}, t_{50}, and P are summarised in Table 4.9. The R^2 of the model explained ≥ 99% of the variability in the residual activities of the PPO enzymes. The tailing effect was observed by the A_{min} values ≥ 0 for PPO inactivation (Pankaj et al., 2013). The A_{min} values were decreased with an increase in temperature, suggesting a more tailing phenomenon at lower temperatures and showing an inverse association with the temperature. The t_{50} denotes the time to diminish half of the residual activity, and it was observed that the t_{50} was in the range of 0.375 to 1.085 min. As the treatment temperature increased, a drop in t_{50} values indicated that the enzyme inactivation was inversely associated with the temperature. The power term, P, was in the range of 0.826 to 1.138. The high R^2 (> 0.990) and low RMSE (< 0.008), SSE (< 0.00021), and R_d value less than 2.2% also showed the accuracy of the model (Table 4.10). However, it is also to be noted that the t_{50} values at 30 V/cm and 35 V/cm showed an increasing trend instead of a decreasing trend when the temperature rose from 70 °C to 90 °C. Because of this, the logistic model under these conditions was not suitable. Meanwhile, the model at 40 V/cm showed a good fit and was acceptable under these conditions.

On the other hand, the fractional conversion model assumed the presence of a heat-resistant fraction while modelling enzyme inactivation (Shalini et al., 2008). The model characteristic parameters like A_o, A_r, and K (min^{-1}) are summarised in Table 4.9. The heat-resistant fractions, A_r, ranged from 0.342 to 0.700. The rate constant parameters, K, ranged from 1.920 to 2.842 min^{-1}. With the increase in temperature, a drop in A_r values indicated an inverse association of

heat-resistant fraction with temperature. In contrast, an increase in K values suggested a direct association of the inactivation rate being constant with temperature, suggesting rapid enzyme inactivation. The $R^2 > 0.990$ with low RMSE (< 0.019), SSE (< 0.0007), and R_d (< 1.8%) values suggested the fitness of the model (Table 4.10). It is to be noted that the PPO enzyme's rate constant was found to show a decreasing trend at 30 V/cm and 35 V/cm and an unclear pattern at 40 V/cm when the temperature increased from 70 °C to 90 °C. With uncertainties and unpatterned model parameters, this model was also regarded as unsuitable for prediction purposes, even though the goodness of fit parameters showed acceptable accuracy (Brochier et al., 2016; Icier et al., 2008). Gomes et al. (2018) also observed a satisfactory adjustment of the fractional conversion model to the experimental data, but the model was disregarded because of lower statistical criteria than other models.

4.5.1.3 Validation of PPO inactivation kinetic models

The validation of the predictability of the performance of the fitted models was carried out using the accuracy factor (A_f) and bias factor (B_f) (Pipliya et al., 2022; Vega et al., 2016). The A_f and B_f of the PPO inactivation kinetic models are summarised in Table 4.11.

Table 4.11 Model validation of PPO inactivation using accuracy factor (A_f) and bias factor (B_f)

EFS (V/cm)	T (°C)	Models									
		First Order		Weibull Distribution		Distinct Isozymes		Sigmoidal Logistic		Fractional Conversion	
		A_f	B_f	A_f	B_f	A_f	B_f	A_f	B_f	A_f	B_f
30	70	1.036	1.010	1.007	1.000	1.000	1.000	1.000	1.000	1.002	1.000
	80	1.047	1.009	1.005	1.000	1.001	1.000	1.004	1.004	1.006	0.999
	90	1.062	1.002	1.006	1.001	1.005	1.000	1.007	1.000	1.018	0.998
35	70	1.039	1.011	1.004	1.000	1.029	1.021	1.007	1.007	1.005	1.000
	80	1.048	1.008	1.008	1.002	1.001	0.999	1.001	1.000	1.004	0.999
	90	1.063	0.999	1.010	1.000	1.007	1.000	1.008	1.001	1.010	1.000
40	70	1.036	1.010	1.003	1.001	1.002	0.998	1.021	1.021	1.006	1.000
	80	1.038	1.006	1.006	1.004	1.020	0.981	1.006	1.006	1.008	0.992
	90	1.067	0.996	1.007	1.000	1.005	1.000	1.006	1.000	1.014	1.000

The highest accuracy factor, A_f, of PPO was estimated for the Weibull model (A_f = 1.003 to 1.010), followed by the fractional conversion, sigmoidal logistic, distinct isozymes, and first-order model. The distinct isozymes model observed a lower A_f and B_f than the Weibull, Sigmoidal logistic, and fractional conversion model. Even though the A_f of the sigmoidal logistic and fractional conversion model showed acceptable accuracy, the presence of uncertainties and unpatterned model parameters (Sections 4.5.1.2) pointed out the unsuitability

of the models for prediction purposes. The B_f of the Weibull model for PPO (B_f = 1.000 to 1.004) lies very close to the simulation line (B_f very close to 1), followed by fractional conversion, first order, sigmoidal logistic and distinct isozymes model.

Based on the A_f and B_f values, the Weibull model was the first preference for predicting the PPO inactivation with reasonable accuracy, followed by the first-order model. Nevertheless, the A_f and B_f are criteria for validating and selecting the model's accuracy. Still, it should not be the only criterion for selecting or rejecting any model. Therefore, additional measures, like Akaike information criteria and statistical parameters, should also be employed to choose the best-fit model (Pipliya et al., 2022).

4.5.1.4 Model selection for PPO inactivation kinetic using Akaike information criteria (AIC) and statistical parameters

The AIC and Δ_i values of all five kinetic models of PPO inactivation were calculated and summarised in Table 4.12. These criteria, along with statistical parameters like residual relative deviation (Fig. 4.27) and overall RMSE and R^2 values, were used for comparing and selecting the best-fit kinetic model. The AIC parameters of the first-order model were found to be the least for PPO enzymes, followed by the Weibull distribution model. The distinct isozymes obtained $\Delta_i > 5$; the sigmoidal logistic and fractional conversion model obtained $\Delta_i > 3$ (Δ_i very close to 4).

Table 4.12 Model selection for PPO inactivation by AIC and Akaike increment (Δ_i)

EFS (V/cm)	T (°C)	Models									
		First Order		Weibull Distribution		Distinct Isozymes		Sigmoidal Logistic		Fractional Conversion	
		AIC	Δi	AIC	Δi	AIC	Δi	AIC	Δi	AIC	Δi
30	70	-6.02	0.00	-4.05	1.97	-0.05	5.97	-2.05	3.97	-2.05	3.97
	80	-6.00	0.00	-4.05	1.96	-0.05	5.96	-2.05	3.96	-2.05	3.96
	90	-6.00	0.00	-4.05	1.95	-0.05	5.95	-2.05	3.95	-2.04	3.96
35	70	-6.01	0.00	-4.05	1.96	-0.03	5.98	-2.05	3.96	-2.05	3.96
	80	-6.00	0.00	-4.05	1.96	-0.05	5.96	-2.05	3.96	-2.05	3.96
	90	-6.01	0.00	-4.05	1.96	-0.05	5.96	-2.05	3.96	-2.05	3.96
40	70	-6.02	0.00	-4.05	1.97	-0.05	5.97	-2.04	3.98	-2.05	3.97
	80	-6.02	0.00	-4.05	1.98	-0.04	5.98	-2.05	3.98	-2.05	3.98
	90	-6.01	0.00	-4.05	1.96	-0.05	5.96	-2.05	3.96	-2.05	3.96

According to the Akaike increment thumb rule, these models showed substantially less significant support and should not be considered for overall model selection (Pipliya et al., 2022; Vega et al., 2016). On the other hand, the first-order model demonstrated the lowest AIC values and $\Delta_i = 0$. As a result, the first-order model should be the best-fit model for prediction

purposes. However, looking into the comparatively lower A_f and B_f (Table 4.11) and relatively higher residuals (-0.072 to 0.053) and relative deviation (0.00 to 12.41%) than the Weibull model, as shown in Fig. 4.27, the first order model should not be the primary choice. It is also well known that information theory criteria penalize models more with a higher number of parameters (Vega et al., 2016). Finally, the Weibull distribution model estimated the second least AIC values with $\Delta_i < 2$ for PPO. Thus, the Weibull model had significant support for the model selection. This was also supported by better A_f and B_f values, which were closer to the line of equivalence (close to 1), as well as comparatively lower residuals (-0.014 to 0.008) and relative deviations (0.00 to 2.47%) than the first-order model. The overall R^2 of the Weibull model ($R^2 = 0.999$) was higher than the first-order model ($R^2 = 0.947$). Also, the overall RMSE value of the Weibull model (RMSE = 0.005) was comparatively lower than the first-order model (RMSE = 0.039). Thus, Akaike's information criteria and statistical parameters suggested that the Weibull distribution model should be the primary choice for predicting PPO inactivation in COH-treated pineapple juice.

4.5.2 Peroxidase (POD)

4.5.2.1 Effect of COH on POD Inactivation

POD was inactivated significantly ($p < 0.05$) during the CUT period, as shown in Fig. 4.28. Approximately 30% of POD inactivation occurred when juice was heated to 90 °C at 40 V/cm from room temperature. This was due to the inactivation of highly thermal-sensitive fractions of the POD enzymes during the rise in temperature of ohmic heating. Time and temperature had a significant ($p < 0.05$) effect on POD inactivation during isothermal holding (Fig. 4.28). POD inactivation increased significantly ($p < 0.05$) from 31.8% to 82.2%, with an increase in the treatment time from 0 s to 60 s at 90 °C and 40 V/cm. Also, with a rise in temperature from 70 °C to 90 °C, the inactivation of POD increased significantly from 59.5% to 82.2% at a constant treatment time of 60 s and EFS 40 V/cm. Similar results were observed in different treatment conditions. Also, POD residual activity decreased numerically with an increase in EFS at constant temperature and time, but the reduction was statistically non-significant ($p > 0.05$) in most conditions. Apart from the reason explained for enzyme inactivation during ohmic heating in Section 4.5.1.1, the presence of an electric field might have altered the POD surface charge and enzyme environment by ionizing solution components, and distributing these ions might have resulted in additional POD inactivation during ohmic heating (Kanjanapongkul and Baibua, 2021). Treatment time was reduced from 9.0 to 6.0 min when the temperature increased from 85 °C to 95 °C for the complete inactivation of POD in

pineapple (Lee et al., 2009). Similarly, during the blanching of garlic, POD inactivation increased from 90.76% to 94.47% with a rise in water temperature from 80 °C to 90 °C (Fante and Norena, 2012).

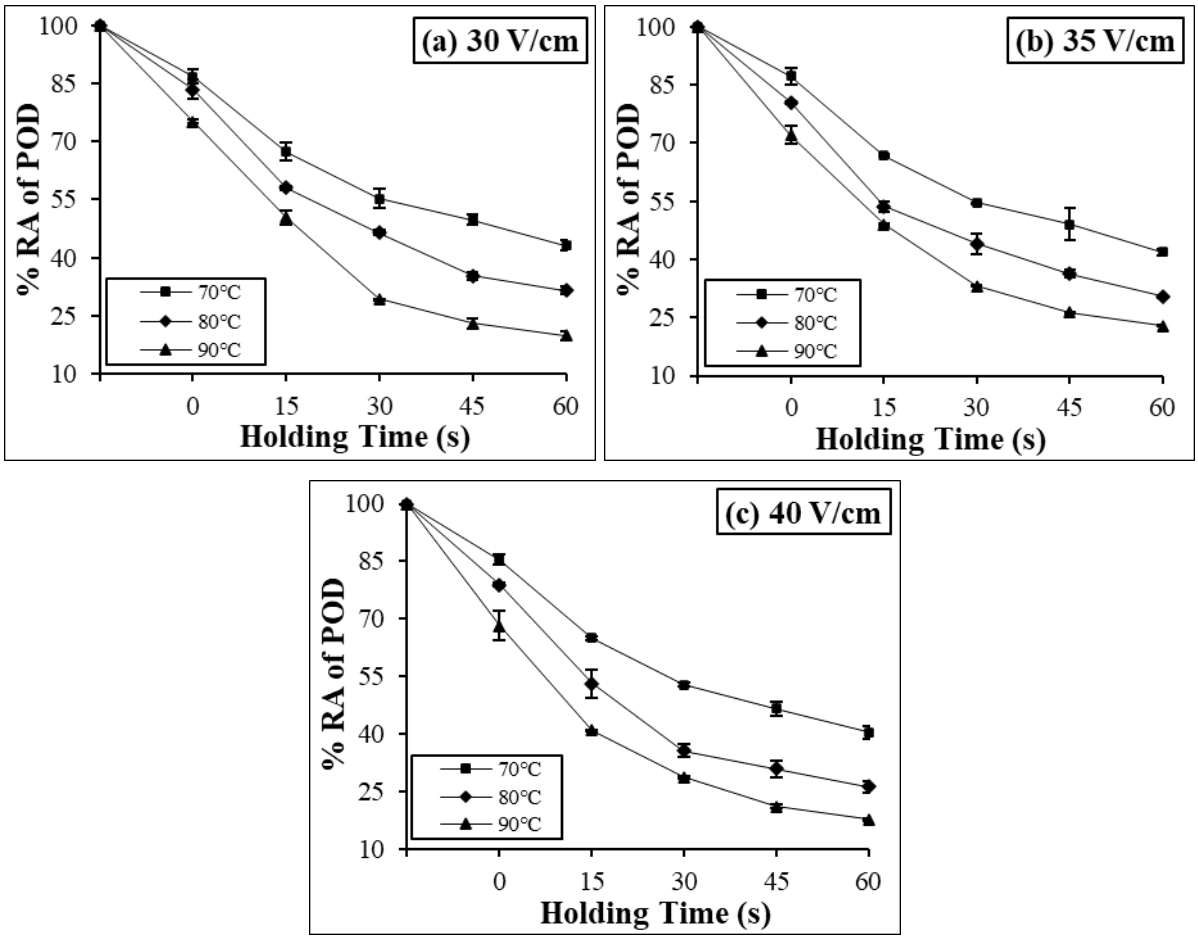

Fig. 4.28 Effect of continuous ohmic heating on POD inactivation at EFS (a) 30 V/cm, (b) 35 V/cm, and (c) 40 V/cm

It was also observed that the inactivation of the POD enzyme was higher than PPO under each treatment condition. A maximum inactivation of 82.2% of POD was observed. In comparison, it was only 68.2% inactivation for the PPO under the same treatment conditions. The present study aligned with the observation of Kanjanapongkul and Baibua (2021), who also reported a higher heat sensitivity of POD compared to PPO during the ohmic pasteurization of coconut water. Similarly, Rodriguez et al. (2021) reported more than 99% of POD inactivation during the ohmic pasteurization of carrot juice, while approximately 80% of PPO inactivation occurred during the same treatment. Fante and Norena (2012) also reported 90.76% inactivation of POD during hot water blanching of garlic at 80 °C compared to 80.24% inactivation of the PPO. On the contrary, Lee et al. (2009) observed a higher inactivation of PPO than POD during the thermal treatment of pineapple. The addition of sugar to standardize

the pineapple juice has contributed to the reduction of the thermal stability of the POD due to the interaction of sugar with the protein amino acid which has resulted in higher POD inactivation than PPO in the present study (Matsui et al., 2007). The other reasons may be due to the variation of source, nature, species, cultivar, geography, and behaviour of the food samples, as well as physico-chemical and environmental conditions (Fante and Norena, 2012).

4.5.2.2 Inactivation kinetic modelling of POD enzyme

The model parameters and goodness of fit parameters of the first-order, distinct isozymes, Weibull distribution, sigmoidal logistic, and fractional conversion models for POD inactivation kinetic are shown in Table 4.13 and Table 4.14, respectively. The reaction rate constant (k) was significantly increased with an increase in temperature at any particular EFS applied. The k-values increased more than 1.6-fold when the temperature rose from 70 °C to 90 °C at any constant EFS. Also, a maximum increment of 1.18-fold in the k-values at 80 °C was observed when the EFS increased from 30 V/cm to 40 V/cm. It was also observed that the POD had a higher inactivation rate constant than the PPO, suggesting that the PPO was more thermally resistant than the POD enzyme in the pineapple juice, as also explained in Section 4.5.1.1 and Section 4.5.2.1. The coefficient of determination, R^2, was ≥ 0.950 for all treatment conditions. The RMSE and SSE were lower than 0.055 and 0.012, respectively. Also, POD's relative deviation (Rd) was lower than 9.5%, respectively. This model showed comparatively lower R^2 values and higher RMSE, SSE, and R_d than other models, which was also in line with the observation of Gomes et al. (2018), who suggested that the first-order kinetic model that is based on the assumption of single bond or structure rupture sufficient for enzyme inactivation is too simplistic to explain the mechanism of POD inactivation.

The model parameters of the distinct isozymes viz., k_L, k_s, A_L, and A_s and goodness of fit parameters viz., R^2, RMSE, SSE, and R_d are shown in Tables 4.13 and Table 4.14, respectively. The R^2 (≥ 0.985) was high, and RMSE (< 0.043) and SSE (< 0.0036) values were low for POD inactivation. Even though the goodness of fit statistical parameters were in acceptable accuracy, the distinct isozymes model for POD inactivation was also found unsuitable because of uncertainties and unpatterned model parameters. The reaction rate constant directly relates to temperature and should increase with the increase in temperature. The unsuitability of the distinct isozymes model was also explained by Gomes et al. (2018), Brochier et al. (2016), and Icier et al. (2008), who also rejected the model in the absence of acceptable physical parameters and the presence of uncertainties and unpatterned in the model parameters. A very high relative deviation of POD inactivation (up to 40%) also suggested the unsuitability of the model.

Table 4.13 Model parameters of different inactivation kinetic modelling of POD enzymes in COH-treated pineapple juice

	EFS (V/cm)	Parameters	POD		
			70 °C	80 °C	90 °C
First Order	30	k (min^{-1})	0.778 ± 0.038^{aA}	1.122 ± 0.024^{bA}	1.596 ± 0.055^{cA}
	35	k (min^{-1})	0.812 ± 0.010^{aA}	1.123 ± 0.047^{bA}	1.363 ± 0.051^{cA}
	40	k (min^{-1})	0.838 ± 0.005^{aA}	1.328 ± 0.100^{bA}	1.622 ± 0.125^{bA}
Weibull Distribution	30	δ (min)	1.707 ± 0.301^{bA}	0.998 ± 0.015^{abB}	0.635 ± 0.024^{aA}
		n	0.712 ± 0.192^{aA}	0.736 ± 0.072^{aA}	0.851 ± 0.011^{aA}
	35	δ (min)	1.576 ± 0.161^{bA}	1.065 ± 0.016^{aB}	0.771 ± 0.028^{aA}
		n	0.707 ± 0.073^{aA}	0.638 ± 0.057^{aA}	0.776 ± 0.027^{aA}
	40	δ (min)	1.504 ± 0.125^{bA}	0.816 ± 0.060^{aA}	0.630 ± 0.057^{aA}
		n	0.710 ± 0.068^{aA}	0.709 ± 0.063^{aA}	0.717 ± 0.057^{aA}
Distinct Isozymes	30	K_L (min^{-1})	3.248 ± 1.696^{aA}	4.003 ± 2.979^{aA}	2.352 ± 0.050^{aA}
		K_S (min^{-1})	0.357 ± 0.070^{aA}	0.358 ± 0.494^{aA}	0.000 ± 0.000^{aA}
		A_L	0.317 ± 0.005^{aA}	0.493 ± 0.342^{aA}	0.841 ± 0.005^{aB}
		A_S	0.683 ± 0.005^{aA}	0.507 ± 0.342^{aA}	0.168 ± 0.007^{aA}
	35	K_L (min^{-1})	4.024 ± 3.017^{aA}	3.655 ± 3.727^{aA}	2.326 ± 0.160^{aA}
		K_S (min^{-1})	0.300 ± 0.265^{aA}	0.772 ± 0.256^{aA}	0.000 ± 0.000^{aA}
		A_L	0.379 ± 0.252^{aA}	0.635 ± 0.453^{aA}	0.770 ± 0.007^{aAB}
		A_S	0.621 ± 0.253^{aA}	0.345 ± 0.481^{aA}	0.234 ± 0.006^{aAB}
	40	K_L (min^{-1})	3.697 ± 0.275^{aA}	2.596 ± 0.356^{aA}	3.376 ± 0.166^{aB}
		K_S (min^{-1})	0.430 ± 0.135^{aA}	0.000 ± 0.000^{aA}	0.483 ± 0.174^{aB}
		A_L	0.278 ± 0.083^{aA}	0.727 ± 0.009^{bA}	0.609 ± 0.082^{bA}
		A_S	0.722 ± 0.082^{aA}	0.276 ± 0.007^{aA}	0.390 ± 0.083^{aB}
Sigmoid Logistic	30	A_{min}	0.163 ± 0.231^{aA}	0.013 ± 0.018^{aA}	0.226 ± 0.033^{aB}
		t_{50}	0.687 ± 0.414^{aA}	0.576 ± 0.002^{aB}	0.285 ± 0.001^{aA}
		P	1.046 ± 0.004^{aA}	1.006 ± 0.110^{aA}	2.312 ± 0.307^{bB}
	35	A_{min}	0.081 ± 0.114^{aA}	0.000 ± 0.000^{aA}	0.233 ± 0.001^{aB}
		t_{50}	0.805 ± 0.242^{aA}	0.586 ± 0.040^{aB}	0.304 ± 0.015^{aA}
		P	0.954 ± 0.189^{aA}	0.858 ± 0.060^{aA}	1.744 ± 0.001^{bAB}
	40	A_{min}	0.135 ± 0.190^{aA}	0.281 ± 0.032^{aB}	0.039 ± 0.055^{aA}
		t_{50}	0.668 ± 0.291^{aA}	0.275 ± 0.019^{aA}	0.347 ± 0.078^{aA}
		P	1.027 ± 0.106^{aA}	1.863 ± 0.240^{bB}	1.150 ± 0.052^{aA}
Fractional Conversion	30	K (min^{-1})	1.973 ± 0.970^{aA}	2.107 ± 0.307^{aA}	2.352 ± 0.049^{aA}
		A_O	0.999 ± 0.000^{aA}	0.998 ± 0.002^{aA}	1.009 ± 0.002^{bB}
		A_R	0.391 ± 0.125^{aA}	0.287 ± 0.037^{aA}	0.168 ± 0.007^{aA}
	35	K (min^{-1})	1.934 ± 0.290^{aA}	2.516 ± 0.449^{aA}	2.326 ± 0.161^{aA}
		A_O	0.998 ± 0.002^{aA}	0.994 ± 0.003^{aA}	1.004 ± 0.000^{aAB}
		A_R	0.401 ± 0.047^{bA}	0.337 ± 0.026^{abA}	0.234 ± 0.006^{aB}
	40	K (min^{-1})	1.962 ± 0.352^{aA}	2.597 ± 0.354^{aA}	2.721 ± 0.402^{aA}
		A_O	0.999 ± 0.001^{aA}	1.004 ± 0.002^{aA}	0.999 ± 0.000^{aA}
		A_R	0.391 ± 0.052^{bA}	0.276 ± 0.007^{abA}	0.209 ± 0.012^{aB}

Values in the same row with different small superscripts significantly ($p < 0.05$) different with change in temperature at constant EFS. Also, values in the same column with different capital superscripts are significantly ($p < 0.05$) different with a change in EFS at a constant temperature.

Table 4.14 Goodness of fit parameters for different inactivation kinetic modelling of POD enzymes in continuous ohmic-treated pineapple juice

	EFS (V/cm)	Parameters	POD		
			70 °C	80 °C	90 °C
First Order	30	R^2	0.954	0.973	0.980
		RMSE ($\times10^{-2}$)	3.738	4.076	4.339
		SSE ($\times10^{-3}$)	7.076	6.844	7.578
	35	R^2	0.961	0.950	0.978
		RMSE ($\times10^{-2}$)	3.926	5.425	4.179
		SSE ($\times10^{-3}$)	6.445	11.937	7.017
	40	R^2	0.965	0.962	0.975
		RMSE ($\times10^{-2}$)	3.808	5.310	4.668
		SSE ($\times10^{-3}$)	6.024	11.366	8.938
Weibull	30	R^2	0.997	0.997	0.986
		RMSE ($\times10^{-2}$)	1.116	1.534	4.180
		SSE ($\times10^{-4}$)	5.016	7.124	53.405
	35	R^2	0.995	0.999	0.993
		RMSE ($\times10^{-2}$)	1.543	0.812	2.643
		SSE ($\times10^{-4}$)	8.717	2.930	20.950
	40	R^2	0.998	0.991	0.999
		RMSE ($\times10^{-2}$)	0.903	3.013	1.132
		SSE ($\times10^{-4}$)	3.550	27.940	4.061
Distinct Isozymes	30	R^2	0.998	0.997	0.992
		RMSE ($\times10^{-2}$)	1.436	2.544	3.913
		SSE ($\times10^{-4}$)	3.385	6.472	31.810
	35	R^2	0.996	0.985	0.998
		RMSE ($\times10^{-2}$)	2.128	4.264	2.495
		SSE ($\times10^{-4}$)	7.193	35.842	6.252
	40	R^2	0.999	0.996	1.000
		RMSE ($\times10^{-2}$)	1.100	2.598	1.012
		SSE ($\times10^{-4}$)	2.133	11.776	1.121
Sigmoid Logistic	30	R^2	0.998	0.997	1.000
		RMSE ($\times10^{-2}$)	1.056	1.819	0.469
		SSE ($\times10^{-4}$)	3.749	6.624	0.774
	35	R^2	0.995	0.998	1.000
		RMSE ($\times10^{-2}$)	1.609	1.304	0.224
		SSE ($\times10^{-4}$)	8.126	5.218	0.103
	40	R^2	0.999	0.999	1.000
		RMSE ($\times10^{-2}$)	0.845	1.345	0.685
		SSE ($\times10^{-4}$)	2.276	3.982	1.174
Fractional Conversion	30	R^2	0.997	0.997	0.992
		RMSE ($\times10^{-2}$)	1.202	1.988	3.913
		SSE ($\times10^{-4}$)	4.641	7.989	31.810
	35	R^2	0.993	0.994	0.998
		RMSE ($\times10^{-2}$)	1.805	2.531	1.764
		SSE ($\times10^{-4}$)	10.739	13.766	6.252
	40	R^2	0.998	0.996	1.000
		RMSE ($\times10^{-2}$)	1.185	2.290	0.876
		SSE ($\times10^{-4}$)	3.226	11.776	1.580

R^2, RMSE, SSE, and R_d are the coefficient of determination, residual sum of square errors, sum of square errors, and relative deviation, respectively.

The scale factor, δ (min), of the Weibull distribution model significantly ($p < 0.05$) decreased with an increase in temperature. Higher temperatures typically result in a greater inactivation rate of enzymes due to increased denaturation or structural changes leading to lowering δ-values (Gomes et al., 2018). The δ-value of the POD inactivation decreased more than 2.0-fold when the temperature rose from 70 °C to 90 °C at any constant EFS between 30 to 40 V/cm. The δ-value of POD inactivation was lower than the PPO under each treatment condition, suggesting a higher thermal stability of the PPO enzymes than POD in the pineapple juice. EFS also influences the overall rate of inactivation. A maximum increment of 1.2-fold in the δ-value was also observed at 80 °C when the applied EFS increased from 30 to 40 V/cm. A stronger EFS may result in more rapid inactivation because of electrothermal effects, affecting the δ-value. The reasons for thermal and electric field effects on enzyme inactivation are explained in Section 4.5.1.1. The shape factor, $n < 1$, also suggested the concave nature of the model curve for POD inactivation (Fig. 4.29) and explained the 'tailing phenomena' that indicated the presence of highly heat-resistant POD enzyme fractions (Gomes et al., 2018). The R^2 was ≥ 0.986, and the RMSE, SSE, and R_d were lower than 0.042, 0.0054, and 6.95%, respectively. Thus, the goodness of fit parameters like high R^2 and low RMSE, SSE, and R_d values suggested the acceptability and accuracy of the Weibull distribution model. This was also explained by Gomes et al. (2018) in *Tetsukabuto* pumpkin (POD inactivation by ohmic blanching) and Pipliya et al. (2022) in pineapple juice (PPO and POD inactivation by cold plasma) and selected the Weibull distribution model as the best kinetic model for the enzyme inactivation.

The R^2 of the sigmoidal logistic model explained ≥ 99% of the variability in the residual activities of the POD enzymes. The tailing effect was observed by the A_{min} values ≥ 0 for POD inactivation (Pankaj et al., 2013). The A_{min} values of POD were found to be unpatterned. The t_{50} denotes the time to diminish half of the residual activity and was observed in the 0.275 to 0.805 min range. As the treatment temperature increased, a drop in t_{50} values indicated that the enzyme inactivation was inversely associated with the temperature. The higher t_{50} value of the PPO than the POD enzyme also suggested that the PPO was more thermally stable than POD in the COH-treated pineapple juice. The t_{50} values were also used to compare the thermal stability of PPO and POD enzymes in pineapple juice (Pipliya et al., 2022) and tender coconut water (Chutiya et al., 2019) during cold plasma treatment. The power term, P, was in the range of 0.858 to 2.312. The high R^2 values (≥ 0.995) and low RMSE (< 0.019), SSE (< 0.00082), and R_d value (< 2.2%) also showed the accuracy of the logistic model (Table 4.14).

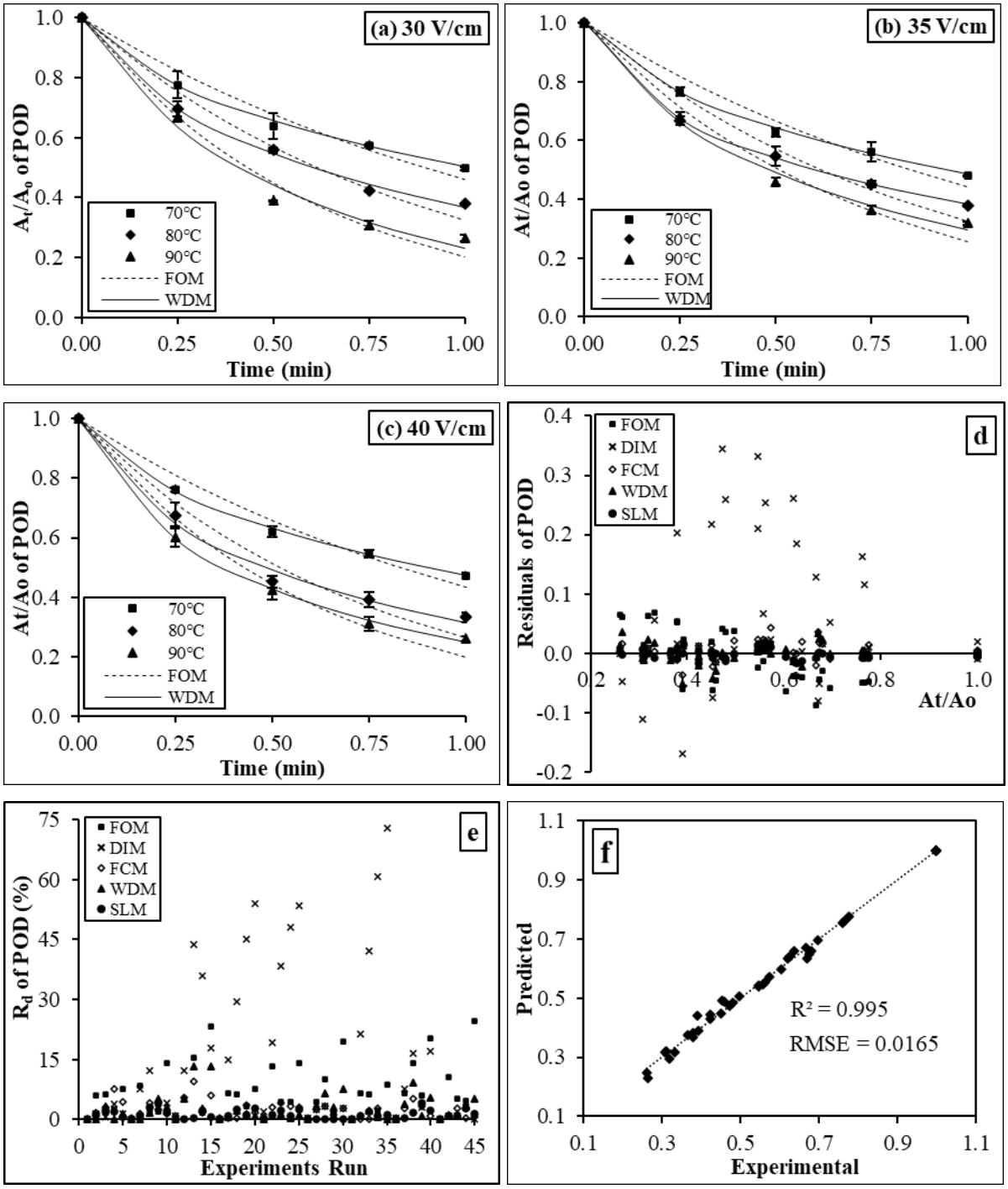

Fig. 4.29 Model curve fitting of experimental and predicted values of POD enzymes at EFS (a) 30 V/cm, (b) 35 V/cm, and (c) 40 V/cm, (d) residual plot of POD inactivation, (e) relative deviation plot of POD inactivation, (f) predicted vs experimental residual activity of POD using Weibull distribution model. Where FOM, DIM, FCM, WDM, and SLM are first-order model, distinct isozymes model, fractional conversion model, Weibull distribution model, and sigmoidal logistic model, respectively

However, it is also to be noted that the t_{50} values of POD at 40 V/cm had shown an unclear pattern. Because of this, the logistic model under these conditions was not suitable. Meanwhile, the models at 30 V/cm and 35 V/cm for POD showed a good fit and were acceptable under

these conditions. The suitability of the sigmoidal logistic model for enzyme inactivation like POD in tomato (Pankaj et al., 2013), PPO and POD in pineapple juice (Pipliya et al., 2022) and tender coconut water (Chutiya et al., 2019) has been reported.

The fractional conversion model characteristic parameters like A_o, A_r, and K (min^{-1}) of the POD inactivation are summarised in Table 4.13. The heat-resistant fractions of the PPO (A_r = 0.342 to 0.700) were higher than the POD (A_r = 0.168 to 0.401) enzymes. This also suggested that the PPO enzyme required higher treatment time at the same temperature to achieve the same level of POD inactivation. In other words, the PPO enzymes in the pineapple juice were observed to be more thermally resistant than the POD enzyme. The rate constant parameters of the POD enzymes were in the range of 1.934 to 2.721 min^{-1}. With the increase in temperature, a drop in A_r values indicated an inverse association of heat-resistant fraction with temperature. In contrast, an increase in K values suggested a direct association of the inactivation rate being constant with temperature, suggesting rapid enzyme inactivation. The $R^2 \geq 0.992$ with low RMSE (< 0.0392), SSE (< 0.0032), and R_d (< 4.8%) values suggested the fitness of the model (Table 4.14). It is to be noted that the POD enzyme's rate constant showed an unclear pattern at 35 V/cm when the temperature increased from 70 °C to 90 °C. With uncertainties and unpatterned model parameters, this model was also regarded as unsuitable for prediction purposes, even though the goodness of fit parameters showed acceptable accuracy (Brochier et al., 2016; Icier et al., 2008). Gomes et al. (2018) also observed a satisfactory adjustment of the fractional conversion model to the experimental data, but the model was disregarded because of lower statistical criteria than other models.

4.5.2.3 Validation of POD inactivation kinetic models

The validation of the predictability of the performance of the fitted models was carried out using the accuracy factor (A_f) and bias factor (B_f) (Table 4.15) (Pipliya et al., 2022; Vega et al., 2016). The POD enzyme's highest accuracy factor, A_f, was estimated by the sigmoidal logistic model (A_f = 1.000 to 1.019), followed by fractional conversion, Weibull, first-order, and distinct isozymes model. The distinct isozymes model observed a very low A_f (1.835) for POD and an extensive range of bias factor (B_f = 0.545 to 1.211) around the line of equivalence, which showed the unsuitability and inaccuracy for predicting the POD inactivation. Even though the A_f of the sigmoidal logistic and fractional conversion model showed acceptable accuracy, the presence of uncertainties and unpatterned model parameters (Section 4.5.2.2) pointed out the unsuitability of the models for prediction purposes.

Table 4.15 Model validation of POD inactivation using accuracy factor (A_f) and bias factor (B_f)

EFS (V/cm)	T (°C)	Models									
		First Order		Weibull Distribution		Distinct Isozymes		Sigmoidal Logistic		Fractional Conversion	
		A_f	B_f	A_f	B_f	A_f	B_f	A_f	B_f	A_f	B_f
30	70	1.046	1.003	1.010	1.009	1.015	0.986	1.011	1.003	1.035	0.966
	80	1.056	0.994	1.020	1.000	1.057	0.946	1.019	1.001	1.019	0.996
	90	1.089	0.973	1.072	0.992	1.211	1.211	1.007	0.997	1.048	1.000
35	70	1.048	1.003	1.011	1.002	1.459	0.685	1.015	1.010	1.013	0.997
	80	1.075	0.994	1.007	1.000	1.533	0.652	1.014	1.001	1.029	0.996
	90	1.077	0.982	1.042	0.997	1.020	0.999	1.000	1.000	1.020	0.999
40	70	1.048	1.002	1.007	1.002	1.835	0.545	1.010	1.006	1.008	0.995
	80	1.102	0.981	1.039	0.997	1.093	1.003	1.017	0.999	1.025	0.997
	90	1.100	0.965	1.023	0.997	1.010	1.006	1.012	1.002	1.009	0.995

The B_f of the sigmoidal logistic model (B_f = 0.997 to 1.010) showed greater closeness to the simulation line, followed by the Weibull, first-order, and fractional conversion model. Based on the A_f and B_f values, the Weibull model was the first preference for predicting the POD inactivation with reasonable accuracy, followed by the first-order model. Nevertheless, the A_f and B_f are criteria for validating and selecting the model's accuracy. Still, it should not be the only criterion for selecting or rejecting any model. Therefore, additional measures, like Akaike information criteria and statistical parameters, should also be employed to choose the best-fit model (Pipliya et al., 2022).

4.5.2.4 Model selection for POD inactivation kinetic using AIC and statistical parameters

The AIC and Δ_i values of all five kinetic models for POD inactivation were calculated and summarised in Table 4.16. These criteria, along with statistical parameters like residuals and relative deviation (Fig. 4.29) and overall RMSE and R^2 values, were used for comparing and selecting the best-fit model. The AIC parameters of the first-order model were found to be the least for POD enzymes, followed by the Weibull distribution model. The distinct isozymes obtained $\Delta_i > 5$; the sigmoidal logistic and fractional conversion model obtained $\Delta_i > 3$ (Δ_i very close to 4). According to the Akaike increment thumb rule, these models showed substantially less significant support and should not be considered for overall model selection (Pipliya et al., 2022; Vega et al., 2016). On the other hand, the first-order model demonstrated the lowest AIC values and $\Delta_i = 0$. As a result, this model should be the best-fit model for prediction purposes. However, looking into the comparatively lower A_f and B_f (Table 4.15) and relatively higher

residuals (-0.088 to 0.068) and relative deviation (0.00 to 24.53%) than the Weibull model, as shown in Fig. 4.29, the first-order model should not be the primary choice.

Table 4.16 Model selection for POD inactivation by AIC and Akaike increment (Δ_i)

EFS (V/cm)	T (°C)	Models									
		First Order		Weibull Distribution		Distinct Isozymes		Sigmoidal Logistic		Fractional Conversion	
		AIC	Δi	AIC	Δi	AIC	Δi	AIC	Δi	AIC	Δi
30	70	-6.02	0.00	-4.04	1.97	-0.04	5.98	-2.05	3.97	-2.03	3.99
	80	-6.01	0.00	-4.04	1.97	-0.01	6.01	-2.04	3.97	-2.04	3.97
	90	-6.01	0.00	-4.02	1.99	0.20	6.21	-2.05	3.96	-2.03	3.98
35	70	-6.02	0.00	-4.05	1.97	0.85	6.87	-2.04	3.97	-2.04	3.97
	80	-5.99	0.00	-4.05	1.94	0.70	6.69	-2.05	3.94	-2.04	3.95
	90	-6.01	0.00	-4.04	1.98	-0.04	5.97	-2.05	3.97	-2.04	3.97
40	70	-6.02	0.00	-4.05	1.97	1.58	7.60	-2.05	3.97	-2.05	3.97
	80	-5.99	0.00	-4.03	1.96	0.01	6.00	-2.05	3.95	-2.04	3.95
	90	-6.00	0.00	-4.05	1.96	-0.05	5.96	-2.05	3.96	-2.05	3.96

It is also well known that information theory criteria penalize models more with a higher number of parameters (Vega et al., 2016). Finally, the Weibull distribution model estimated the second least AIC values with $\Delta_i < 2$. Thus, the Weibull model had significant support for the model selection. This was also supported by better A_f and B_f values, which were closer to the line of equivalence (close to 1), as well as comparatively lower residuals (-0.052 to 0.035) and relative deviations (0.00 to 13.33%) than the first-order model. The overall R^2 of the Weibull model ($R^2 = 0.995$) was higher than the first-order model ($R^2 = 0.972$), and also, the RMSE value of the Weibull model (RMSE = 0.016) was comparatively lower than the first-order model (RMSE = 0.039). Thus, Akaike's information criteria and statistical parameters suggested that the Weibull distribution model should be the primary choice for predicting POD inactivation in COH-treated pineapple juice.

Using the AIC and Δ_i parameters, Pipliya et al. (2022) also selected the Weibull model as their first choice for predicting PPO and POD inactivation in cold plasma-treated pineapple juice. Brochier et al. (2016) also chose the Weibull model for POD inactivation in ohmic-treated sugarcane juice while rejecting other models because of low R^2, high RMSE and Chi-square values, and the presence of negative model parameters. In contrast, Icier et al. (2008) selected only the first-order kinetic model. They rejected other models based on considerable uncertainty and inconsistent trends in the rate constant during PPO deactivation in ohmic-treated grape juice. However, in another study of POD inactivation kinetics of ohmic blanched

Tetsukabuto pumpkin, the Weibull model was observed to be the best-fit model based on statistical criteria and the fewest number of parameters (Gomes et al., 2018).

In contradiction, Sulaiman et al. (2015a) observed the first-order biphasic model as an appropriate model for the inactivation kinetics of PPO in Camarosa strawberry and Royal Gala apples during high-pressure processing. While the first-order kinetic model was the most suitable for PPO inactivation in thermosonicated pear, apple, and strawberry purees and the other models like biphasic, fractional conversion, and Weibull model were rejected based on lower R^2 values and patterned residual plots (Sulaiman et al., 2015b). Thus, different kinetic models can be suitable depending on the variations in the sources of enzymes, processing conditions, and technologies employed. So, different mathematical models should be studied in a given data set to find the best kinetic model for the spoilage enzyme inactivation. The present study showed the suitability of the Weibull model in predicting PPO and POD inactivation. It provided valuable insights into how these enzymes will respond to varying conditions, especially changes in temperature and time exposures. The shape and scale parameters of the Weibull model offer insights into the enzyme's resistance to thermal inactivation. Understanding these parameters helps quantify and compare the stability of different enzymes under various treatment conditions. Also, the predictive capability of the Weibull model allows for the anticipation of enzyme activity levels. It helps determine their stability profile, which can be used to identify optimal conditions for enzyme inactivation based on specific needs.

4.5.3 Bromelain

4.5.3.1 Effect of COH on Bromelain Inactivation

The residual activity (%) of bromelain enzyme during continuous ohmic heating-assisted isothermal holding is shown in Fig. 4.30. It was observed that more than 50.0% bromelain inactivation occurred during the CUT period, irrespective of the treatment conditions. A maximum of 80.0% bromelain inactivation occurred during the CUT period at 90 °C and 40 V/cm. This showed the thermal sensitivity of the bromelain enzyme in pineapple juice. No studies have been reported on bromelain inactivation during the CUT period of ohmic heating, so the results cannot be compared. However, the authors reported a 7.0% and 22.0% loss of initial bromelain activity in pineapple juice at 45 °C and 70 °C during the CUT period in high-pressure thermal treatment (Chakraborty et al., 2016). The other authors also reported a significant reduction in the activity of other enzymes during the CUT period. For example, the inactivation of 27.0% of peroxidase at 80 °C and 91.0% polyphenol oxidase at 70 °C was

observed during the CUT period of ohmic heating of sugarcane juice (Brochier et al., 2016). While the residual activity of the tyrosinase inactivation in *Agaricus bisporus* during the CUT period of ohmic heating was reported to be 24.46 ± 1.24, 24.40 ± 3.54, and 18.29 ± 0.59%, respectively, at 25, 30, and 35 V/cm with treatment temperature of 58 °C (Barron-Garcia et el., 2019).

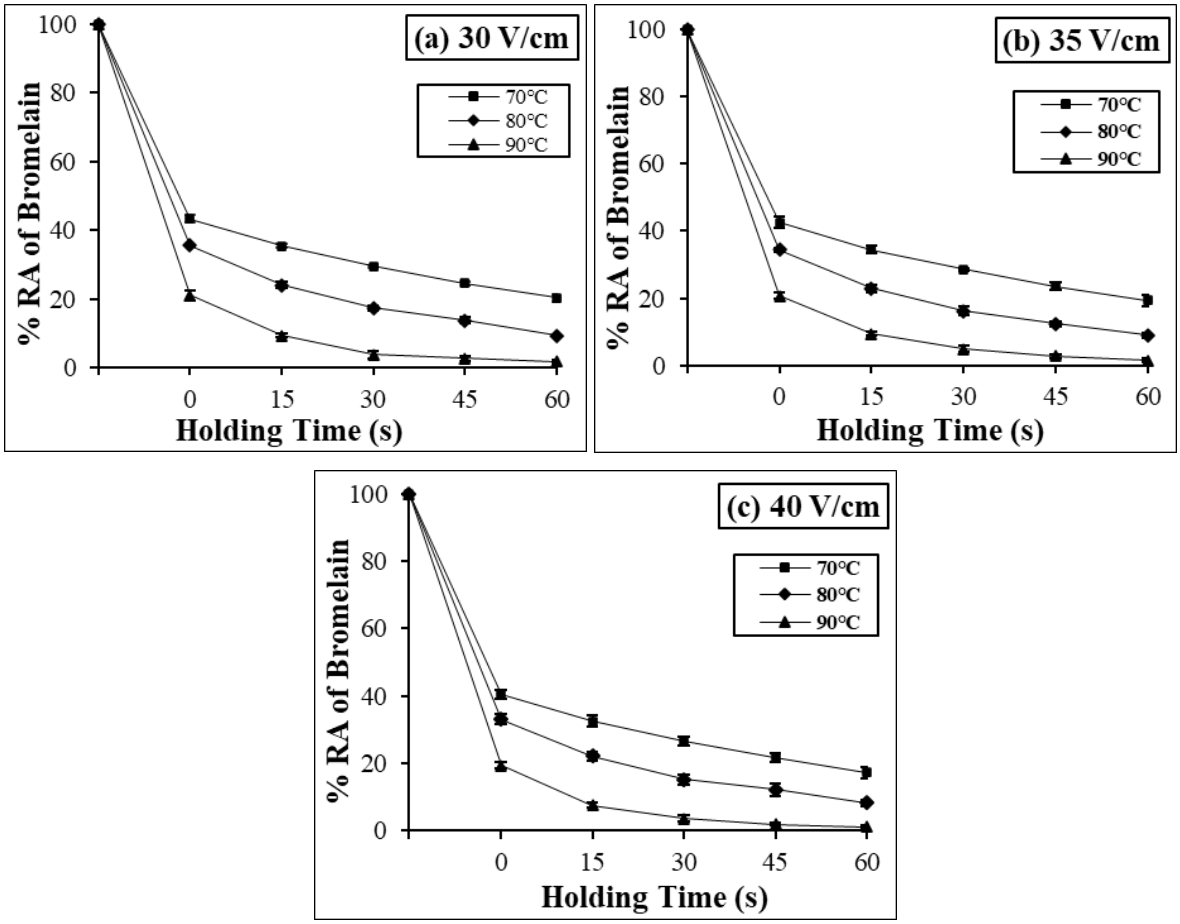

Fig. 4.30 Effect of continuous ohmic heating on bromelain inactivation at EFS (a) 30 V/cm, (b) 35 V/cm, and (c) 40 V/cm

Bromelain inactivation increased significantly ($p < 0.05$) with an increase in temperature at any constant treatment time and EFS, as shown in Fig. 4.30. Inactivation of bromelain was also significantly increased ($p < 0.05$) with an increase in isothermal holding time at any constant temperature and EFS. Bromelain was inactivated completely to a negligible value (less than 2.0% of the initial activity) when the pineapple juice was treated for 60 s at 90 °C. It was also reported that 90.0% of bromelain inactivation in pineapple juice was achieved in 25 min and 5 min, respectively, at 60 °C and 65 °C while it was inactivated entirely at 67 °C in 5 min (Sriwatanapongse et al., 2000). In another study, 51.0% residual activity of bromelain in pineapple juice was observed after 8 min at 60 °C while complete inactivation was observed at

80 °C after 8 min treatment time (Jutamongkon and Charoenrein, 2010). Though at any particular holding time and treatment temperature, the residual activity of bromelain was reduced with an increase in EFS, but it was statistically non-significant ($p > 0.05$). The residual activity of bromelain was more than 15.0% when treated for 60 s at a temperature of 70 °C. This showed that a small thermal resistant fraction of bromelain enzyme at 70°C was present. However, the findings showed that bromelain activity in the standardized pineapple juice was highly thermal sensitive and could be inactivated to a negligible level during thermal processing. A significant effect of the electric field on the enzyme activity was observed by Delfiya and Thangavel (2016), Kanjanapongkul and Baibua (2021), and Zhong et al. (2007). Biochemical reactions may have influenced the presence of an electric field by altering molecular spacing and increasing inter-chain reactions that resulted in the additional inactivation of the enzymes when the voltage gradient increased from 16 V/cm to 36 V/cm during ohmic treatment (Makroo et al., 2022).

4.5.3.2 Inactivation kinetic modelling of bromelain enzyme

The model parameters and goodness of fit parameters of first-order, Weibull distribution, and logistic models for bromelain inactivation are shown in Table 4.17 and Table 4.18, respectively. The reaction rate constant (k) of the first-order model was increased significantly ($p < 0.05$) with an increase in temperature at any constant EFS (Chakraborty et al., 2016). The k-values increased more than 3.6-fold with an increase in temperature from 70 °C to 90 °C at any particular EFS. Also, the scale factor (δ-values) of the Weibull model and time for half-inactivation (t_{50}-values) of the logistic model decreased significantly ($p < 0.05$) with an increase in temperature. The δ-values of the Weibull model and t_{50}-values of the logistic model increased more than 3.9-fold when the temperature increased from 70 °C to 90 °C. The increase in k-values or reduction in δ-values and t_{50}-values with increased temperature suggested a higher bromelain inactivation rate at higher treatment temperatures.

It was also observed that a maximum increment of 1.11-fold in the k-value of the first-order model and 1.14-fold in the δ-value of the Weibull model for bromelain inactivation when the EFS increased from 30 to 40 V/cm at 90 °C, while the maximum increment of 1.13-fold in t_{50}-values was observed at 70 °C when EFS increased from 30 to 40 V/cm. The n-values of the Weibull model were found to be in the range of 0.812 to 0.991. The shape factor, $n < 1$, showed the curve's concave nature, explaining the ‘tailing phenomenon’ and suggesting heat-resistant fractions.

Table 4.17 Model parameters of different inactivation kinetic modelling of bromelain enzymes in COH-treated pineapple juice

Model	EFS (V/cm)	Parameters	Bromelain		
			70 °C	80 °C	90 °C
First order	30	k (min^{-1})	0.764 ± 0.072^{aA}	1.365 ± 0.070^{bA}	3.119 ± 0.183^{cA}
	35	k (min^{-1})	0.792 ± 0.113^{aA}	1.435 ± 0.144^{abA}	2.916 ± 0.202^{bA}
	40	k (min^{-1})	0.844 ± 0.044^{aA}	1.450 ± 0.110^{abA}	3.466 ± 0.326^{bA}
Weibull	30	δ (min)	1.351 ± 0.161^{cA}	0.751 ± 0.040^{bA}	0.307 ± 0.010^{aA}
		n	0.962 ± 0.032^{aA}	0.870 ± 0.015^{aA}	0.854 ± 0.070^{aA}
	35	δ (min)	1.309 ± 0.239^{bA}	0.713 ± 0.071^{abA}	0.331 ± 0.019^{aA}
		n	0.970 ± 0.057^{aA}	0.856 ± 0.074^{aA}	0.868 ± 0.042^{aA}
	40	δ (min)	1.194 ± 0.070^{cA}	0.706 ± 0.062^{bA}	0.270 ± 0.025^{aA}
		n	0.991 ± 0.013^{bA}	0.864 ± 0.028^{aA}	0.812 ± 0.020^{aA}
Logistic	30	A_{min}	0.000 ± 0.000	0.000 ± 0.000	0.063 ± 0.024
		t_{50}	0.929 ± 0.110^{bA}	0.476 ± 0.029^{aA}	0.213 ± 0.006^{aAB}
		P	1.186 ± 0.059^{aA}	1.221 ± 0.001^{aA}	2.326 ± 0.759^{aA}
	35	A_{min}	0.000 ± 0.000	0.000 ± 0.000	0.000 ± 0.000
		t_{50}	0.900 ± 0.161^{bA}	0.450 ± 0.060^{aA}	0.227 ± 0.006^{aB}
		P	1.205 ± 0.105^{aA}	1.223 ± 0.068^{aA}	1.578 ± 0.127^{aA}
	40	A_{min}	0.000 ± 0.000	0.000 ± 0.000	0.000 ± 0.000
		t_{50}	0.820 ± 0.048^{cA}	0.446 ± 0.033^{bA}	0.191 ± 0.010^{aA}
		P	1.245 ± 0.024^{aA}	1.239 ± 0.072^{aA}	1.591 ± 0.110^{aA}

Values in the same row with different small superscripts significantly ($p < 0.05$) different with change in temperature at constant EFS. Also, values in the same column with different capital superscripts are significantly ($p < 0.05$) different with a change in EFS at a constant temperature.

Since the n-values are closer to 1.0 and more than 50.0% of bromelain already got inactivated during the CUT period, this suggested the presence of a very minor fraction of heat-resistant bromelain enzymes. This was also supported by the A_{min} values of the logistic model where $A_{min} = 0$ suggested no tailing phenomenon, i.e., no heat-resistant fraction. The P-values of the logistic model were in the range of 1.186 to 2.326. Poh and Majid (2011) also studied the first-order reaction kinetics of free bromelain and bromelain-polyphenol complex in pineapple juice to study its thermal stability and studied the bromelain denaturation rate using model reaction rate constant. Similarly, Sriwatanapongse et al. (2000) also reported a pseudo-first-order reaction kinetic modelling for the thermal inactivation of bromelain in the temperature range of 55 to 67 °C. Jutamongkon and Charoenrein (2010) also described a first-order kinetic model for the thermal inactivation of fruit bromelain in the temperature range of 40 – 80 °C. On the

other hand, Chakraborty et al. (2016) observed a slight deviation from the log-linearity of fruit bromelain inactivation during isothermal treatment at 45 to 70 °C at 0.1 MPa.

The coefficient of determination, R^2, was greater than 0.990 for all the three models. Also, the RMSE of the first-order, Weibull, and logistic model were less than 0.0341, 0.0293, and 0.0230, respectively, and the SSE value was less than 0.0047, 0.0021, and 0.0014, respectively. Even though the logistic model's statistical parameters like RMSE and SSE were found to be least followed by the Weibull distribution and first-order model, they all were in acceptable range irrespective of the model.

Table 4.18 Goodness of fit parameters for different inactivation kinetic modelling of bromelain enzymes in continuous ohmic-treated pineapple juice

	EFS (V/cm)	Parameters	Bromelain		
			70 °C	80 °C	90 °C
First order	30	R^2	0.999	0.993	0.992
		RMSE ($\times10^{-2}$)	0.561	2.381	3.403
		SSE ($\times10^{-3}$)	0.152	2.268	4.633
	35	R^2	0.999	0.993	0.997
		RMSE ($\times10^{-2}$)	0.521	2.279	1.994
		SSE ($\times10^{-3}$)	0.164	2.407	1.666
	40	R^2	0.999	0.992	0.996
		RMSE ($\times10^{-2}$)	0.485	2.543	2.542
		SSE ($\times10^{-3}$)	0.122	2.668	2.609
Weibull	30	R^2	1.000	0.998	0.995
		RMSE ($\times10^{-2}$)	0.425	1.480	2.928
		SSE ($\times10^{-3}$)	0.050	0.525	2.080
	35	R^2	1.000	1.000	1.000
		RMSE ($\times10^{-2}$)	0.305	0.514	0.667
		SSE ($\times10^{-3}$)	0.061	0.151	0.065
	40	R^2	0.999	0.997	1.000
		RMSE ($\times10^{-2}$)	0.470	1.647	0.802
		SSE ($\times10^{-3}$)	0.158	0.639	0.187
Logistic	30	R^2	0.998	0.996	1.000
		RMSE ($\times10^{-2}$)	1.076	2.291	0.820
		SSE ($\times10^{-3}$)	0.278	1.347	0.144
	35	R^2	0.999	0.999	0.999
		RMSE ($\times10^{-2}$)	1.016	1.352	1.304
		SSE ($\times10^{-3}$)	0.248	0.365	0.484
	40	R^2	0.998	0.997	1.000
		RMSE ($\times10^{-2}$)	1.226	1.936	1.087
		SSE ($\times10^{-3}$)	0.404	1.110	0.239

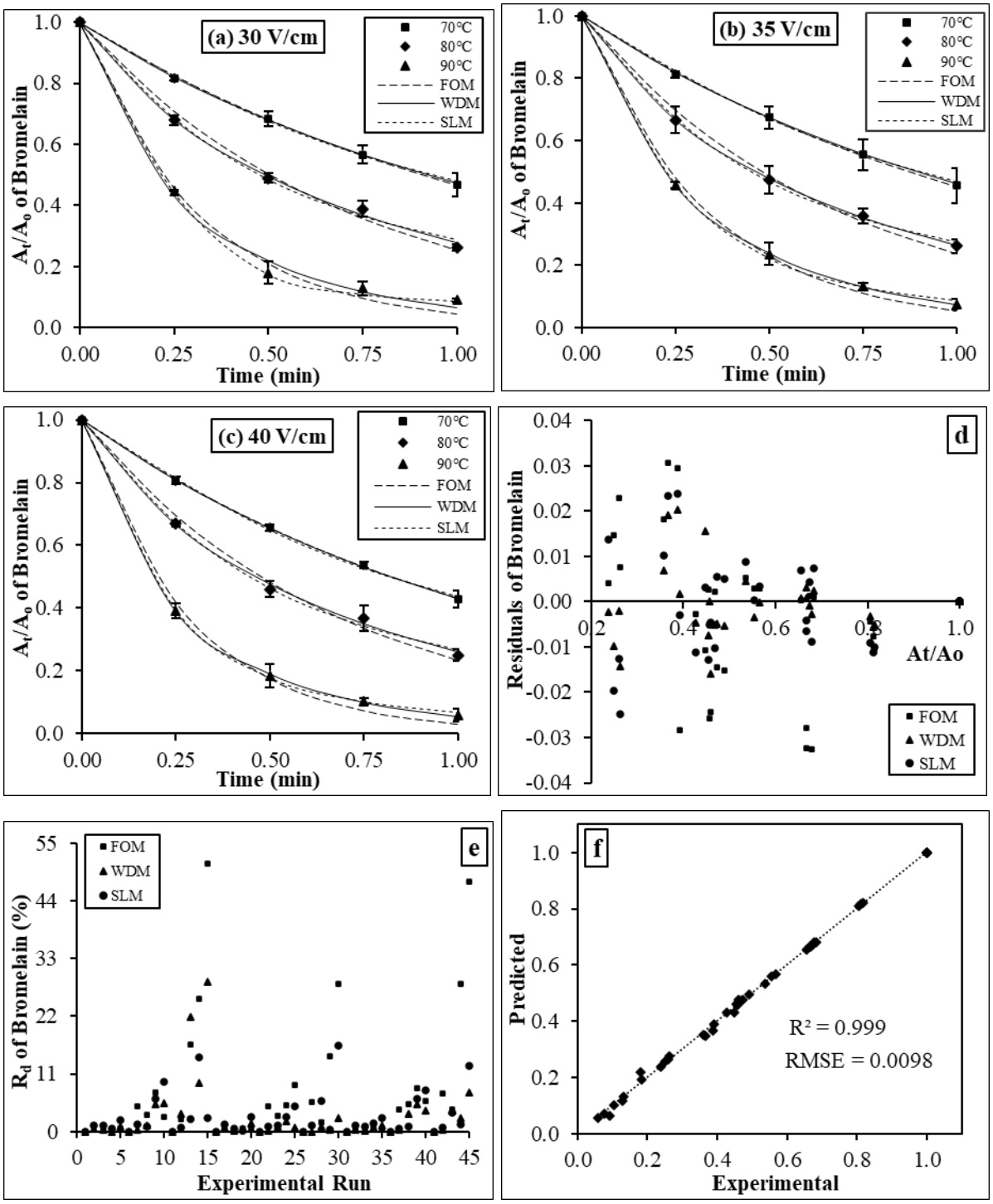

Fig. 4.31 Model curve fitting of experimental and predicted values of bromelain enzymes at EFS (a) 30 V/cm, (b) 35 V/cm, and (c) 40 V/cm, (d) residual plot of bromelain inactivation, (e) relative deviation plot of bromelain inactivation, (f) predicted vs experimental residual activity of bromelain using Weibull distribution model. Where FOM, WDM, and SLM are first-order model, Weibull distribution model, and sigmoidal logistic model, respectively

Thus, the goodness of fit parameters alone was insufficient in comparing and selecting the best kinetic model for bromelain inactivation during COH-assisted isothermal treatment of

pineapple juice. So, to distinguish and rank the several competing models, parameters like accuracy factor (A_f), bias factor (B_f), and Akaike information theory were employed to validate the models' performance and select the best-fit model for bromelain inactivation.

4.5.3.3 Validation of bromelain inactivation kinetic models

Accuracy factor (A_f) and bias factor (B_f) were used to validate the performance of the kinetic models of the bromelain inactivation, as shown in Table 4.19 (Pipliya et al., 2022; Vega et al., 2016). The A_f of the first-order, Weibull distribution, and logistic model of bromelain inactivation ranged from 1.005 to 1.268, 1.004 to 1.143, and 1.010 to 1.046, respectively.

Table 4.19 Model validation of bromelain inactivation using accuracy factor (A_f) and bias factor (B_f)

EFS (V/cm)	T (°C)	Models					
		First Order		Weibull Distribution		Logistic	
		A_f	B_f	A_f	B_f	A_f	B_f
30	70	1.005	1.000	1.004	1.003	1.010	1.003
	80	1.038	0.994	1.025	1.003	1.036	1.006
	90	1.268	0.847	1.143	0.947	1.043	0.959
35	70	1.004	0.999	1.006	1.006	1.010	1.007
	80	1.045	0.987	1.008	0.999	1.020	1.003
	90	1.118	0.914	1.008	0.996	1.046	1.022
40	70	1.005	1.000	1.005	1.001	1.013	1.002
	80	1.049	0.989	1.026	1.003	1.032	1.005
	90	1.244	0.827	1.030	0.986	1.036	1.015

It was observed that in 88.9% of the treatment conditions, the Weibull model had a comparatively better A_f value (closest to the simulation line) compared to the logistic model (11.1%) and the first-order model (0%). The B_f of the Weibull model for bromelain inactivation was found to be better and closest to the simulation line (close to 1) (Table 4.19). It was observed that in 55.6% of the treatment conditions, the Weibull model showed better B_f (values closest to 1) followed by first-order (33.3%) and logistic model (11.1%). Thus, the A_f and B_f parameters suggested that the Weibull distribution model better predicted bromelain inactivation in COH-treated pineapple juice (Pipliya et al., 2022; Vega et al., 2016).

4.5.3.4 Model selection for bromelain inactivation kinetic using AIC and statistical parameters

The AIC and Δ_i values of all three models for bromelain inactivation were calculated and are summarised in Table 4.20. The logistic model observed the highest AIC values for each

treatment condition, followed by the Weibull and first-order model. Also, the logistic model obtained $\Delta_i > 3.9$ (close to or greater than 4), and therefore, this model showed less significant support and should not be considered for model selection (Pipliya et al., 2022; Vega et al., 2016). On the other hand, the Weibull model obtained $\Delta_i \leq 2$ and, therefore, showed significant support and should be considered while making inferences for model selection. The first-order model obtained $\Delta i = 0$, so this model should be the primary choice for prediction purposes. The Akaike increment criteria (Δ_i) is an easy tool to discriminate, rank, and compare several competing models, but this should not be used in isolation for model selection as the AIC penalizes the models more with a higher number of parameters (Vega et al., 2016). So, to select the best-fit model, Δ_i should be used along with statistical parameters.

Table 4.20 Model selection for bromelain inactivation by AIC and Akaike increment (Δ_i)

EFS (V/cm)	T (°C)	Models					
		First Order		Weibull Distribution		Logistic	
		AIC	Δi	AIC	Δi	AIC	Δi
30	70	-6.05	0.00	-4.05	2.00	-2.05	4.00
	80	-6.04	0.00	-4.04	1.99	-2.04	4.00
	90	-6.03	0.00	-4.03	1.99	-2.05	3.98
35	70	-6.05	0.00	-4.05	2.00	-2.05	4.00
	80	-6.04	0.00	-4.05	1.99	-2.05	3.99
	90	-6.04	0.00	-4.05	1.99	-2.05	3.99
40	70	-6.05	0.00	-4.05	2.00	-2.05	4.00
	80	-6.03	0.00	-4.04	1.99	-2.04	3.99
	90	-6.03	0.00	-4.05	1.99	-2.05	3.99

The Weibull distribution model showed better accuracy and bias factor (Table 4.19) with comparatively lower RMSE values (0.003 to 0.029) (Table 4.18) and residuals (-0.039 to 0.026) (Fig. 4.31) than the first order model (RMSE = 0.005 to 0.034; residuals = -0.033 to 0.046). So, the parameters Δ_i, A_f, B_f, R^2, RMSE, and residuals suggested that the Weibull distribution model should be the primary choice for predicting bromelain inactivation in COH-treated pineapple juice.

4.6 Effect of COH on total microbial load reduction and kinetic modelling

4.6.1 Effect of COH on total microbial load reduction

The effect of treatment temperature and time at different EFS (30 to 40 V/cm) on the total microbial load reduction is shown in Fig. 4.32. A significant ($p < 0.05$) reduction in the total microbial load was observed during the CUT period that ranged from 2.40 ± 0.05 to 2.93 ±

0.00 log CFU/mL from an initial microbial load of 6.00 ± 0.06 log CFU/mL. During isothermal treatment, a significant ($p < 0.05$) reduction in total microbial load was observed with increased treatment time. Microbial inactivation increased significantly ($p < 0.05$) from 2.84 ± 0.04 log CFU/mL to 4.29 ± 0.08 log CFU/mL at 90 °C when the treatment time increased from 0 s to 60 s at an EFS of 40 V/cm. Similar results were observed at other EFS and temperatures. A minimum microbial load of 1.65 ± 0.07 log CFU/mL was observed at 90 °C after 60 s treatment at 40 V/cm. Several studies also reported the efficacy of ohmic heating in microbial inactivation (Makroo et al., 2020; Abedelmaksoud et al., 2019; Kanjanapongkul and Baibua, 2021; Rodriguez et al., 2021). Makroo et al. (2020) reviewed the effectiveness of OH in sugarcane juice processing in which the total plate count was reduced to 3.47 log CFU/mL at 90 °C from an initial load of 6.3 log CFU/mL when treated for 15.0 min.

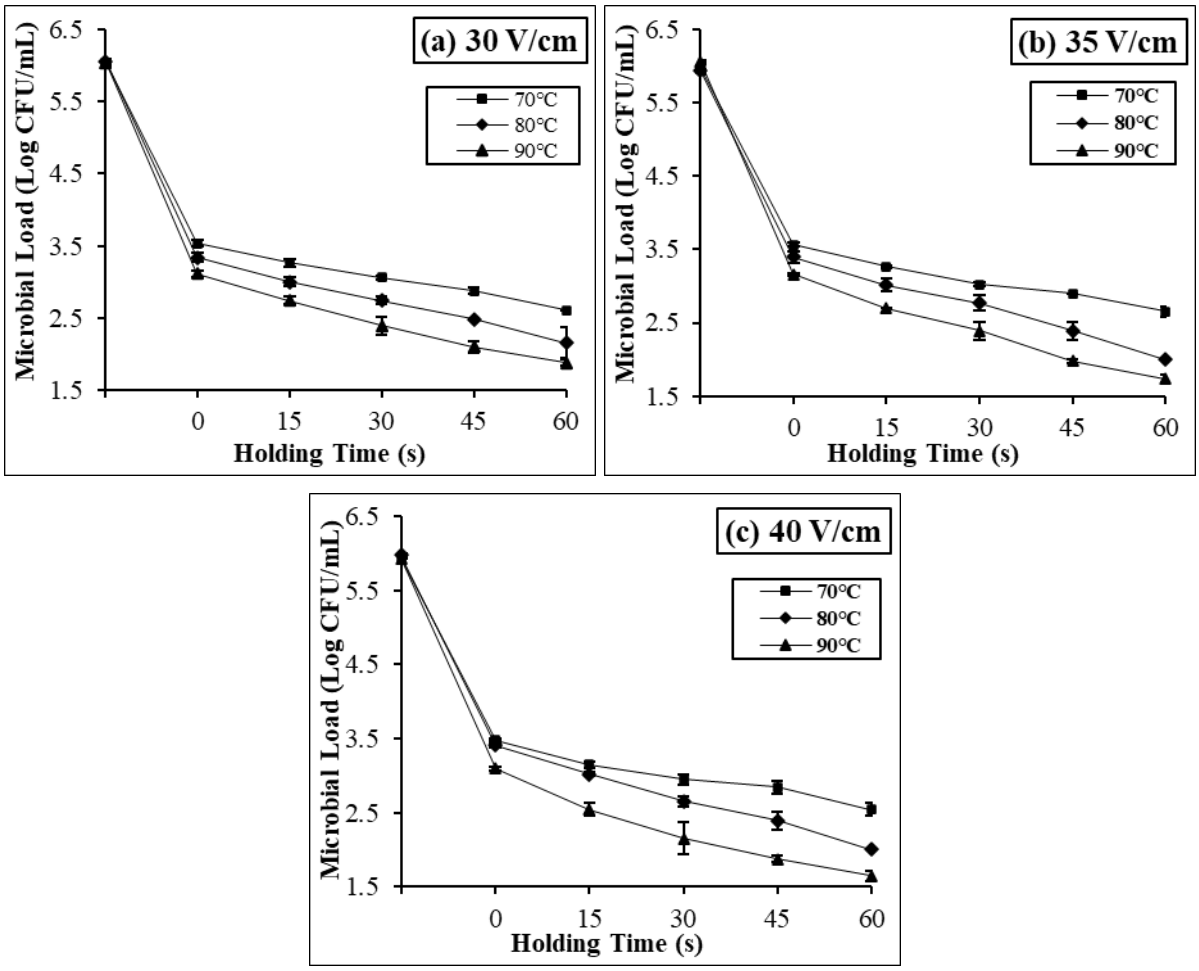

Fig. 4.32 Effect of continuous ohmic heating on microbial inactivation at EFS (a) 30 V/cm, (b) 35 V/cm, and (c) 40 V/cm

Lee et al. (2012) reported a reduction of 1.32 log CFU/mL and more than 6.52 log CFU/mL *Salmonella typhimurium* when orange juice was treated in COH for 60 s and 90 s, respectively.

They reached an undetectable level when treated for 180 s at 30 V/cm. In contrast, *Listeria monocytogenes* inactivation in orange juice increased from 1.23 log to 5.1 log reduction when the treatment time increased from 1.0 min to 2.5 min during OH at 35 V/cm (Makroo et al., 2020). These findings suggested that the processing time greatly affected the microbial load, which was in accordance with the present study.

A significant ($p < 0.05$) reduction in the microbial load was observed with an increase in temperature from 70 °C to 90 °C during the CUT period and isothermal holding. Microbial inactivation increased significantly from 2.47 ± 0.01 log CFU/mL at 70 °C to 2.84 ± 0.04 log CFU/mL at 90 °C at a constant EFS of 40 V/cm during the CUT period. At the same time, the microbial reduction increased from 3.40 ± 0.08 log CFU/mL at 70 °C to 4.29 ± 0.08 log CFU/mL at 90 °C at a similar EFS of 40 V/cm when the juice was isothermally treated for 60 s. Similar observations were made in other treatment conditions. Hashemi et al. (2019) also reported a negative effect of treatment temperature on the microbial population.

Similarly, the *Enterobacteriaceae* reduced significantly with an increase in temperature from an initial load of 2.7 log CFU/g to 1.6 log CFU/g at 70 °C and further to an undetectable limit (< 1.0 log CFU/g) at 90 °C during OH of Chilean blue mussels (Bastias et al., 2015). Also, at a constant temperature and treatment time, EFS positively affected the microbial inactivation, i.e., the microbial inactivation was increased with an increase in the applied EFS across the juice. The main reason for microbial inactivation was the thermal effect leading to cell membrane destruction during OH. However, the non-thermal effect due to the electric field also influenced microbial growth inhibition through chemical and mechanical effects (Doan et al., 2023). The mechanical effects mainly resulted in the rupture or disruption of cell membranes through electroporation that leads to the release of inner cellular contents, resulting in microbial inhibition, while the chemical effects lead to the formation of free radicals and ions, resulting in microbial inactivation (Alkanan et al., 2021; Saxena et al., 2016). During electroporation, in the presence of an electric field during OH, the electrically charged intercellular compounds in microorganisms are attracted to the opposite polarity. The membrane conductance increases intensely when the applied EFS exceeds the cell membrane's elastic limit, resulting in pore formation and changes in cell permeability, ultimately leading to microbial death (Doan et al., 2023; Makroo et al., 2020). Similarly, Wagner et al. (2020) concluded that the non-thermal effect of electroporation on microbial cells during OH occurs in a specific temperature range, i.e., thermal effect (protein denaturation) and non-thermal effect (electroporation) occur at lower processing temperature, whereas after a threshold temperature microbial inactivation occur only due to the thermal effect.

4.6.2 Inactivation kinetic modelling of microorganisms

The model parameters and goodness of fit parameters of the first-order modified Gompertz and Weibull distribution models for microbial inactivation are shown in Table 4.21 and Table 4.22, respectively. The reaction rate constant (k) of the first-order model was increased significantly ($p < 0.05$) with an increase in temperature at any constant EFS.

Table 4.21 Model parameters of different inactivation kinetic modelling of microbial load in COH-treated pineapple juice.

Model	EFS (V/cm)	Parameters	Microbial load		
			70 °C	80 °C	90 °C
First order	30	k (min^{-1})	2.134 ± 0.068^{aA}	2.547 ± 0.119^{bA}	3.019 ± 0.066^{cA}
	35	k (min^{-1})	2.150 ± 0.175^{aA}	3.139 ± 0.022^{bAB}	3.454 ± 0.240^{bA}
	40	k (min^{-1})	2.162 ± 0.182^{aA}	3.245 ± 0.259^{bB}	3.654 ± 0.150^{bA}
Modified Gompertz	30	A	1.300 ± 0.139^{aA}	1.168 ± 0.105^{aA}	1.400 ± 0.117^{aA}
		k_{max} (min^{-1})	1.026 ± 0.037^{aA}	1.357 ± 0.053^{abA}	1.662 ± 0.175^{bA}
		t_S (min)	0.048 ± 0.014^{aB}	0.035 ± 0.015^{aA}	0.052 ± 0.002^{aA}
	35	A	1.037 ± 0.136^{aA}	2.418 ± 0.861^{aA}	1.684 ± 0.066^{aA}
		k_{max} (min^{-1})	1.069 ± 0.060^{aA}	1.631 ± 0.107^{abA}	1.799 ± 0.225^{bA}
		t_S (min)	0.014 ± 0.003^{aAB}	0.111 ± 0.068^{aA}	0.041 ± 0.005^{aA}
	40	A	1.176 ± 0.008^{aA}	1.954 ± 0.474^{aA}	1.490 ± 0.037^{aA}
		k_{max} (min^{-1})	0.999 ± 0.110^{aA}	1.672 ± 0.272^{aA}	2.245 ± 0.506^{aA}
		t_S (min)	0.000 ± 0.000^{aA}	0.068 ± 0.010^{aA}	0.034 ± 0.048^{aA}
Weibull	30	δ (min)	1.105 ± 0.054^{bA}	0.941 ± 0.068^{abB}	0.756 ± 0.023^{aB}
		n	0.935 ± 0.043^{aB}	0.793 ± 0.058^{aA}	0.830 ± 0.072^{aA}
	35	δ (min)	1.171 ± 0.142^{bA}	0.737 ± 0.003^{aAB}	0.645 ± 0.063^{aAB}
		n	0.793 ± 0.037^{aA}	1.049 ± 0.127^{aA}	0.837 ± 0.064^{aA}
	40	δ (min)	1.162 ± 0.119^{bA}	0.704 ± 0.068^{aA}	0.565 ± 0.027^{aA}
		n	0.784 ± 0.011^{abA}	0.933 ± 0.083^{bA}	0.663 ± 0.033^{aA}

Values in the same row with different small superscripts significantly ($p < 0.05$) different with change in temperature at constant EFS. Also, values in the same column with different capital superscripts are significantly ($p < 0.05$) different with a change in EFS at a constant temperature.

The k-value increased from 2.134 ± 0.068 min^{-1} at 70 °C, 30 V/cm to a maximum of 3.654 ± 0.150 min^{-1} when the temperature and EFS increased to 90 °C and 40 V/cm, respectively. The k-value increased by 1.69-fold when the temperature was increased from 70 °C to 90 °C at constant EFS 40 V/cm. The k-value also increased numerically with an increase in applied EFS from 30 to 40 V/cm, but the increment was mainly non-significant ($p > 0.05$). A maximum of 1.27-fold increment in k-value was observed when the EFS was increased from 30 to 40 V/cm at a constant treatment temperature of 80 °C. Although the first-order kinetic model or linear

model for microbial inactivation is an old method and is still in use. In this model, all the members in a population have equal probability of dying which is not likely possible for genetic and probabilistic reasons. Also, most of the survival curves of microbial inactivation are either concave or convex in nature (Buzrul, 2022). For this reason, several non-linear survival curves for microbial inactivation are developed over the years including the Weibull distribution model, the modified Gompertz model, and many others (Buzrul, 2022; Silva et al., 2021; Schottroff et al., 2019; Shao et al., 2019; Pereira et al., 2020). The Weibull model is just a simple alternative to the first-order kinetic model that can be used to describe concave, convex, and linear survival curves for microbial inactivation (Buzrul, 2022).

The scale factor (δ) of the Weibull model decreased significantly ($p < 0.05$) with an increase in temperature, suggesting a higher microbial inactivation rate at higher treatment temperatures. The δ-values of the Weibull model increased a maximum of 2.06-fold when the temperature increased from 70 °C to 90 °C at a constant EFS of 40 V/cm. Significant ($p < 0.05$) reduction in the δ-value (1.34-fold) was also observed with an increase in EFS from 30 to 40 V/cm at a constant treatment temperature of 80 °C and 90 °C, suggesting a positive relation of microbial inactivation with an increase in EFS. The n-values of the Weibull model were found to be in the range of 0.663 to 1.049. The shape factor (n) in almost all the conditions except at 35 V/cm and 80 °C was found to be > 1, which showed the concave nature of the curve (Fig. 4.33), which explained the 'tailing phenomenon' and suggested the presence of heat-resistant fractions. Pereira et al. (2020) also reported a good fit of the Weibull model with better R^2 and RMSE values for the inactivation kinetics of *Listeria monocytogenes* in ohmic-treated whey dairy beverages. Similarly, Schottroff et al. (2019) also observed a similar goodness of fit of the Weibull model during the inactivation of wild-type *B. subtilis* PS533 spores during ohmic and conventional heat treatment. Similarly, Silva et al. (2021) also showed an excellent fit of the Weibull model to the experimental data of all the conditions for survival kinetics of *Listeria monocytogenes* in ohmic heating processed milk. Chen (2007) compared the linear model with the Weibull model to study the inactivation kinetics of foodborne pathogens in milk and observed a better fit of the Weibull model to the inactivation data than a linear model.

Table 4.22 Goodness of fit parameters for different inactivation kinetic modelling of microbial load reduction in continuous ohmic-treated pineapple juice

	EFS (V/cm)	Parameters	Bromelain		
			70 °C	80 °C	90 °C
First order	30	R^2	0.994	0.980	0.984
		RMSE ($\times 10^{-1}$)	0.282	0.567	0.594
		SSE ($\times 10^{-1}$)	0.032	0.130	0.159
	35	R^2	0.975	0.991	0.983
		RMSE ($\times 10^{-1}$)	0.554	0.490	0.750
		SSE ($\times 10^{-1}$)	0.124	0.106	0.226
	40	R^2	0.964	0.989	0.932
		RMSE ($\times 10^{-1}$)	0.658	0.558	1.508
		SSE ($\times 10^{-1}$)	0.173	0.125	0.911
Modified Gompertz	30	R^2	0.981	0.990	0.994
		RMSE ($\times 10^{-1}$)	0.690	0.575	0.550
		SSE ($\times 10^{-1}$)	0.096	0.066	0.062
	35	R^2	0.973	0.987	0.986
		RMSE ($\times 10^{-1}$)	0.819	0.875	0.912
		SSE ($\times 10^{-1}$)	0.139	0.154	0.172
	40	R^2	0.954	0.984	0.975
		RMSE ($\times 10^{-1}$)	1.055	0.920	1.054
		SSE ($\times 10^{-1}$)	0.223	0.185	0.316
Weibull	30	R^2	0.995	0.998	0.997
		RMSE ($\times 10^{-1}$)	0.275	0.183	0.310
		SSE ($\times 10^{-1}$)	0.024	0.012	0.034
	35	R^2	0.992	0.994	0.994
		RMSE ($\times 10^{-1}$)	0.351	0.480	0.464
		SSE ($\times 10^{-1}$)	0.045	0.074	0.078
	40	R^2	0.981	0.992	0.984
		RMSE ($\times 10^{-1}$)	0.541	0.512	0.848
		SSE ($\times 10^{-1}$)	0.088	0.087	0.226

Apart from the Weibull model, several studies also showed the suitability and better accuracy of the modified Gompertz model for fitting the survival curves of microbial inactivation (Vega et al., 2016; Shao et al., 2019). The maximum inactivation rate constant (k_{max}) of the modified Gompertz model was increased significantly ($p < 0.05$) with an increase in temperature (Table 4.21), suggesting a higher microbial inactivation rate at a higher treatment temperature. A maximum of 2.25-fold increment in the k_{max} value was observed when the temperature was increased from 70 °C to 90 °C at a constant EFS of 40 V/cm.

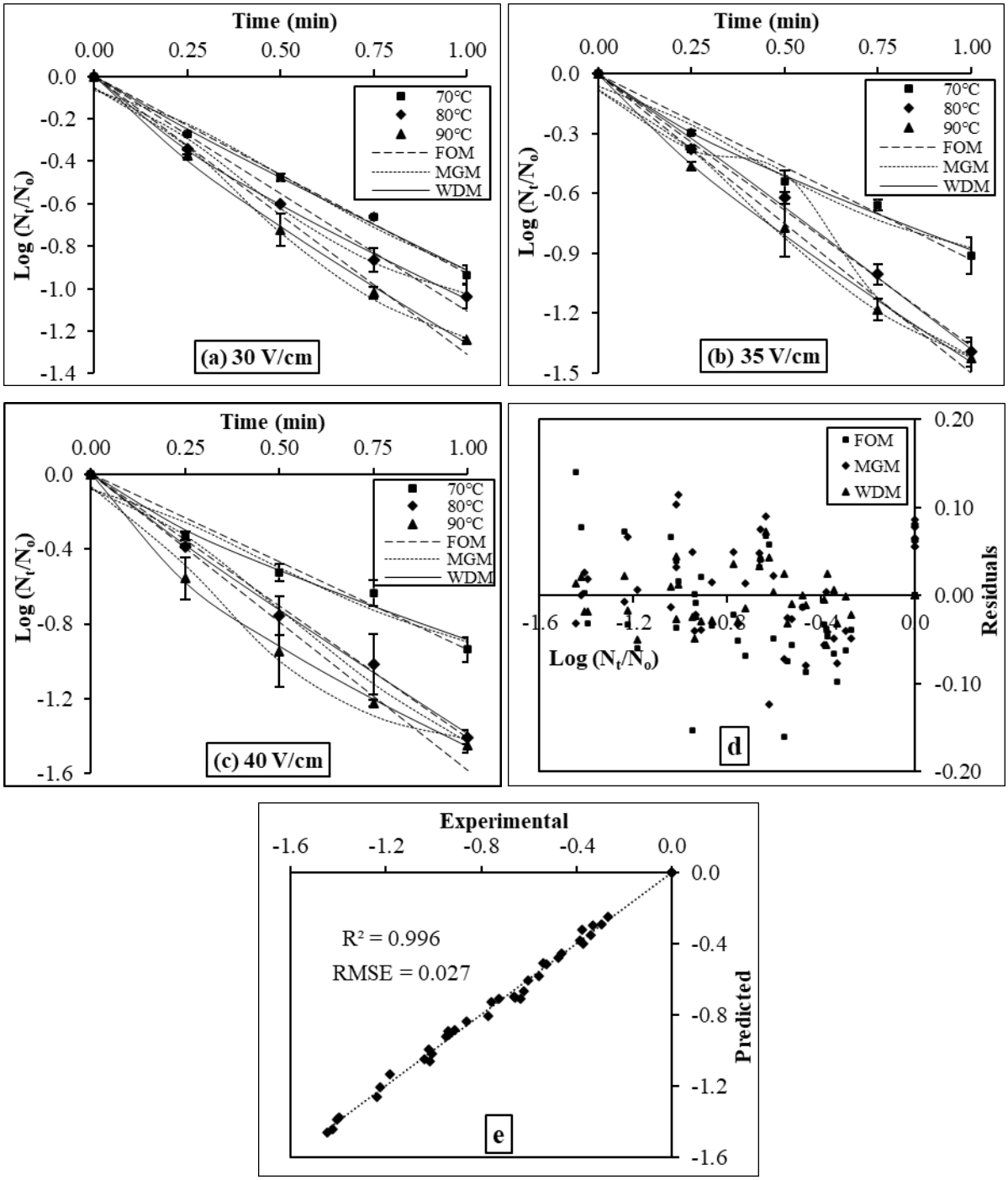

Fig. 4.33 Model curve fitting of experimental and predicted values of microbial load reduction at EFS (a) 30 V/cm, (b) 35 V/cm, and (c) 40 V/cm, (d) residual plot of microbial load reduction, and (e) predicted vs experimental microbial load reduction using Weibull distribution model. FOM, MGM, and WDM are the first-order, modified Gompertz and Weibull distribution models, respectively.

Similarly, k_{max} values also increased numerically but were statistically non-significant ($p > 0.05$) with an increase in EFS from 30 to 40 V/cm at a constant temperature of 80 °C and 90 °C. A 1.35-fold increment in k_{max} value was observed when the EFS was increased from 30 to 40 V/cm at a constant treatment temperature of 90 °C. The duration of the lag phase time

parameter, t_s, was in the range of 0.000 to 0.111 min, and the asymptote value for the time approaching infinity, A-value, was in the range of 1.037 to 2.418, as shown in Table 4.21. The t_s values should decrease with an increase in the treatment temperature as it is indirectly related to temperature, but in the current study, the trend was unclear. Therefore, the modified Gompertz model needs further consideration before selection.

The R^2 was ≥ 0.932, 0.954, and 0.981 for the first-order, modified Gompertz and Weibull distribution models, respectively. Also, the RMSE of the first-order modified Gompertz and Weibull distribution model was found to be less than 0.151, 0.106, and 0.085, respectively, and the SSE value was less than 0.092, 0.032, and 0.023, respectively as shown in Table 4.22. Even though the statistical parameters like R^2, RMSE, and SSE showed that the Weibull distribution was the best-fit model followed by modified Gompertz and first-order model, they all were in acceptable range irrespective of the model. Thus, the goodness of fit parameters alone was insufficient in comparing and selecting the best kinetic model for microbial inactivation. Therefore, statistical parameters like accuracy factor (A_f), bias factor (B_f), and Akaike information theory were employed to validate the performance and select the best fit kinetic model.

4.6.3 Validation of microbial inactivation kinetic model

Accuracy factor (A_f) and bias factor (B_f) were used to validate the performance of the kinetic models of microbial inactivation, as shown in Table 4.23 (Pipliya et al., 2022; Vega et al., 2016). The A_f of the microbial inactivation ranged from 1.051 to 1.172, 1.044 to 1.130, and 1.017 to 1.073, respectively, for the first-order, modified Gompertz and Weibull distribution model. Weibull distribution model showed the highest A_f in 88.9% of the treatment conditions, followed by the first order (11.1%). On the other hand, if the comparison was made between the first-order and modified Gompertz models only, then the modified Gompertz showed better A_f in 66.7% of the treatment conditions. At the same time, the first-order model showed better A_f in only 33.3% of the treatment conditions.

Similarly, the B_f of the Weibull distribution model was better compared to other models and was closest to the simulation line (close to 1) (Table 4.23). The Weibull model showed better B_f in almost 88.9% of the overall treatment conditions, followed by the first-order model (11.1%). Among the first-order and modified Gompertz models, only the modified Gompertz model showed better B_f in 77.8% of the treatment conditions. The first-order model showed better B_f in only 22.2% of the treatment conditions. Thus, the accuracy and bias factor study

suggested that the Weibull distribution showed better accuracy for predicting microbial inactivation in COH-treated pineapple juice.

Table 4.23 Model validation for microbial inactivation using accuracy factor (A_f) and bias factor (B_f)

EFS (V/cm)	T (°C)	Models					
		First Order		Modified Gompertz		Weibull Distribution	
		A_f	B_f	A_f	B_f	A_f	B_f
30	70	1.062	0.964	1.082	0.957	1.041	0.985
	80	1.106	0.933	1.056	0.973	1.017	1.000
	90	1.084	0.949	1.044	0.982	1.033	1.009
35	70	1.124	0.928	1.090	0.968	1.041	0.992
	80	1.060	0.995	1.093	0.978	1.065	0.976
	90	1.089	0.943	1.067	0.971	1.032	0.999
40	70	1.151	0.915	1.130	0.946	1.073	0.985
	80	1.051	0.971	1.082	0.979	1.027	0.995
	90	1.172	0.894	1.068	0.986	1.023	1.003

4.6.4 Model selection for microbial inactivation kinetic using AIC and statistical parameters

The AIC and Δ_i value of the first-order, modified Gompertz, and Weibull distribution model for microbial inactivation kinetic are summarised in Table 4.24. The modified Gompertz model observed the highest AIC values for each treatment condition, followed by the Weibull distribution and first-order model. Also, the modified Gompertz model obtained $\Delta_i \geq 3.77$, which was closer to 4, and therefore, this model showed less significant support for its selection (Pipliya et al., 2022; Vega et al., 2016). On the other hand, the Weibull distribution model obtained $\Delta_i \leq 2$ and showed significant support and should be considered while making inferences for model selection. The first-order model obtained $\Delta i = 0$, so this model should be the primary choice for prediction purposes. The Akaike increment criteria (Δ_i) is an easy tool to discriminate, rank, and compare several competing models, but this should not be used in isolation for model selection as the AIC penalise the models more with a higher number of parameters (Pipliya et al., 2022; Vega et al., 2016). So, to select the best-fit model, the Δ_i should be used along with other statistical parameters.

Therefore, the Weibull distribution model should be the primary choice based on Δ_i, supported by better A_f and B_f values (Table 4.23) than other models. The Weibull model also observed

lower residuals (-0.056 to 0.073) than the first-order (-0.160 to 0.141) and modified Gompertz model (-0.124 to 0.115), as shown in Fig. 4.33.

Table 4.24 Model selection for microbial inactivation by AIC and Akaike increment (Δ_i)

EFS (V/cm)	T (°C)	Models					
		First Order		Modified Gompertz		Weibull Distribution	
		AIC	Δi	AIC	Δi	AIC	Δi
30	70	-3.53	0.00	0.48	4.01	-1.54	2.00
	80	-3.50	0.00	0.47	3.96	-1.54	1.95
	90	-3.49	0.00	0.47	3.96	-1.54	1.95
35	70	-3.50	0.00	0.49	3.99	-1.53	1.97
	80	-3.52	0.00	0.57	4.09	-1.52	2.00
	90	-3.47	0.00	0.49	3.97	-1.53	1.95
40	70	-3.48	0.00	0.52	4.00	-1.51	1.97
	80	-3.52	0.00	0.52	4.04	-1.53	1.99
	90	-3.27	0.00	0.51	3.77	-1.54	1.73

The overall relative deviation, R_d, of the Weibull model was less than 3.8%, while the first-order and modified Gompertz model observed more than 7.2%. Also, the overall R^2 and RMSE of the Weibull model were 0.996 and 0.027, respectively, which was comparatively better than the other two models. Thus, AIC and statistical parameters suggested the Weibull distribution model as the first preference for predicting microbial inactivation in COH-treated pineapple juice.

4.7 Effect of COH on vitamin C content and degradation kinetic modelling

4.7.1 Effect of COH on vitamin C content

The initial vitamin C content in the untreated juice was 7.38 ± 0.12 mg/100 mL. The effect of treatment time and temperature at different EFS on the vitamin C content of the pineapple juice is shown in Fig. 4.34. Significant ($p < 0.05$) loss of vitamin C occurred at 90 °C, but non-significant ($p > 0.05$) change was observed at 70 °C and 80 °C during the CUT period. A maximum of one-fourth of the vitamin C degradation occurred during the CUT period at 90 °C, 35 V/cm. Also, a significant ($p < 0.05$) effect of treatment time and temperature was observed on vitamin C degradation during isothermal treatment. It was reduced significantly to 63.3 ± 4.7%, 55.6 ± 0.0%, and 45.5 ± 0.0%, respectively, at 70 °C, 80 °C and 90 °C from the initial concentration when the juice was treated for 60 s at 30 V/cm. Similar trends were observed at 35 V/cm and 40 V/cm at each treatment temperature and holding time. Vitamin C content reached a minimum level of 2.82 ± 0.15 mg/100 mL, i.e., 38.2 ± 2.6% retention was

observed when the juice was treated at 90 °C for 60 s at 40 V/cm. The significant ($p < 0.05$) reduction in vitamin C content agrees with Abedelmaksoud et al. (2018), who also observed a significant decrease in ascorbic acid during ohmic heating of apple juice from an initial content of 4.49 ± 0.24 mg/100 mL to 1.92 ± 0.28 mg/100 mL at 80 °C, 40 V/cm. The study also agrees with Saxena et al. (2016), who observed a significant reduction in ascorbic acid during ohmic heating of sugarcane juice.

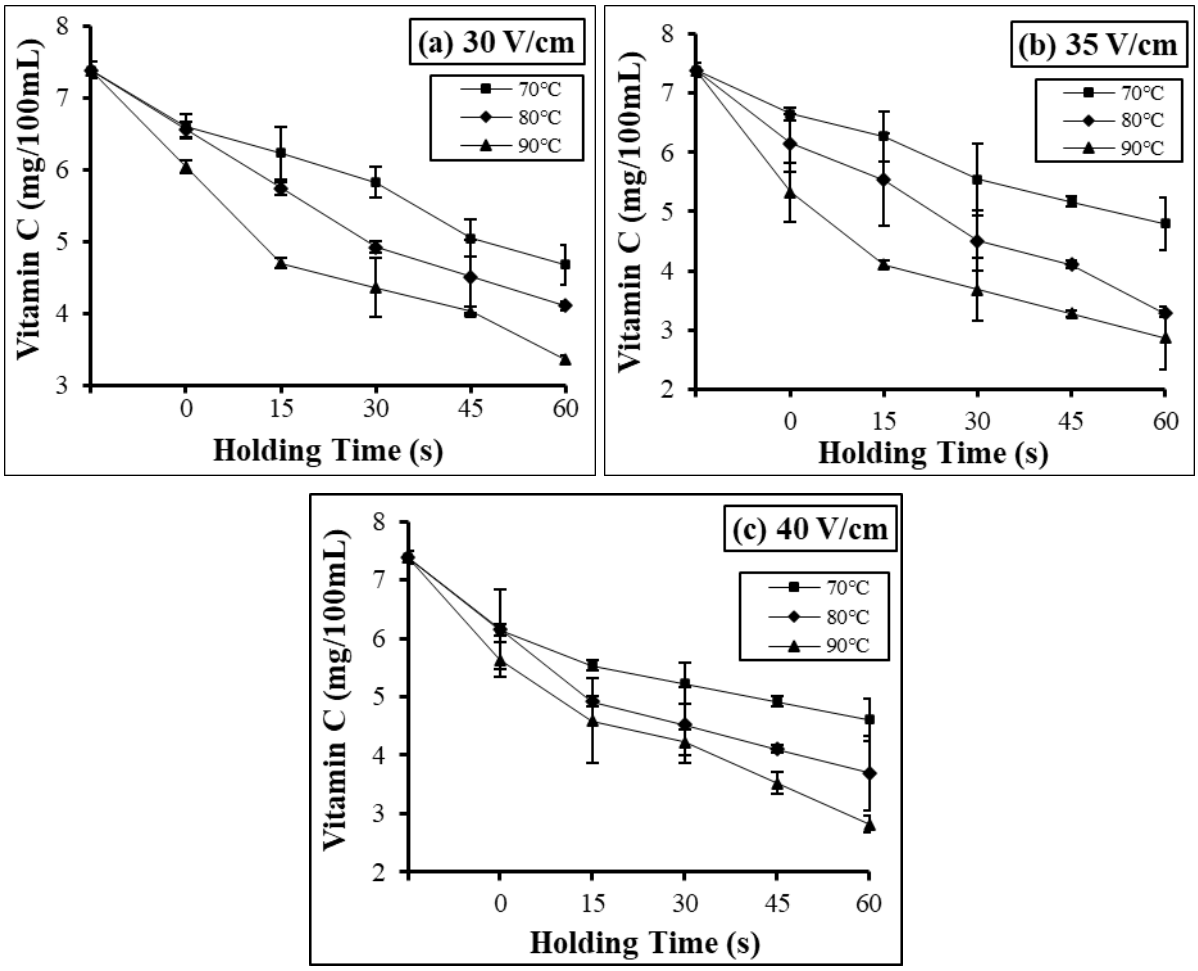

Fig. 4.34 Effect of continuous ohmic heating on vitamin C content at EFS (a) 30 V/cm, (b) 35 V/cm, and (c) 40 V/cm

The main reason for vitamin C degradation during ohmic heating was chemical decomposition due to heating temperature and processing time (Abedelmaksoud et al., 2019). Also, temperature, oxygen, metal catalysts, pH, enzymes, and light affect its degradation, while during ohmic heating, the strength of the electric field and frequency below 100 Hz significantly affected the degradation of vitamin C (Doan et al., 2023; Alkanan et al., 2021).

4.7.2 Degradation kinetic modelling of vitamin C

The model and goodness of fit parameters of different kinetic models of vitamin C degradation are shown in Table 4.25 and Table 4.26, respectively. The reaction rate constant (k) of the first-order model was significantly ($p < 0.001$) affected by the treatment conditions, while a non-significant ($p > 0.05$) effect was observed in the model parameters of the Weibull distribution and logistic models.

Table 4.25 Model parameters of different degradation kinetic modelling of vitamin C in COH-treated pineapple juice.

Model	EFS (V/cm)	Parameters	Vitamin C		
			70 °C	80 °C	90 °C
First order	30	k (min^{-1})	0.328 ± 0.041^{aA}	0.503 ± 0.055^{abA}	0.611 ± 0.042^{cA}
	35	k (min^{-1})	0.330 ± 0.038^{aA}	0.582 ± 0.050^{bA}	0.679 ± 0.017^{bA}
	40	k (min^{-1})	0.304 ± 0.073^{aA}	0.562 ± 0.022^{bA}	0.657 ± 0.029^{bA}
Weibull	30	δ (min)	2.188 ± 0.052^{aA}	2.421 ± 0.412^{aA}	2.652 ± 0.357^{aA}
		n	1.322 ± 0.088^{bA}	0.845 ± 0.031^{aA}	0.641 ± 0.115^{aA}
	35	δ (min)	2.899 ± 1.059^{aA}	1.717 ± 0.636^{aA}	2.617 ± 1.342^{aA}
		n	1.097 ± 0.229^{aA}	1.149 ± 0.432^{aA}	0.660 ± 0.301^{aA}
	40	δ (min)	6.108 ± 3.084^{aA}	3.865 ± 2.401^{aA}	1.636 ± 0.380^{aA}
		n	0.745 ± 0.076^{aA}	0.638 ± 0.291^{aA}	0.981 ± 0.341^{aA}
Logistic	30	A_{min}	0.375 ± 0.530^{aA}	0.271 ± 0.383^{aA}	0.000 ± 0.000^{a}
		t_{50}	1.128 ± 0.887^{aA}	1.162 ± 1.046^{aA}	1.583 ± 0.026^{aA}
		P	10.075 ± 12.283^{aA}	1.467 ± 0.746^{aA}	0.754 ± 0.115^{aA}
	35	A_{min}	0.389 ± 0.550^{aA}	0.137 ± 0.194^{aA}	0.000 ± 0.000^{a}
		t_{50}	1.054 ± 0.993^{aA}	1.097 ± 0.559^{aA}	1.402 ± 0.384^{aA}
		P	11.254 ± 13.953^{aA}	1.564 ± 0.823^{aA}	0.795 ± 0.356^{aA}
	40	A_{min}	0.000 ± 0.000^{aA}	0.000 ± 0.000^{aA}	0.000 ± 0.000^{a}
		t_{50}	4.455 ± 2.272^{aA}	2.077 ± 0.827^{aA}	1.126 ± 0.134^{aA}
		P	0.816 ± 0.097^{aA}	0.747 ± 0.333^{aA}	1.166 ± 0.415^{aA}

Values in the same row with different small superscripts significantly ($p < 0.05$) different with change in temperature at constant EFS. Also, values in the same column with different capital superscripts are significantly ($p < 0.05$) different with a change in EFS at a constant temperature.

At 30 V/cm, the k-values of the first-order model increased 1.86-fold when the treatment temperature increased from 70 °C to 90 °C, while at 40 V/cm, the increment was 2.16-fold. This showed that the vitamin C degraded at a faster rate at higher temperature and EFS (Basak et al., 2023; Salari and Jafari, 2020). It was also observed that the δ-values of the Weibull distribution model increased numerically with an increase in temperature at 30 V/cm, while an unclear pattern was observed at 35 V/cm. Also, the t_{50} values of the logistic model increased

numerically with an increase in treatment temperature at 30 V/cm and 35 V/cm. This showed the unsuitability of the Weibull and logistic kinetic modelling for vitamin C degradation. Zheng and Lu (2011) also studied the kinetic modelling of ascorbic acid retention in pasteurized pineapple juice stored at different temperature ranges of 5 to 45 °C using zero-order, first-order, Weibull and PLSR models. They reported that the first-order model was the best-fit model and best for predictive purposes based on high R^2 values and low residuals, mean absolute error (MAE), mean relative error (MRE), and mean squared error (MSE) than other models.

Table 4.26 Goodness of fit parameters for different degradation kinetic modelling of vitamin C in continuous ohmic-treated pineapple juice

	EFS (V/cm)	Parameters	Vitamin C		
			70 °C	80 °C	90 °C
First order	30	R^2	0.901	0.958	0.906
		RMSE ($\times10^{-2}$)	3.924	3.112	5.113
		SSE ($\times10^{-3}$)	6.262	3.876	10.519
	35	R^2	0.847	0.953	0.889
		RMSE ($\times10^{-2}$)	4.652	4.048	5.693
		SSE ($\times10^{-3}$)	9.271	6.655	14.088
	40	R^2	0.917	0.881	0.954
		RMSE ($\times10^{-2}$)	2.716	5.122	3.688
		SSE ($\times10^{-3}$)	2.954	11.488	6.375
Weibull	30	R^2	0.923	0.966	0.960
		RMSE ($\times10^{-2}$)	4.008	3.225	3.736
		SSE ($\times10^{-3}$)	4.870	3.120	4.379
	35	R^2	0.853	0.977	0.961
		RMSE ($\times10^{-2}$)	5.188	2.909	4.187
		SSE ($\times10^{-3}$)	8.838	2.740	5.268
	40	R^2	0.943	0.961	0.971
		RMSE ($\times10^{-2}$)	2.629	3.609	2.913
		SSE ($\times10^{-3}$)	2.074	3.912	4.061
Logistic	30	R^2	0.966	0.974	0.957
		RMSE ($\times10^{-2}$)	23.256	29.035	42.045
		SSE ($\times10^{-3}$)	2.155	2.258	4.731
	35	R^2	0.966	0.978	0.959
		RMSE ($\times10^{-2}$)	23.284	26.685	42.595
		SSE ($\times10^{-3}$)	2.155	2.389	5.455
	40	R^2	0.942	0.960	0.966
		RMSE ($\times10^{-2}$)	29.405	44.810	34.940
		SSE ($\times10^{-3}$)	2.102	4.021	4.697

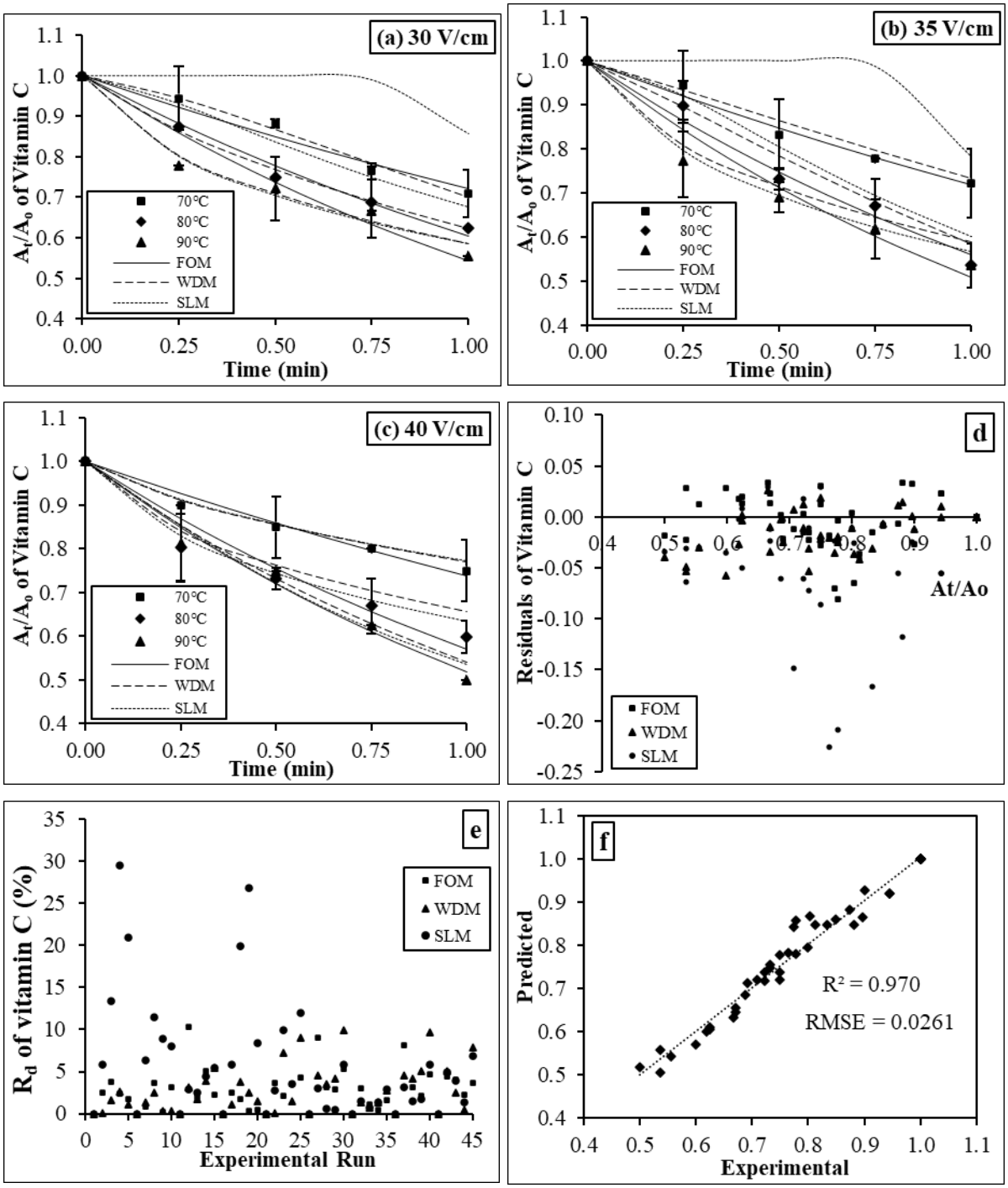

Fig. 4.35 Model curve fitting of experimental and predicted values of vitamin C at EFS (a) 30 V/cm, (b) 35 V/cm, and (c) 40 V/cm, (d) residual plot of vitamin C, (e) relative deviation plot of vitamin C, (f) predicted vs experimental vitamin C using first-order model. Where FOM, WDM, and SLM are first-order model, Weibull distribution model, and sigmoidal logistic model, respectively

Similarly, Akyildiz et al. (2021) also observed the first-order model as the best-fit model to study the degradation kinetics of vitamin C in thermally treated orange juice in the temperature range of 70 to 90 °C. Badin et al. (2021) also reported a similar finding where the first-order

model was suitable to study the kinetic modelling of thermal degradation of ascorbic acid in crushed tomatoes. The R^2 of the first order, Weibull, and logistic model ranged from 0.847 to 0.958, 0.853 to 0.977, and 0.942 to 0.978, respectively. Even though the R^2 of the logistic model was comparatively better than the other two models, the RMSE (< 0.4482), SSE (< 0.0055), and R_d (> 10%) were comparatively higher. The RMSE, SSE, and R_d of both the first-order and Weibull model were found to be comparatively lower than the logistic model, and the values were lower than 0.0570, 0.0141, and 5.0%, respectively, as shown in Table 4.26 and Fig. 4.35.

4.7.3 Validation of vitamin C kinetic model

Accuracy factor (A_f) and bias factor (B_f) were used to validate the performance of the kinetic models of vitamin C degradation, as shown in Table 4.27 (Pipliya et al., 2022; Vega et al., 2016). The A_f of the vitamin C degradation ranged from 1.010 to 1.041, 1.009 to 1.046, and 1.013 to 1.135, respectively, for the first-order, Weibull distribution, and logistic model. The first-order model showed the highest A_f in 44.5% of the treatment conditions, followed by the Weibull distribution (33.3%) and logistic model (22.2%). The B_f of the first-order model for vitamin C degradation was found to be better and closest to the simulation line (close to 1) (Table 4.27). It was observed that the first-order model showed better B_f in 77.8% of the treatment conditions, followed by both Weibull (11.1%) and the logistic model (11.1%). Thus, the A_f and B_f parameters suggested that the first-order model showed better accuracy for predicting vitamin C degradation in COH-treated pineapple juice.

Table 4.27 Model selection for vitamin C degradation by using accuracy factor (A_f) and bias factor (B_f)

EFS (V/cm)	T (°C)	Models					
		First Order		Weibull Distribution		Logistic	
		A_f	B_f	A_f	B_f	A_f	B_f
30	70	1.021	0.995	1.011	1.000	1.135	1.135
	80	1.016	1.002	1.009	1.002	1.069	1.069
	90	1.040	1.009	1.029	1.005	1.031	1.002
35	70	1.010	0.998	1.017	1.013	1.118	1.118
	80	1.027	0.998	1.035	1.035	1.055	1.055
	90	1.041	1.007	1.044	1.044	1.019	1.019
40	70	1.012	1.004	1.012	1.012	1.013	1.013
	80	1.036	1.008	1.046	1.046	1.024	1.024
	90	1.029	1.003	1.031	1.021	1.034	1.012

4.7.4 Model selection for Vitamin C degradation kinetic

The AIC and Δ_i values of all three kinetic models for vitamin C degradation were calculated and are summarised in Table 4.28. The logistic model observed the highest AIC values for each treatment condition, followed by the Weibull and first-order model. Also, the logistic model obtained $\Delta_i > 3.9$ (close to or greater than 4), and therefore, this model showed less significant support and should not be considered for model selection. On the other hand, the Weibull model obtained $\Delta_i \leq 2$ and, therefore, showed significant support and should be considered while making inferences for model selection. The first-order model obtained $\Delta i = 0$, so this model should be the primary choice for prediction purposes. The Akaike increment criteria (Δ_i) is an easy tool to discriminate, rank, and compare several competing models, but this should not be used in isolation for model selection as the AIC penalise the models more with a higher number of parameters (Pipliya et al., 2022; Vega et al., 2016). So, to select the best-fit model, Δ_i should be used along with statistical parameters.

Table 4.28 Model selection for vitamin C degradation by AIC and Akaike increment (Δ_i)

EFS (V/cm)	T (°C)	Models					
		First Order		Weibull Distribution		Logistic	
		AIC	Δi	AIC	Δi	AIC	Δi
30	70	-6.04	0.00	-4.04	1.99	-1.60	4.44
	80	-6.04	0.00	-4.04	2.00	-1.96	4.08
	90	-6.01	0.00	-4.04	1.97	-2.03	3.97
35	70	-6.04	0.00	-4.04	2.00	-1.66	4.39
	80	-6.04	0.00	-4.02	2.01	-1.99	4.04
	90	-6.01	0.00	-4.02	1.99	-2.04	3.98
40	70	-6.04	0.00	-4.04	2.00	-2.04	4.00
	80	-6.02	0.00	-4.01	2.00	-2.04	3.98
	90	-6.03	0.00	-4.03	2.00	-2.03	4.01

For vitamin C degradation, the first-order model should be the primary choice based on $\Delta_i = 0$, which was also supported by better A_f and B_f (Table 4.27) along with comparatively lower RMSE (0.027 to 0.057) (Table 4.26) and overall similar residuals (Fig. 4.35) when compared with the Weibull model. Also, according to the Principle of Parsimony, the model with the lowest number of parameters among several competing models should be considered (Pipliya et al., 2022; Vega et al., 2016). Therefore, the first-order model should be the primary choice for vitamin C degradation prediction in COH-treated pineapple juice.

4.8 Decimal reduction time of enzyme and microbial inactivation

The decimal reduction time (D-value) of PPO, POD, bromelain enzyme, and microbial inactivation was calculated using Weibull model parameters summarised in Table 4.29. The D-value was decreased significantly ($p < 0.05$) with an increase in temperature at any constant EFS for all parameters viz., PPO, POD, bromelain, and microbial, which showed that the time required to inactivate 90% of the enzyme activity and microbial load was directly proportional to the treatment temperature. This was because, at higher temperatures, the enzyme and microbial inactivation rate was high due to a higher rate of protein denaturation and biochemical reactions (Makroo et al., 2022; Makroo et al., 2020). Augusto et al. (2011) also reported a reduction in the D-value of the *L. Plantarum* in 0.3% carboxymethyl cellulose suspension from 76.3 s to 7.3 s when the temperature was increased from 52 °C to 61 °C.

Table 4.29 Decimal reduction time of enzyme and microbial inactivation

Parameter	EFS (V/cm)	D – value (min)		
		70 °C	80 °C	90 °C
PPO	30	6.54 ± 0.24^{cA}	4.62 ± 0.09^{bB}	2.94 ± 0.02^{aB}
	35	6.70 ± 0.14^{cA}	4.31 ± 0.21^{bAB}	2.78 ± 0.10^{aAB}
	40	6.21 ± 0.11^{cA}	4.02 ± 0.06^{bA}	2.50 ± 0.05^{aA}
POD	30	3.30 ± 0.08^{cA}	2.30 ± 0.03^{bB}	1.56 ± 0.04^{aA}
	35	3.16 ± 0.12^{cA}	2.40 ± 0.03^{bB}	1.88 ± 0.04^{aB}
	40	3.06 ± 0.10^{cA}	2.00 ± 0.08^{bA}	1.66 ± 0.06^{aA}
Bromelain	30	3.07 ± 0.32^{cA}	1.80 ± 0.08^{bA}	0.84 ± 0.10^{aA}
	35	2.97 ± 0.48^{bA}	1.73 ± 0.10^{aA}	0.88 ± 0.09^{aA}
	40	2.74 ± 0.15^{cA}	1.70 ± 0.15^{bA}	0.79 ± 0.08^{aA}
Microbial	30	2.52 ± 0.11^{bA}	2.19 ± 0.13^{abB}	1.83 ± 0.01^{aA}
	35	2.60 ± 0.24^{bA}	1.67 ± 0.06^{aA}	1.60 ± 0.09^{aA}
	40	2.59 ± 0.21^{bA}	1.66 ± 0.10^{aA}	1.58 ± 0.08^{aA}

Values in the same row, respectively, for each parameter with different small superscripts are significantly ($p < 0.05$) different with change in temperature at constant EFS. Values in the same column, respectively, for each parameter with different capital superscripts are significantly ($p < 0.05$) different with a change in EFS at a constant temperature.

The D-value of PPO, POD, bromelain, and microbial load was reduced significantly ($p < 0.05$) by ≥ 2.2-fold, 1.7-fold, 3.4-fold, and 1.4-fold, respectively, when the treatment temperature increased from 70 °C to 90 °C at an EFS ranging from 30 to 40 V/cm. In the same line, Lee et al. (2009) also observed a reduction in the D-value of PPO and POD in pineapple juice from 10.42 ± 0.48 to 2.62 ± 0.11 min and 13.02 ± 2.23 to 1.09 ± 0.15 min, respectively when the

treatment temperature increased from 75 °C to 95 °C. In comparison, Vishwasrao and Ananthanarayan (2018) observed a D-value of 2.8 ± 0.1 min at 75 °C and 1.9 ± 0.0 min at 85 °C for PPO inactivation during the thermal processing of pink guava pulp. On a similar line, Chakraborty et al. (2016) also reported a multiple-fold reduction in the bromelain activity in pineapple pulp when the treatment temperature and pressure were increased during high-pressure and thermal treatments. The main reason for the differences in the D-value was the variations in the samples, their geographical locations, seasonal variations, and the type of technologies involved in the processing. A Weibull model was also best described for the POD inactivation of Tetsukabuto pumpkin during ohmic heating with a D-value of 1.5 min compared to 2.6 min during conventional blanching (Gomes et al., 2018). The study also showed that the D-value obtained from the Weibull model was comparatively higher than the first-order model for all the enzyme activity. Since the Weibull model was more accurate than the first-order model, the D-value obtained from the Weibull model should be used for the process design. The first-order model might give under-estimated or over-estimated D-values, leading to the failure of the processing designs. Chakraborty et al. (2016) also reported that the first-order model gave underestimated and overestimated D-value at 100-300 MPa/30-60 °C and 400-600/70 °C, respectively, during high pressure-thermal treatment of fruit bromelain in pineapple and suggested the use of n^{th} order model.

Also, at any particular temperature, the D-value of the enzymes and microbial inactivation was reduced numerically with an increase in the EFS from 30 to 40 V/cm. However, the change was statistically non-significant ($p > 0.05$) for bromelain enzyme at all temperatures, while for PPO, POD, and microbial inactivation, a non-significant ($p > 0.05$) change was observed at 70 °C and significant ($p < 0.05$) change was observed at 80 °C and 90 °C as shown in Table 4.29. The results also showed that the D-value of PPO was higher than the POD under each treatment condition, suggesting a higher thermal stability of the PPO than the POD enzyme in pineapple juice. A significant ($p < 0.05$) effect of EFS on the D-value was also observed by Barron-Garcia et al. (2019) during ohmic heating of *Agaricus bisporus* for tyrosinase inactivation and found that the D-value reduced from 11.98 ± 0.59 min at 25 V/cm to 6.44 ± 0.16 min at 35 V/cm at 58 °C. The effect of EFS on the D-value of enzyme inactivation was also verified by other authors (Kanjanapongkul and Baibua, 2021; Zhong et al., 2007).

4.9 Activation energy of enzyme inactivation

The activation energy (E_a) of PPO, POD, and bromelain was obtained from the Arrhenius plot of ln(k) versus 1/T using the kinetic parameter of the Weibull distribution model and is

summarised in Table 4.30. The E_a of PPO, POD, and bromelain was in the range of 41.4 ± 1.6 to 47.2 ± 2.1 kJ/mol, 26.8 ±3.1 to 38.6 ± 2.7 kJ/mol, and 62.6 ± 3.6 to 66.9 ± 11.6 kJ/mol, respectively. Though the E_a values changed with a change in the EFS, the change was statistically non-significant ($p > 0.05$). The E_a of PPO in pineapple during thermal inactivation was reported to be 80.15 ± 6.69 kJ/mol at a temperature range of 45 to 95 °C. Similarly, the E_a of POD during the same treatment condition in pineapple was 68.98 and 93.23 kJ/mol, respectively, for heat-labile and heat-resistant fractions (Lee et al., 2009). At the same time, the E_a of PPO in pink guava pulp during thermal processing was found to be 60.36 ± 1.21 kJ/mol (Vishwasrao and Ananthanarayan, 2018).

On the other hand, the E_a of heat-labile fractions of POD and PPO in garlic during thermal blanching was 37.41 and 4.04 kJ/mol, respectively, and for heat resistant fraction was 50.46 and 12.93 kJ/mol, respectively (Fante et al., 2012).

Table 4.30 Activation energy of PPO, POD, and bromelain enzymes

EFS (V/cm)	Activation Energy, Ea (kJ/mol)		
	PPO	POD	Bromelain
30	41.4 ± 1.6[a]	38.6 ± 2.7[a]	66.9 ± 11.6[a]
35	45.5 ± 0.9[a]	26.8 ± 3.1[a]	62.6 ± 3.6[a]
40	47.2 ± 2.1[a]	32.0 ± 3.7[a]	64.1 ± 2.3[a]

Values in the same column, respectively, for each parameter with different small superscripts are significantly ($p < 0.05$) different with a change in EFS.

Similarly, the E_a of POD in carrots was 148 kJ/mol for heat resistant fraction and 89.6 kJ/mol for heat-labile fraction (Soysal and Soylemez, 2005). In comparison to the current E_a of bromelain enzyme, the previous authors have reported an E_a of 41.7 kcal/mol (i.e., 174.5 kJ/mol) during thermal treatment of industrially purified bromelain in the temperature range of 45 to 60 °C (Yoshioka et al., 1991). In comparison, Jutamongkon and Charoenrein (2010) reported an elevated E_a of 313 ± 57.44 kJ/mol during thermal inactivation of fruit bromelain from Smooth Cayenne pineapple in the temperature range of 40 to 80 °C which was in comparable range of Sriwatanapongse et al. (2000) who reported an E_a of 326 kJ/mol in pineapple juice in the temperature range of 55 to 67 °C. The E_a for crude bromelain in pineapple fruit was 31 kJ/mol during isothermal treatment at atmospheric pressure (Chakraborty et al., 2016). Also, during high-pressure processing (200 to 500 MPa) of pineapple puree, the E_a was in the range of 24 to 51 kJ/mol, which was in the comparable range of the current study (Chakraborty et al., 2014).

The variations in these values might be because of the differences in the fruit and sample preparation, mode of thermal processing technologies, temperature gradient, and type of technology involved in processing (Lee et al., 2009). The E_a of any enzyme refers to the amount of energy needed to form an activated and quasi-state complex that eventually results in its inactivation. At higher temperatures, say 70 °C, the chances to regain the unfolded conformation for the enzyme are diminished, and so further increases in the temperature show additive or synergistic effects during inactivation (Chakraborty et al., 2016). Thus, the variations in the activation energies are observed with changes in treatment conditions. However, no such processing destroys the enzymes because of the presence of the resistant enzymes, so the focus must not be on the complete inactivation but instead on finding the optimum temperature-time combination to bring it to a minimum level so that it does not have a significant effect during storage and consumption (Kanjanapongkul and Baibua, 2021).

4.10 Optimization of COH process parameters

4.10.1 Full factorial modelling

Statistical summaries for different models, viz., linear, 2FI, quadratic, and cubic, are shown in Table 4.31. The standard deviation, $R^{2,}$ and predicted R^2 values of the linear and 2FI models were higher, and the cubic model was found to be aliased for each response parameter; thus, these models were rejected. The quadratic model, i.e., second-order polynomial model, was found to be well-fitted at a significance level of 5.0%, having lower standard deviation and comparatively higher R^2 and predicted R^2 values for all the response parameters and, thus, selected.

The wellness and adequacy of the quadratic models were determined by analyzing ANOVA parameters, as shown in Table 4.32 (Faizan and Amardeep, 2018). The model was found to be highly significant ($p < 0.0001$) for all the response parameters. The F-values of the respective response parameters demonstrated that the models were effective and that there was only a 0.01% chance that F-values this large could occur because of noise. The R^2 was greater than 0.985 for PPO, POD, bromelain, and microbial inactivation. For Vitamin C, the R^2 value was 0.956. The developed models for each response parameter were appropriate since the p-value was very low and R^2 was closer to 1.0. The significance level of each model term, viz., linear, interaction, and quadratic, is shown in Table 4.33. Model terms were significant if $p < 0.05$ were selected, while those with $p > 0.10$ were non-significant and rejected in the final model equations (Hashemi et al., 2019).

Table 4.31 Model summary statistics for selecting the best model

Parameter	Model	Std. Dev.	R^2	Pred. R^2	Remarks
Polyphenol oxidase (%RA)	Linear	5.28	0.897	0.873	Rejected: High SD, low R^2
	2FI	4.57	0.928	0.895	Rejected: High SD, low R^2
	Quadratic	1.65	0.992	0.985	Selected
	Cubic	0.61	0.999	0.997	Rejected: Aliased
Peroxidase (%RA)	Linear	6.19	0.912	0.892	Rejected: High SD, low R^2
	2FI	6.30	0.915	0.875	Rejected: High SD, low R^2
	Quadratic	2.43	0.988	0.981	Selected
	Cubic	1.49	0.997	0.991	Rejected: Aliased
Bromelain (%RA)	Linear	2.66	0.956	0.946	Rejected: High SD, low R^2
	2FI	2.62	0.960	0.941	Rejected: High SD, low R^2
	Quadratic	1.45	0.989	0.980	Selected
	Cubic	0.51	0.999	0.997	Rejected: Aliased
Microbial load (Log reduction)	Linear	0.11	0.961	0.952	Rejected: High SD, low R^2
	2FI	0.08	0.982	0.973	Rejected: High SD, low R^2
	Quadratic	0.07	0.986	0.975	Selected
	Cubic	0.05	0.995	0.985	Rejected: Aliased
Vitamin C (%)	Linear	3.77	0.933	0.919	Rejected: High SD, low R^2
	2FI	3.64	0.943	0.918	Rejected: High SD, low R^2
	Quadratic	3.32	0.956	0.926	Selected
	Cubic	2.30	0.984	0.944	Rejected: Aliased

Table 4.32 ANOVA for enzyme inactivation, microbial load reduction, and vitamin C retention using a second-order polynomial model

Response	Model Type	Sum of squares		F-value	p-value	R^2	RMSE	Adj R^2	Pred R^2	Adeq Precision
		Model	Residual							
PPO (%RA)	Quadratic	11002.7	94.8	451.3	<0.0001	0.992	1.451	0.989	0.985	76.2
POD (%RA)	Quadratic	17556.8	206.6	330.4	<0.0001	0.988	2.143	0.985	0.981	63.5
Bromelain (%RA)	Quadratic	6474.4	73.3	343.7	<0.0001	0.989	1.278	0.986	0.980	66.6
TPC (Log reduction)	Quadratic	11.95	0.17	271.6	<0.0001	0.986	0.062	0.982	0.975	60.7
Vitamin C (%)	Quadratic	8364.4	384.9	84.5	<0.0001	0.956	2.925	0.945	0.926	35.2

PPO (% RA) = 60.95 – (2.12 × EFS) – (10.13 × T) – (17.31 × t) – (4.75 × T × t) – (1.91 × T^2) + (9.13 × t^2) (Eq.4.1)

POD (% RA) = 42.99 – (2.06 × EFS) – (10.47 × T) – (23.83 × t) – (1.93 ×T × t) – (1.57 × EFS^2) + (12.71 × t^2) (Eq. 4.2)

Bromelain (% RA) = 16.88 – (0.96 × EFS) – (10.94 × T) – (10.83 × t) + (1.31 × T × t) + (4.81 × t^2) (Eq. 4.3)

TPC (log reduction) = 3.28 + (0.36 × T) + (0.59 × t) + (0.12 × T × t) + (0.044 × EFS^2) – (0.057 × t^2) (Eq. 4.4)

Vit. C (% retention) = 62.8 – (2.74 × EFS) – (9.34 × T) – (15.38 × t) – (2.24 × T × t) + (2.16 × EFS^2) + (3.01 × t^2) (Eq. 4.5)

It was observed that linear terms viz., EFS, temperature (T), and time (t) were found to be highly significant ($p < 0.001$) except linear term EFS of the microbial inactivation, which was non-significant ($p > 0.05$). The interaction term T × t was significant ($p < 0.05$). In contrast, EFS × T and EFS × t was non-significant ($p > 0.05$) for all the response parameters and, thus, omitted from the model as shown in Eq. 4.1, Eq. 4.2, Eq. 4.3, Eq. 4.4, and Eq. 4.5. Quadratic term t^2 was the only significant ($p < 0.05$) for all the response parameters. However, the PPO residual activity model also contained significant quadratic term $T^{2,}$ while the rest of the response model had a non-significant ($p > 0.05$) effect. Similarly, the POD and vitamin C models had significant quadratic term EFS^2, while PPO, bromelain, and TPC had non-significant terms.

Table 4.33 Significance level of the model terms

	p-value				
	PPO (%RA)	**POD (%RA)**	**Bromelain (%RA)**	**TPC (Log reduction)**	**Vitamin C (%retention)**
EFS	<0.0001*	<0.0001*	0.0009*	0.9793#	<0.0001*
T	<0.0001*	<0.0001*	<0.0001*	<0.0001*	<0.0001*
t	<0.0001*	<0.0001*	<0.0001*	<0.0001*	<0.0001*
EFS × T	0.2201#	0.3979#	0.1539#	0.1187#	0.8221#
EFS × t	0.2703#	0.5187#	0.6210#	0.1171#	0.5674#
T × t	<0.0001*	0.0040*	0.0012*	<0.0001*	0.0131*
EFS^2	0.1144#	0.0488*	0.4921#	0.0527#	0.0473*
T^2	0.0008*	0.3600#	0.1657#	0.4925#	0.9248#
t^2	<0.0001*	<0.0001*	<0.0001*	0.0279*	0.0153*

*Show that the model terms are significant ($p < 0.05$) and #show that the model terms are non-significant ($p > 0.05$)

The negative and positive terms in the model equations showed the negative and positive effects on the response parameters (Hashemi et al., 2019). From Eq. 4.1, it can be observed that the model terms EFS, t, T, T × t, and T^2 had a negative effect on PPO residual activity, i.e., with the increase in these parameters, the PPO residual activity was decreased and vice versa. In contrast, the term t^2 positively affected the PPO residual activity. Similarly, Eq. 4.2, Eq. 4.3, and Eq. 4.5 showed that the linear terms negatively affected the POD, bromelain, and vitamin C, respectively. Interaction term T × t negatively affected POD residual activity and vitamin C retention while positively affecting the residual bromelain activity. The positive effect of quadratic term t^2 was observed on POD, bromelain, and vitamin C, while quadratic term EFS^2 negatively affected the POD residual activity. Total microbial load reduction positively affected linear term temperature and time and their interaction, as shown in Eq. 4.5. The linear term EFS was non-significant ($p > 0.05$) and, therefore, not included in the final equation. The quadratic term EFS^2 had a positive effect, while time negatively affected the microbial load reduction.

4.10.2 Performance of the full factorial model

The model's performance was assessed by statistical parameters like R^2, RMSE, and residuals between predicted and observed values, as shown in Table 4.34 (Faizan and Amardeep, 2018; Aliakbarian et al., 2018). The predicted R^2 value of each response model was in reasonable agreement with the adjusted R^2 value, and adequate precision was greater than 4.0, which was required, as shown in Table 4.32.

The predicted R^2 value was higher than 0.975 for enzyme residual activity and microbial inactivation, while it was 0.926 for vitamin C retention and lower residuals and RMSE values, as shown in Fig. 4.36. The residuals for PPO, POD, bromelain, microbial load reduction, and vitamin C were in the range of -3.06 to 2.61, -4.87 to 3.50, -2.72 to 2.17, -012 to 0.13 and -7.56 to 5.44, respectively as shown in Table 4.34 and Fig. 4.37.

The residuals are a critical determining parameter for the developed model's quality. The residual sum of squares (RSS) was used to determine the amount of variance in a data set, which was not explained by the regression model itself (Hashemi et al., 2019). It was observed that the RSS was found to be small as compared to the model sum of squares (MSS), i.e., RSS was less than 1.0% of the MSS value of PPO residual activity, and it was less than 1.5% for the respective MSS values of POD inactivation, bromelain inactivation, and microbial load reduction. Vitamin C had the maximum RSS values among all the responses, but it still was

less than 5.0% of its MSS values. Thus, the smaller RSS values showed a well-fit model to the data set. Therefore, these models can be used to navigate the design space.

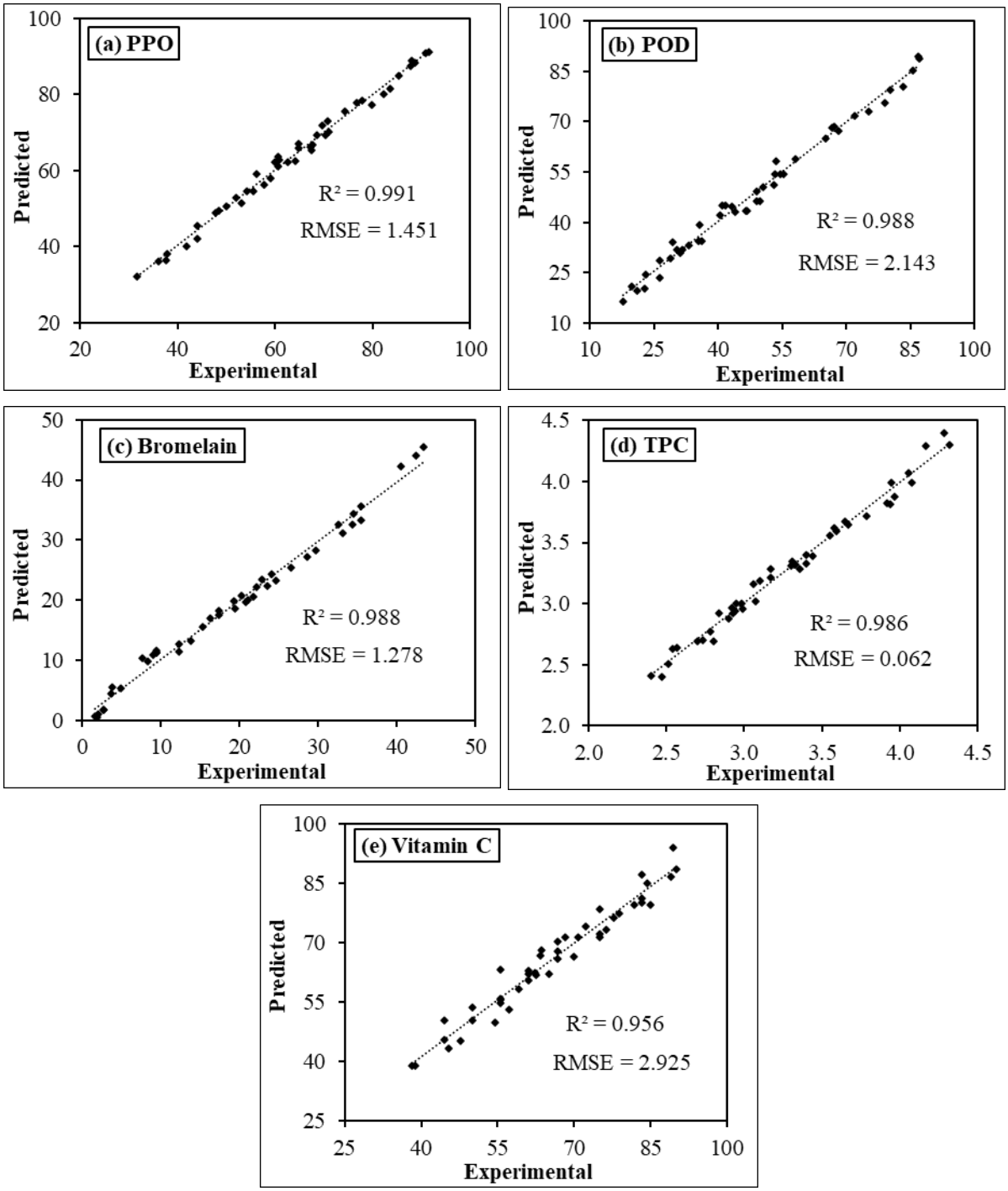

Fig. 4.36 Experimental vs predicted values of (a) PPO (% RA), (b) POD (%RA), (c) bromelain (%RA), (d) microbial load reduction (log reduction), and (e) vitamin C (%)

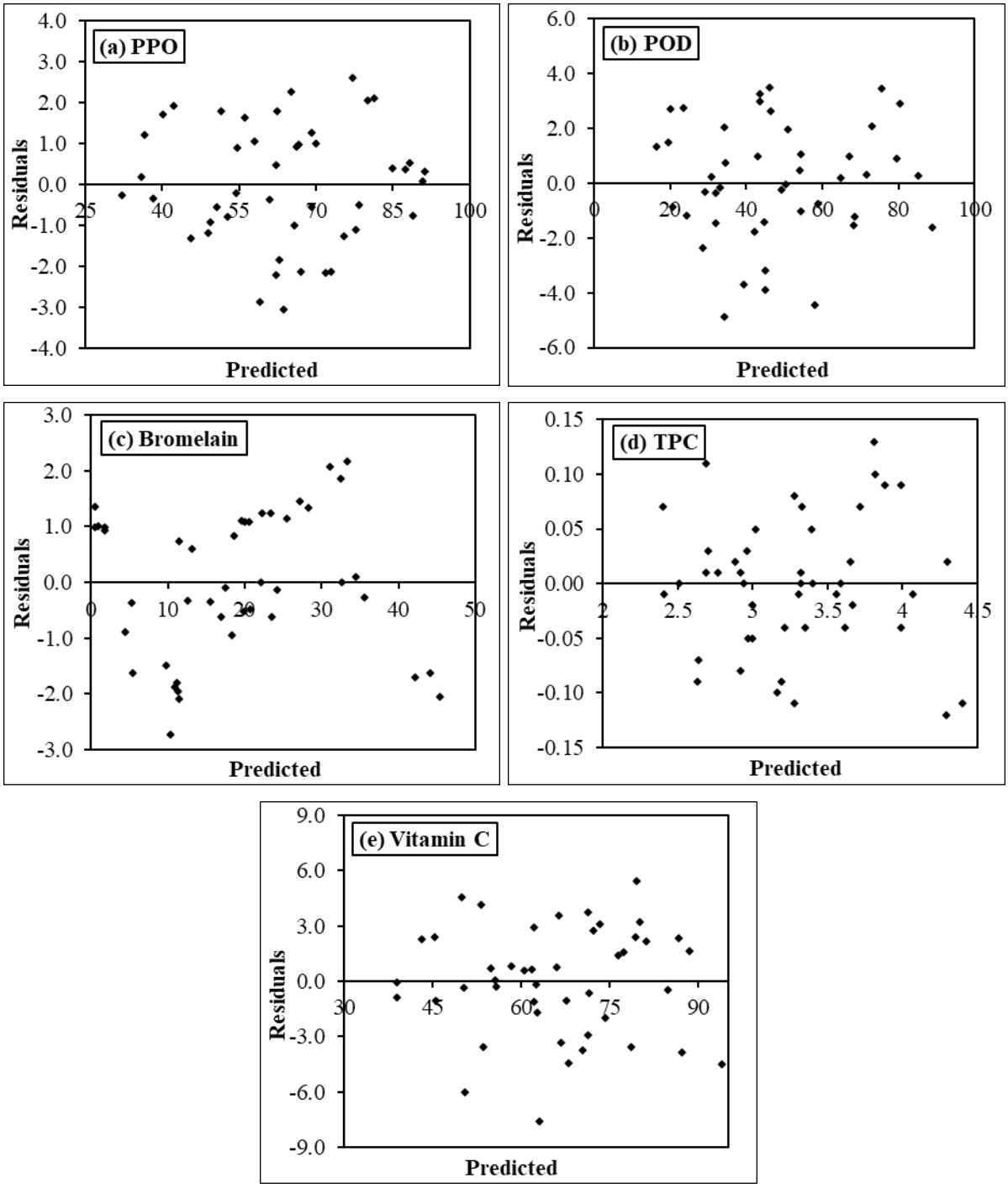

Fig. 4.37 Residual plots of (a) PPO (%RA), (b) POD (%RA), (c) bromelain (%RA), (d) microbial load reduction (log reduction), and (e) vitamin C (%)

Table 4.34 Statistical parameters of the models

Parameters	PPO (% RA)	POD (% RA)	Bromelain (% RA)	Microbial (log reduction)	Vitamin C (%)
R^2	0.992	0.988	0.985	0.986	0.956
RMSE	1.451	2.143	1.278	0.062	2.925
Residuals	-3.06 to 2.61	-4.87 to 3.50	-2.72 to 2.17	-0.12 to 0.13	-7.56 to 5.44

4.10.3 Optimization of the COH process parameters and validation

The process parameters of the continuous ohmic heating of standardized pineapple juice were optimized using the RSM full factorial quadratic model. The optimization was done using the fruit juice spoilage enzyme PPO and POD and total microbial load.

Table 4.35 Constraints of the optimization process and best solution

Parameter	Parameters	Goal	Lower limit	Upper limit	Best solution
Independent	EFS (V/cm)	In range	30	40	40.00
	Temperature (°C)	In range	70	90	88.86
	Time (s)	In range	0	60	59.94
Dependent	PPO (%RA)	Minimize	31.81	91.52	34.25
	POD (%RA)	Minimize	17.84	87.18	17.82
	Total Microbial (log reduction)	Maximize	2.4	4.32	4.34
Desirability					0.986

The constraints of the optimization process for the selected parameters are shown in Table 4.35. The best solution was obtained at EFS 40 V/cm with a treatment temperature of 88.86 °C and a time of 59.94 s. The desirability of the optimized treatment condition was 0.986, which was considerably high. The optimization process was validated by comparing the predicted and experimental values under the optimized treatment conditions, as shown in Table 4.36. The deviation between the predicted and experimental values was less than 5.0% for all the dependent parameters.

Table 4.36 Experimental and predicted values at optimized condition

Parameter	Unit	Predicted Value	Experimental Value	Deviation (%)
PPO	Residual activity (%)	34.25	33.59 ± 0.69	1.93
POD	Residual activity (%)	17.82	18.66 ± 1.47	4.71
Total Microbial	Log reduction	4.34	4.15 ± 0.02	4.38

Further, the standardized pineapple juice was treated with optimized conditions and a hot water bath under similar conditions. The treated juice samples were stored for two months (60 days) at two different temperatures (4 °C and 2 °C), and a comparative storage study was done. The detailed studies are discussed in the follow-up section.

4.11 Storage study of COH and hot water bath (HWB) treated pineapple juice

COH and HWB methods treated the standardized pineapple juice at optimized treatment conditions. For COH treatment, the juice samples were heated in an ohmic heating cell, passed to the holding chamber for the desired duration, and aseptically filled in 20 mL glass vials, capped, and immediately cooled in an ice bath. For HWB treatment, the juice samples were first filled in the glass vials, capped, and then heated in a water bath. After the treatment, the juice samples were immediately cooled in an ice bath. All the glass vials were sealed using parafilm prior to storage. The juice samples were stored away from direct sunlight for two months at 4 °C and 2 °C. The analysis for various juice parameters was done at a regular interval, as discussed in the following section.

4.11.1 Changes in pH, TSS, electrical conductivity, and titratable acidity

The physico-chemical parameters like pH (Fig. 4.38), TSS (Fig. 4.39), titratable acidity (Fig. 4.40), and electrical conductivity (Fig. 4.41) of untreated (UT), COH, and hot water bath (HWB) treated standardized pineapple juice (22 °Brix/Acid) were examined under two different storage temperature of 4 °C and 25 °C.

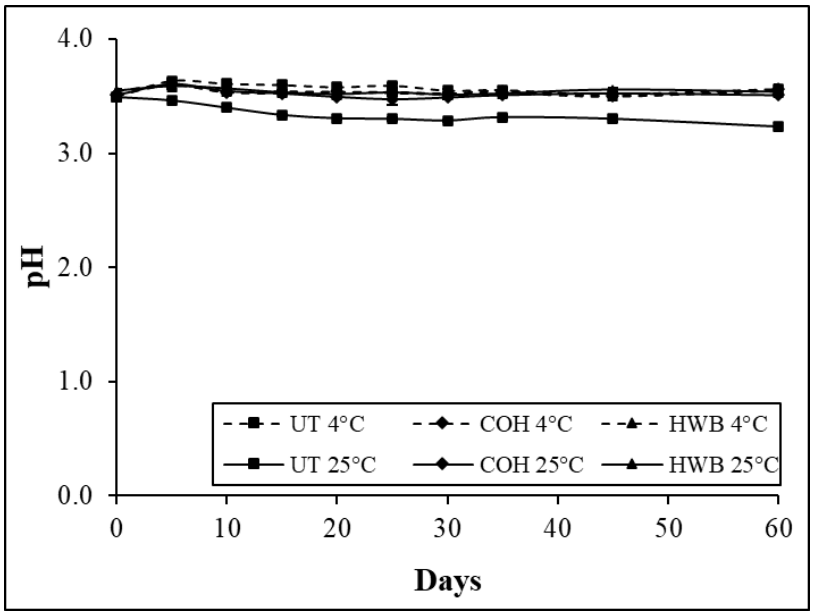

Fig. 4.38 Effect of storage on pH

The initial value of pH, TSS, titratable acidity, and electrical conductivity of the untreated standardized pineapple juice was 3.50 ± 0.01, 11.80 ± 0.00 °Brix, 0.512 ± 0.00%, and 0.164 ± 0.003 S/m, respectively. On the other hand, the initial value of pH, TSS, titratable acidity, and electrical conductivity of COH treated pineapple juice was 3.51 ± 0.00, 11.8 ± 0.00 °Brix, 0.544 ± 0.02%, and 0.162 ± 0.002 S/m, respectively and for HWB treated pineapple juice was 3.55 ± 0.02, 11.8 ± 0.00 °Brix, 0.533 ± 0.00%, and 0.161 ± 0.002 S/m, respectively. These parameters were significantly ($p < 0.005$) affected in untreated pineapple juice, while the change was minor in COH and HWB-treated juice at both storage temperatures. Similarly, the change was observed more at a higher storage temperature of 25 °C than at 4 °C. The pH and TSS of untreated pineapple juice stored at 25 °C significantly ($p < 0.05$) reduced from 3.50 ± 0.01 to 3.23 ± 0.00 and 11.80 ± 0.00 to 5.15 ± 0.07 °Brix, respectively.

On the other hand, the titratable acidity and electrical conductivity significantly ($p < 0.05$) increased from 0.512 ± 0.00 to 1.109 ± 0.03% and 0.164 ± 0.003 to 0.206 ± 0.001 S/m, respectively, when stored at the same temperature of 25 °C. The reduction in pH and TSS was in good synchronization with increased titratable acidity and electrical conductivity during storage. Guan et al. (2016) reported reduced pH and increased acidity while storing high-pressure and thermally treated mango juice. However, the change was minor because of storage conditions, as the samples were refrigerated. A non-significant ($p > 0.005$) change was observed in the pH and TSS values of COH and HWB treated pineapple juice at both storage temperatures suggesting the stable nature of the juice treated with COH and HWB.

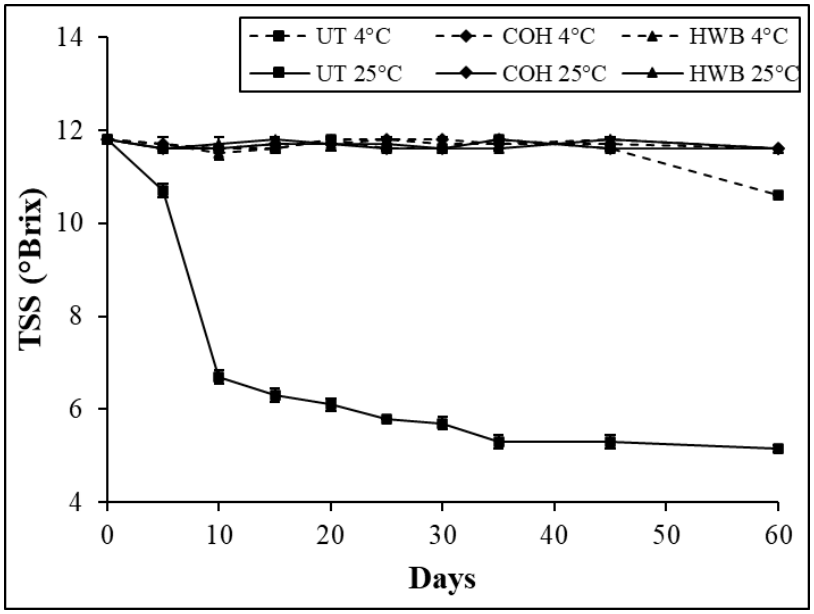

Fig. 4.39 Effect of storage on TSS

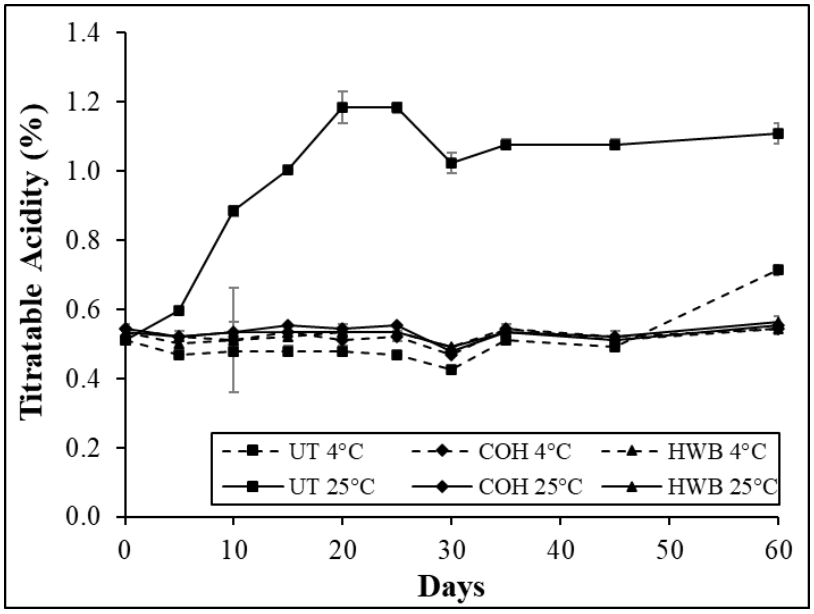

Fig. 4.40 Effect of storage on titratable acidity

The titratable acidity of COH and HWB-treated pineapple juice showed a significant ($p < 0.05$) change at 30 days of storage when the storage temperature was 25 °C, while a non-significant ($p > 0.05$) change was observed at 4 °C suggesting the stability of juice at refrigerated condition. Similarly, the electrical conductivity of the COH and HWB-treated pineapple juice showed a significant change at 15 days of storage at both temperatures. The reason was the increase in the microbial count during storage, which may have resulted in the growth of acid-forming bacteria, resulting in the increase in acidity and degradation of sugar, causing a reduction in pH and an increment in electrical conductivity (Guan et al., 2016; Liu et al., 2014).

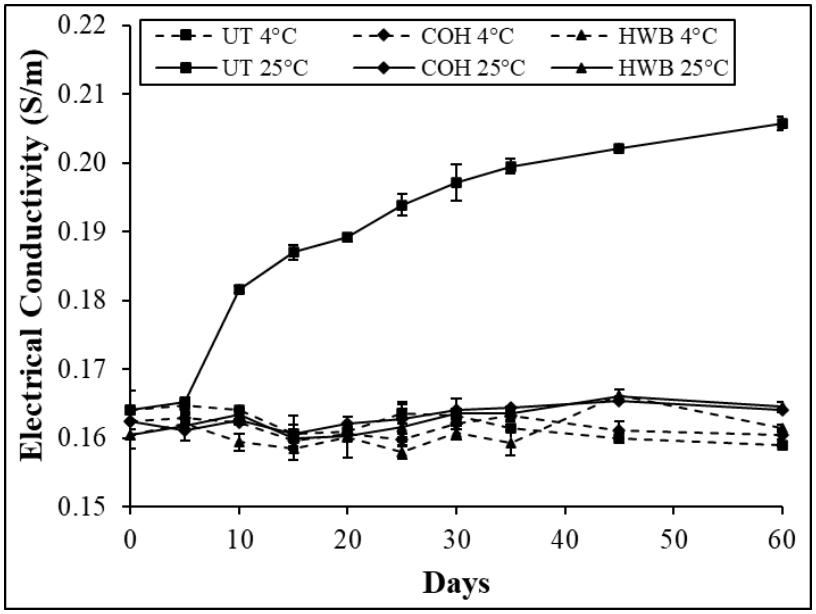

Fig. 4.41 Effect of storage on electrical conductivity

4.11.2 Changes in vitamin C content

The vitamin C content of untreated (UT), COH, and HWB-treated pineapple juice was estimated at a regular period during storage temperatures of 4 °C and 25 °C, respectively, as shown in Fig. 4.42. The kinetic model parameters of vitamin C degradation during storage study are shown in Table 4.37. The initial vitamin C content of the untreated, COH, and HWB-treated pineapple juice was 8.21 ± 0.00, 2.99 ± 0.00, and 2.61 ± 0.53 mg/100 mL of juice, respectively. The vitamin C content of the untreated pineapple juice significantly ($p < 0.05$) reduced with storage time at both temperatures of 4 °C and 25 °C. It was reduced from 8.21 ± 0.00 mg/100 mL to 4.85 ± 0.53 and 3.36 ± 0.53 mg/100 mL, respectively at 4 °C and 25 °C. The reduction rate was higher at higher storage temperatures (Kabasakalis et al., 2000).

There was a slow degradation of vitamin C in COH and HWB-treated pineapple juice, and the change was significant ($p < 0.05$) observed only after 30 days of storage period. The vitamin C content of both COH and HWB-treated pineapple juice was slowly reduced to 1.49 ± 0.00 mg/100 mL at 4 °C and 1.12 ± 0.53 mg/100 mL at 25 °C from the respective initial values during the 60-day storage period. A second-order kinetic model was found to explain better the degradation of vitamin C during the storage study of standardized pineapple juice. The second-order kinetic model's R^2, RMSE, and SSE values were lower than the zero-order and the first-order kinetic models.

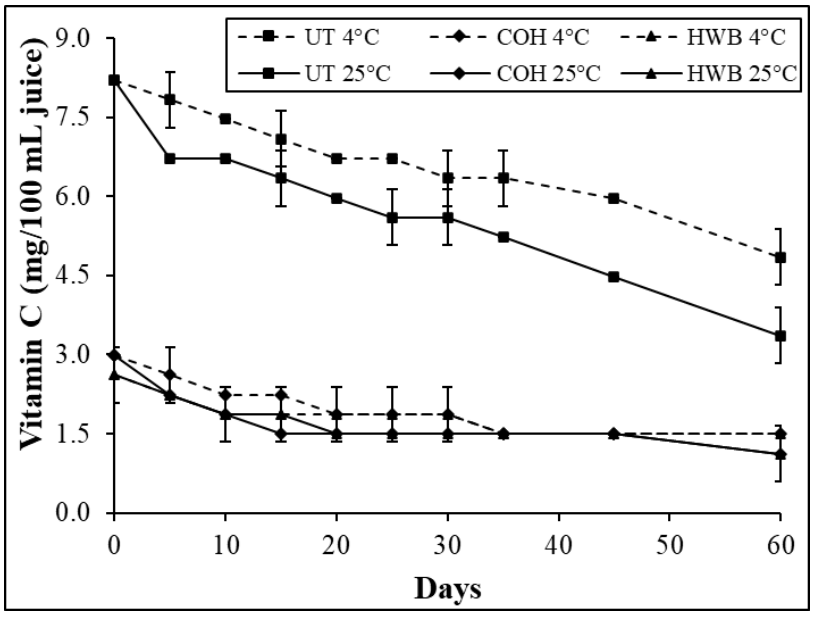

Fig. 4.42 Effect of storage on vitamin C

Table 4.37 Model parameters of degradation kinetic modelling of vitamin C during storage study of pineapple juice

Model	Kinetic Parameter	UT4°C	COH4°C	HWB4°C	UT25°C	COH25°C	HWB25°C
Zero Order	k_o (day^{-1})	0.057	0.035	0.026	0.088	0.042	0.031
	R^2	0.954	0.591	0.351	0.848	-0.089	0.460
	RMSE	0.208	0.323	0.284	0.520	0.558	0.322
	SSE	0.388	0.939	0.724	2.429	2.802	0.934
First Order	k_1 (day^{-1})	0.008	0.017	0.014	0.015	0.024	0.018
	R^2	0.970	0.829	0.596	0.918	0.478	0.739
	RMSE	0.021	0.070	0.086	0.046	0.129	0.086
	SSE	0.004	0.044	0.066	0.019	0.150	0.066
Second Order	k_2 (day^{-1})	0.001	0.007	0.006	0.003	0.010	0.009
	R^2	0.947	0.833	0.673	0.922	0.568	0.813
	RMSE	0.006	0.050	0.055	0.014	0.100	0.062
	SSE	0.0003	0.022	0.027	0.002	0.090	0.035

Results also showed that the increase in storage temperature positively influences vitamin C degradation. This was also confirmed by the reaction rate constant (k_2) parameters, which increased with an increase in storage temperature from 4 °C to 25 °C (Table 4.37). Since vitamin C is a thermolabile compound and is highly sensitive to various processing conditions like temperature and time, it gets readily oxidized and lost during storage. The degradation of vitamin C greatly depends on the storage temperature and duration (Kabasakalis et al., 2000; Tiwari et al., 2009). Kabasakalis et al. (2000) also reported a higher ascorbic acid reduction in orange juice under ambient temperature than when refrigerated samples. Similarly, Choi et al. (2002) also observed a reduction rate of 18% per week of ascorbic acid in fresh blood orange juice stored under refrigerated conditions. On the other hand, Tiwari et al. (2009) also observed a reduction in ascorbic acid during 30 days of storing sonicated and thermally pasteurized orange juice. However, ascorbic acid reduction was higher in thermally treated juice than in sonicated. Therefore, vitamin C degradation also greatly depends on the type of technologies applied during processing.

4.11.3 Changes in total microbial load

The initial microbial load of untreated, COH and HWB-treated pineapple juice was 5.71 ± 0.08, 1.56 ± 0.07, and 1.67 ± 0.06 log CFU/mL of juice, respectively. The microbial load of each sample increased significantly ($p < 0.05$) with time at both the storage temperature of 4 °C and 25 °C, as shown in Fig. 4.43. The kinetic model parameters of microbial growth during storage study are shown in Table 4.38. A maximum of 8.30 ± 0.05 log CFU/mL was observed in the

untreated juice sample stored at 25 °C in the first 25 days, and then it was slowly reduced to 5.51 ± 0.16 log CFU/mL during 60 days of storage. The reason was the juice fermentation and reduction in the pH, as in an acidic medium, the bacterial growth reduces significantly. The microbial growth in untreated juice reached 6.45 ± 0.02 log CFU/mL when stored at 4 °C for 60 days.

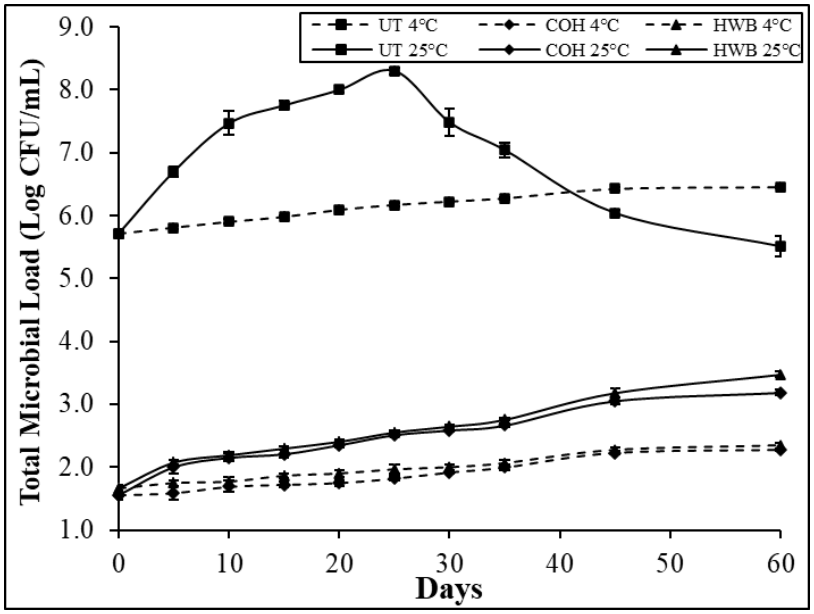

Fig. 4.43 Effect of storage on total microbial load

Table 4.38 Model parameters of kinetic modelling of microbial growth during storage study of pineapple juice

Model	Kinetic Parameter	UT4°C	COH4°C	HWB4°C	UT25°C	COH25°C	HWB25°C
Zero Order	k_o (day^{-1})	0.015	0.013	0.012	0.029	0.032	0.033
	R^2	0.913	0.964	0.981	-1.029	0.845	0.935
	RMSE	0.074	0.047	0.030	1.394	0.191	0.135
	SSE	0.050	0.020	0.008	17.490	0.327	0.163
First Order	k_1 (day^{-1})	0.003	0.007	0.006	0.004	0.014	0.014
	R^2	0.892	0.963	0.969	-1.109	0.644	0.821
	RMSE	0.015	0.030	0.023	0.249	0.185	0.134
	SSE	0.002	0.008	0.005	0.557	0.309	0.163
Second Order	k_2 (day^{-1})	0.001	0.004	0.003	0.001	0.007	0.007
	R^2	0.884	0.966	0.955	-1.124	0.373	0.577
	RMSE	0.002	0.013	0.011	0.032	0.075	0.058
	SSE	0.001	0.001	0.001	0.009	0.051	0.030

On the other hand, the microbial growth was less than 2.50 log CFU/mL when stored at 4 °C and less than 3.50 log CFU/mL when stored at 25 °C during 60 days storage period for both

COH and HWB-treated pineapple juice. However, the microbial growth of COH-treated pineapple juice was comparatively lower than that of HWB-treated juice samples.

A first-order kinetic model was selected to explain the growth kinetics of the microbial load during the storage study of pineapple juice. The R^2 value was found to be comparatively better than that of other models, and the RMSE and SSE were found to be in an acceptable range. The only exception was that the kinetic model of microbial growth in untreated pineapple juice stored at 25 °C (UT25°C) did not explain the growth kinetic behaviour as the microbial load first increased till 25 days and then started decreasing because of the fermentation of the juice. The microbial growth was comparatively more when the juice was stored at a higher temperature of 25 °C than at 4 °C which was also explained by the higher reaction rate constant (k1) at a higher storage temperature of 25 °C than at 4 °C. Although the microbial count of COH and HWB-treated pineapple juice was increased during the storage period, the microbial load was well below the safe limit of 6.0 log CFU/mL, and the fruit juice was fit for human consumption (Kayalvizhi et at., 2016). Guan et al. (2016) also reported a bacterial increment in high-pressure treated mango juice during a storage period of two months. However, the growth was greatly restricted in refrigerated conditions compared to those stored under ambient conditions.

4.11.4 Changes in enzyme activity

The enzyme activity of PPO (Fig. 4.44), POD (Fig. 4.45), and bromelain (Fig. 4.46) were also estimated at a regular interval during 60 days of storage at two different temperatures of 4 °C and 25 °C. Slow degradation of enzyme activity (PPO, POD, and bromelain) was observed during the storage period at both temperatures; however, the degradation was faster at a higher storage temperature of 25 °C compared to 4 °C for all the samples. The kinetic model parameters of enzyme (PPO, POD, and bromelain) degradation during storage study are shown in Table 4.39. The initial activity of PPO, POD, and bromelain of the COH-treated pineapple juice was reduced to 33.6 ± 0.7%, 18.7 ± 1.5%, and 1.5 ± 0.1%, respectively. On the other hand, the initial activity of HWB-treated samples was reduced to 36.9 ± 0.7%, 20.8 ± 1.3%, and 1.7 ± 0.2%, respectively.

Similarly, the POD and bromelain activity of untreated juice samples increased significantly ($p < 0.05$) reduced at both the storage temperatures, but on the other hand, the POD and bromelain activity of COH and HWB-treated pineapple juice reduced significantly ($p < 0.05$) only at a storage temperature of 25 °C.

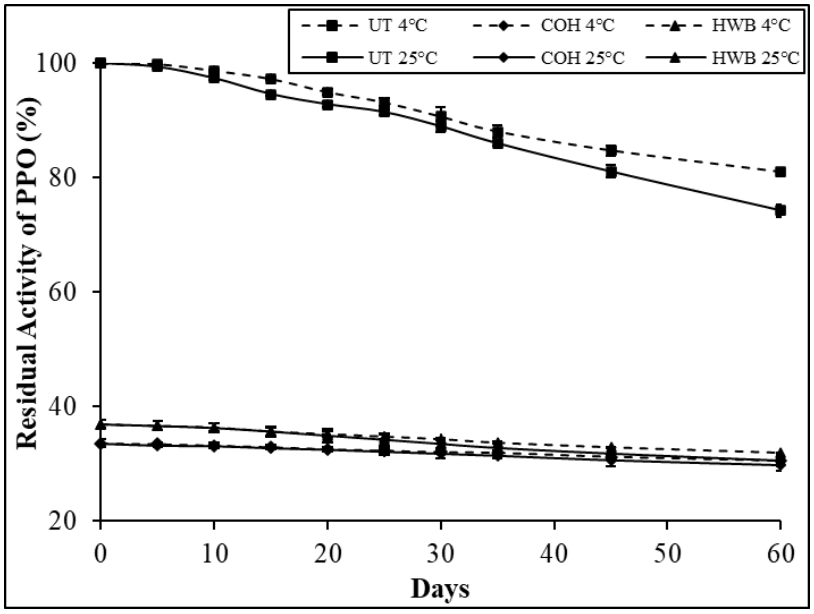

Fig. 4.44 Effect of storage on PPO activity

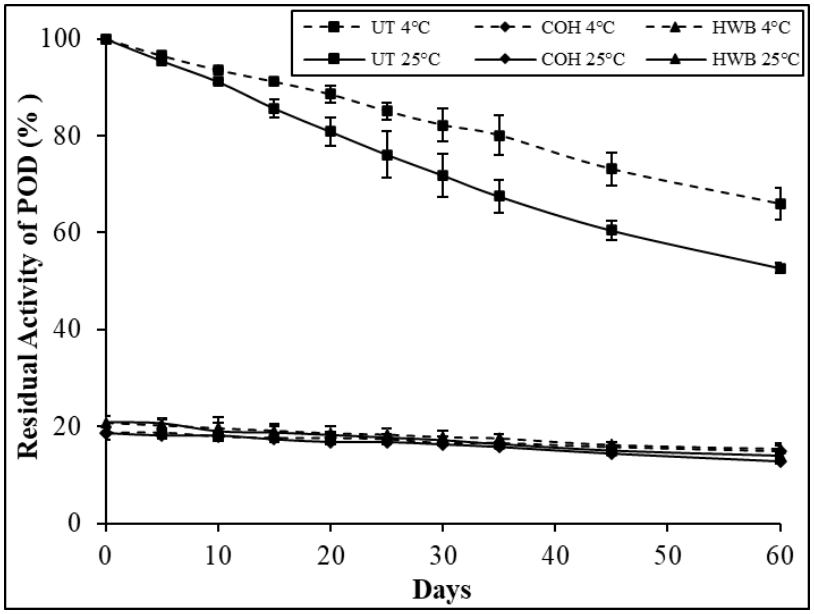

Fig. 4.45 Effect of storage on POD activity

In comparison, the significant ($p < 0.05$) reduction of POD and bromelain activity of COH and HWB treated samples was only observed at 60 days of storage period stored at 4 °C. PPO activity of untreated (UT), COH, and HWB-treated juice was significantly ($p < 0.05$) reduced with storage time at both temperatures. During the storage study, a first-order kinetic model was found to explain better the degradation of PPO and POD enzyme activity in pineapple

juice. In contrast, the second-order kinetic model was better suited for bromelain degradation (Table 4.39).

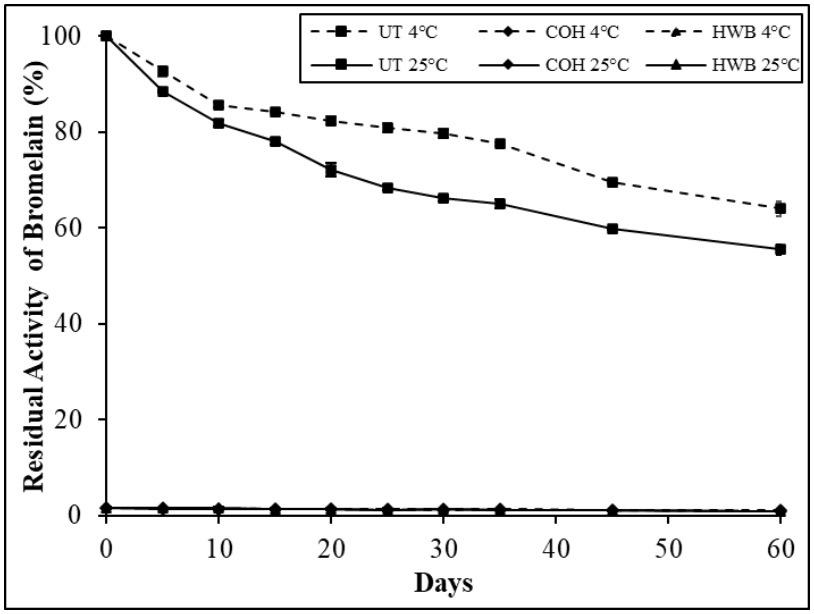

Fig. 4.46 Effect of storage on bromelain activity

The R^2 of the first-order kinetic model of both the PPO and POD degradation was higher than the second-order model. At the same time, the RMSE and SSE values were lower than the zero-order model, which suggested the suitability of the first-order kinetic model. Similarly, the R^2, RMSE, and SSE of the second-order kinetic model of bromelain degradation were comparatively better than the other two models. However, the bromelain was inactivated to less than 2.0% on the initial COH and HWB treatment day. Thus, overall bromelain activity also remained less than 2.0% during their storage; therefore, the kinetic model was not performed. PPO, POD, and bromelain enzyme degradation were lower at lower storage temperatures (4 °C) and vice versa. This was also confirmed by the lower reaction rate constant (k_1: PPO and POD; k_2: bromelain) values, which were lower at 4 °C compared to a higher storage temperature of 25 °C.

The untreated pineapple juice showed a total degradation of 19.0%, 34.1%, and 36.0% of PPO, POD, and bromelain activity, respectively, at a storage temperature of 4 °C. In comparison, degradation was increased to 25.7%, 47.3%, and 44.5%, respectively, at a higher storage temperature of 25 °C. Similar trends were observed for both COH and HWB-treated pineapple juice.

Table 4.39 Model parameters of degradation kinetic modelling of enzyme activity during storage study of pineapple juice

Enzyme	Model	Kinetic Parameter	UT4°C	COH4°C	HWB4°C	UT25°C	COH25°C	HWB25°C
PPO	Zero Order	k_o (day^{-1})	0.312	0.050	0.087	0.404	0.063	0.109
		R^2	0.963	0.991	0.991	0.981	0.991	0.984
		RMSE	1.274	0.096	0.161	1.148	0.118	0.274
		SSE	14.610	0.083	0.233	11.850	0.125	0.676
	First Order	k_1 (day^{-1})	0.003	0.002	0.003	0.004	0.002	0.003
		R^2	0.954	0.988	0.990	0.966	0.987	0.981
		RMSE	0.014	0.003	0.005	0.015	0.004	0.008
		SSE	0.002	0.0001	0.0002	0.002	0.0002	0.001
	Second Order	k_2 (day^{-1})	0.00003	0.00005	0.00007	0.00005	0.00006	0.00009
		R^2	0.950	0.986	0.989	0.946	0.982	0.979
		RMSE	0.0002	0.0001	0.0002	0.0003	0.0002	0.0003
		SSE	0.000	0.000	0.000	0.000	0.000	0.000
POD	Zero Order	k_o (day^{-1})	0.581	0.062	0.095	0.866	0.090	0.124
		R^2	0.998	0.976	0.987	0.980	0.974	0.976
		RMSE	0.504	0.188	0.194	2.153	0.293	0.343
		SSE	2.287	0.317	0.339	41.710	0.774	1.057
	First Order	k_1 (day^{-1})	0.007	0.004	0.005	0.011	0.005	0.007
		R^2	0.995	0.972	0.994	0.998	0.954	0.986
		RMSE	0.007	0.011	0.007	0.008	0.021	0.013
		SSE	0.001	0.001	0.001	0.001	0.004	0.001
	Second Order	k_2 (day^{-1})	0.00008	0.0002	0.0003	0.0001	0.0003	0.0004
		R^2	0.977	0.969	0.991	0.984	0.920	0.985
		RMSE	0.002	0.008	0.005	0.004	0.021	0.009
		SSE	0.00005	0.0005	0.0002	0.0001	0.0040	0.0008
Bromelain	Zero Order	k_o (day^{-1})	0.676	NP	NP	0.947	NP	NP
		R^2	0.845			0.696		
		RMSE	4.063			7.548		
		SSE	148.600			512.700		
	First Order	k_1 (day^{-1})	0.008	NP	NP	0.013	NP	NP
		R^2	0.903			0.863		
		RMSE	0.032			0.051		
		SSE	0.009			0.023		
	Second Order	k_2 (day^{-1})	0.0001	NP	NP	0.0002	NP	NP
		R^2	0.936			0.929		
		RMSE	0.0004			0.0007		
		SSE	0.000			0.000		

'NP' symbolises that the kinetic model was 'not performed.'

Xu et al. (2019) also observed a decreasing trend of PPO and POD enzymes in untreated, hydrothermal treated, calcium chloride treated, and hydrothermal – calcium chloride treated peppers during storage for 32 days at 8 °C which was caused by the decrease in the physiochemical metabolism properties. On the contrary, Suo et al. (2022) observed an increasing trend in the PPO and POD residual activity in ultrasonic-treated pumpkin juice during a storage period of 12 days at 4 °C. They concluded that PPO and POD enzymes appeared reversible in nature and started increasing after 4 days of storage. On the other hand, Tareen et al. (2012) observed a steady increase in the POD activity in salicylic acid-treated peach fruit during the first four weeks of storage at 0 °C. Then they showed a declining trend till the end of the storage period. In contrast, the PPO activity remained stable during the first two weeks and then increased. Overall, the storage conditions, especially temperature, time, pH variations, type of process technology involved, and the presence of certain specific compounds, can influence the activity of the enzymes during storage. Certain compounds present in the fruit or introduced during the processing might act as inhibitors or activators affecting the enzyme's activity during storage. Higher storage temperature can accelerate the enzyme's degradation, resulting in a more rapid decrease in enzyme activity than lower storage temperature. Enzymatic activity often follows a typical temperature-dependent degradation cure. However, the changes in the pH levels during storage might influence the enzyme's stability. Alterations in acidity or alkalinity could impact enzyme activity, potentially accelerating or decelerating its degradation.

4.11.5 Changes in colour parameters

The colour parameters viz., L^*, a^*, b^*, and total colour change (ΔE) of the untreated, COH, and HWB-treated pineapple juice stored at 4 °C and 25 °C for 60 days were estimated as shown in Fig. 4.47. The initial values of L^*, a^*, and b^* of the untreated pineapple juice were 27.36 ± 0.12, -0.95 ± 0.05, and 1.93 ± 0.00, respectively. The COH and HWB treatment increased L^* and b^* values and reduced a^* values. The initial values of L^*, a^*, and b^* were 32.05 ± 0.22, -1.67 ± 0.06, and 2.09 ± 0.05, respectively, for COH-treated pineapple juice and 32.21 ± 0.54, -1.81 ± 0.03, and 2.62 ± 0.04, respectively for HWB treated juice samples. The storage time significantly ($p < 0.05$) affected the values of colour parameters. The L^* values of the COH-treated and HWB-treated juice showed an increasing trend till 20 days of storage at both temperatures and remained relatively stable and then slowly decreased to the end of the storage period.

Tareen et al. (2012) also observed an increasing trend in the L^* values during the first two weeks of storage in the salicylic acid-treated peach fruit, which gradually decreased until the end of the storage period. Similarly, Suo et al. (2022) observed no significant change in the L^*, a^*, and b^* during 4 days of storage in ultrasonic-treated pumpkin juice. However, the colour parameters significantly decreased on the 8^{th} and 12^{th} day of storage. The total colour change of untreated pineapple juice attained a maximum value of 5.32 ± 0.15 and 5.42 ± 0.34, respectively, at 4 °C and 25 °C storage temperatures. On the other hand, the COH-treated pineapple juice observed a total colour change of 2.84 ± 0.08 and 3.69 ± 0.08 at 4 °C and 25 °C storage temperatures, respectively, while the hot water bath-treated juice obtained comparatively higher total colour of 3.30 ± 0.42 and 3.85 ± 0.63, respectively at 4 °C and 25 °C. Suo et al. (2022) observed a non-significant change during 4 days of storage in the total colour change ($\Delta E < 1$) of ultrasonic-treated pumpkin juice, while they observed a significant noticeable change from 8 to 12 days ($\Delta E > 1$) of the storage. The constant change in the colour values of the pumpkin juice during storage was closely related to the chemical, biochemical, enzymatic, and physical changes during the juice processing. Various factors, including enzymatic reactions, oxidation, pH changes, temperature, and microbial growth, influenced the colour parameters in pineapple juice during storage. Pineapple juice is particularly sensitive to these factors due to its composition of natural pigments and enzymes.

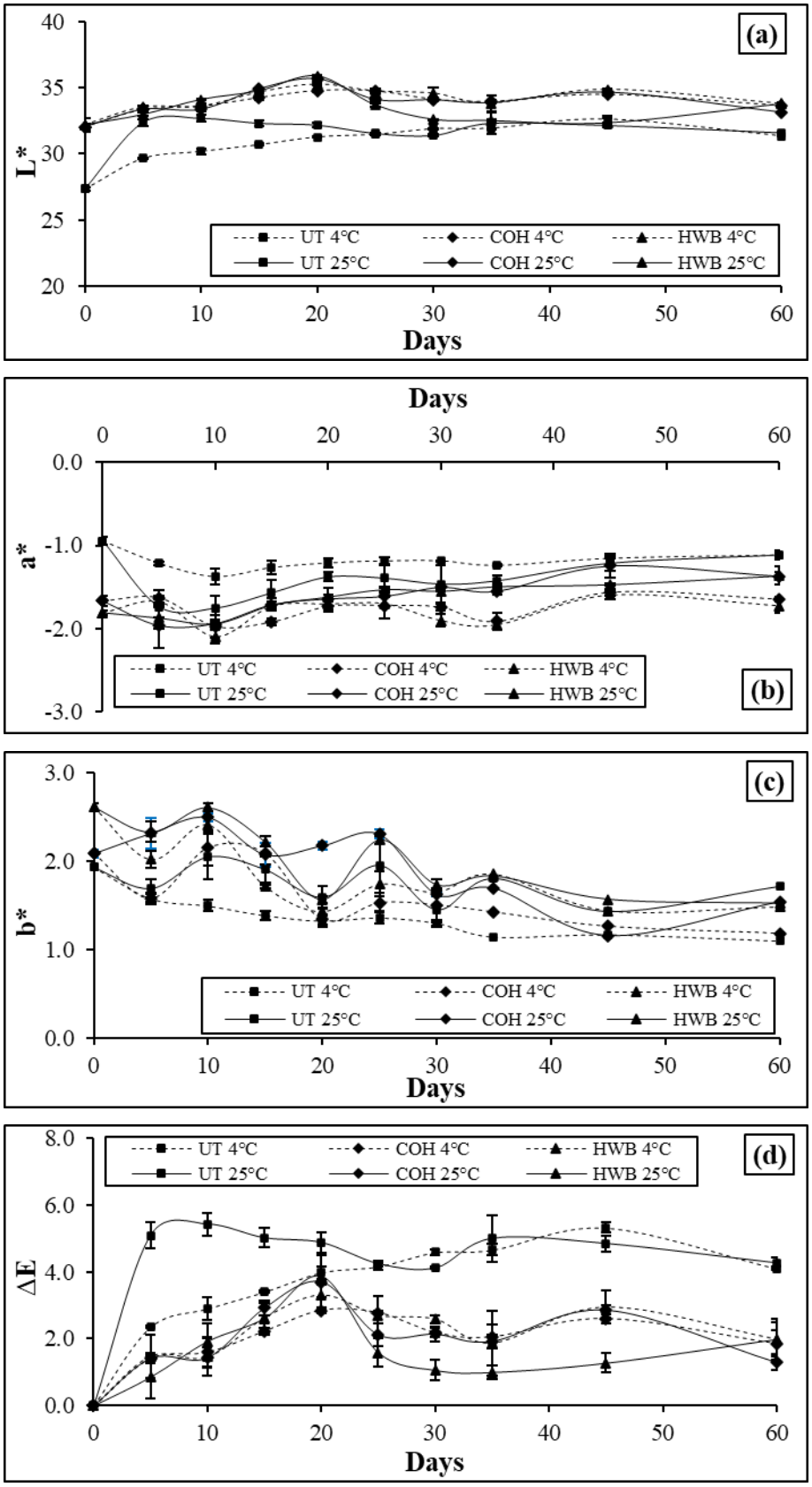

Fig. 4.47 Effect of storage on colour parameters (a) L*, (b) a*, (c) b*, and (d) total colour change